AN INNATE LYPMPHOCYTE CANCER CELL SENSING PROGRAM GOVERNS IMMUNOSURVEILLANCE OF HUMAN AND MURINE MALIGNANCIES

By

Emily R. Kansler

A Dissertation

Presented to the Faculty of the Louis V. Gerstner, Jr.

Graduate School of Biomedical Sciences,

Memorial Sloan Kettering Cancer Center

in Partial Fulfillment of the Requirements for the Degree of

Doctor of Philosophy

New York, NY

May 2021

_____ _____

Ming Li, PhD Date
Dissertation Mentor

To my Mom, I miss you fiercely every day. Your memory motivates all that I do.

ABSTRACT

Malignancy can be suppressed by the immune system. However, the classes of cancer immunosurveillance responses and their mode of tumor sensing remain incompletely understood. This dissertation focuses on investigating tumor-elicited cytotoxic lymphocyte responses, elucidating their method of tumor cell detection and understanding their regulation by the microenvironment in human and mouse malignancies.

By utilizing single-cell RNA sequencing of human tumor samples and flow cytometric analysis of human tumor, adjacent normal kidney and peripheral blood samples, we found that while clear cell RCC (ccRCC) tumors were predominantly infiltrated with phenotypically exhausted $CD8^+$ T cells, chromophobe RCC (chRCC) tumors had abundant infiltration of tissue-resident $CD56^{bright}$ innate lymphocytes that expressed high levels of the cytotoxic molecule granzyme A. Infiltration of phenotypically exhausted $CD8^+$ T cells negatively correlated with patient prognosis in both histologies, while infiltration of granzyme A-expressing tissue-resident innate lymphocytes positively associated with patient survival only among chromophobe patients. These data are, to our knowledge, the first to reveal a tumor suppressive function of tissue-resident group 1 innate lymphocytes in human cancer.

Notably, *in vitro* assays demonstrated that interleukin-15 (IL-15) promoted granzyme A expression and natural killer (NK) cell-like cytotoxicity within the tissue-resident $CD56^{bright}$ innate lymphocyte population in a dose dependent manner. Interestingly, analysis of the TCGA revealed that chRCC tumors express higher levels of IL-15 compared to ccRCC, suggesting that IL-15 expressed by tumor tissue controls the

magnitude of the innate lymphocyte response. In order to investigate the cellular mechanism of IL-15-mediated regulation, we employed a murine model of epithelial cancer in which IL-15 could be specifically ablated in distinct cell types via the use of cell-type specific Cre recombinases. These studies revealed that IL-15 produced by cancer cells, but not hematopoietic or mesenchymal stromal cells, supported the expansion and effector differentiation of tissue-resident cytotoxic innate lymphocytes.

The work in this dissertation uncovers an evolutionarily conserved cancer immunosurveillance mechanism whereby cancer cell-expressed IL-15 functions as an alarmin to be directly sensed by tissue-resident cytotoxic innate lymphocytes. As innate lymphocytes and IL-15 are both actively explored in the clinic for cancer treatment, these findings suggest that distinct differentiation states of innate lymphocytes and the method of IL-15 delivery should be taken into consideration for effective cancer immunotherapy.

BIOGRAPHICAL SKETCH

Emily Rose was born to Christopher Paul and Brigit Marie Kansler on June 21, 1988 along with her twin sister Katie Elizabeth in Baltimore, MD and raised in Abingdon, MD. In 2010, Emily obtained her Bachelor of Arts degree from Salisbury University, where she majored in Cell and Molecular Biology and minored in Chemistry. Upon graduating, Emily worked for the US Army as an ORISE contractor for the Test, Reliability and Evaluation Branch of the Development Command (DEVCOM) Chemical Biological Center. There, she assisted in testing filtration units for masks, vehicles, and shelter systems prior to use in the field. Wanting to pursue a career in biology, Emily started her Master of Science degree in 2011 in the Molecular Microbiology and Immunology (MMI) department at Johns Hopkins Bloomberg School of Public Health, where she worked in the laboratory of Jelena Levitskaya, MD investigating the role of proteinase inhibitor 9 in neuroblastoma. After graduating in 2013, Emily began working as a research technician in the laboratory of Richard White, MD, PhD at MSKCC where she studied the drivers of melanoma metastasis in the zebrafish model. Wanting to merge her interests in immunology and cancer biology, Emily started the PhD program at Louis V. Gerstner, Jr Graduate School of Biomedical Sciences at MSKCC. Following rotations in the laboratories of Dr. Alexander Rudensky and Dr. Frederic Geissmann, Emily joined the laboratory of Dr. Ming Li. With the endless support of Dr. Li, Emily has worked on multiple projects centered around tumor immunology and innate lymphocyte biology and will continue her overarching goal of bridging basic biology and translational medicine to bring health solutions to patients.

ACKNOWLEDGEMENTS

First and foremost, I would like to give my heartfelt thanks to my mentor, Dr. Ming Li, for his steadfast support and guidance throughout this incredible journey. Thank you, Ming, for showing me what true dedication looks like, while having a constantly positive and optimistic attitude. Your curiosity and perseverance have been a true source of inspiration and will continue to be so long into my career.

I would also like to thank my committee members Dr. Alexander Rudensky and Dr. Joseph Sun for their support and helpful advice over these last 5 years. I would like to thank our collaborator Dr. Abraham A. Hakimi for his mentorship and his support throughout my work on the human RCC project. Huge thanks to Dr. Chirag Krishna, whose computational expertise was crucial for the human RCC project. Thank you all for being such a pleasure to work with. An additional thanks to Dr. Morgan Huse for agreeing to chair my committee and Dr. Gregory Sonnenberg of Weill Cornell Medical College for taking on the role of external examiner.

I would also like to express my gratitude to all past and present members of the Li Lab for their friendship and help throughout my PhD. Thank you to Saïda Dadi for laying the groundwork for my projects and her mentorship during my rotation. Thank you to Briana Nixon for your friendship and support on the human RCC project, and to Amy Shyu for making our bay corner a fun and friendly working environment. Thank you to Davina Kang, Kristelle Capistrano, and Chaucie Edwards for help with the never-ending mouse colony and Sofia, Alex, Kristelle and Chaucie for helping the lab function smoothly.

A big thank you to the graduate school leadership and my classmates for making GSK a great place to study, especially Gemma, Paige and Rui. Thank you for always having an ear to listen and advice to give. I can't imagine having gone through this PhD journey without your friendship.

Lastly, I would like to thank my family and friends. First, to my husband Micheal for being my person and a constant source of strength and happiness, and to Cash for making us a family. Thank you, Dad, Kate, Brent, Adam, Alyssa and Brigette, for the unwavering love and support. Thank you, Aunt Courtney, Peyton and Izzy, for being our family in NY. We wouldn't have made it here without you. Thanks to all the Mansfields and Kanslers, especially my grandparents, whose support and love I've felt over these years. Huge thanks to Jackie, Kellie, Sara, Kara, Aysha, Amanda, Frankie and Veronica for our decades of friendship, how lucky are we. And last but not least Emily, Ian, Dawn, Ryan, Shannon and Craig for the adventures, friendship and support all these years.

TABLE OF CONTENTS

LIST OF FIGURES

LIST OF ABBREVIATIONS

ACK	Ammonium Chloride Potassium buffer
ANOVA	Analysis of Variance
B2M	Beta-2 microglobulin
ccRCC	Clear cell renal cell carcinoma
cDC1,2	Classical dendritic cell type 1,2
CFP	Cyan fluorescent protein
chRCC	Chromophobe renal cell carcinoma
CPT	Cell preparation tube
CTLA-4	Cytotoxic T-lymphocyte-associated protein 4
CTV	Cell trace violet
DC	dendritic cell
eGFP	Enhanced green fluorescent protein
FACS	Fluorescence-activated cell sorting
FMO	Fluorescence minus one
GECI	Genetically encoded calcium indicator
GEMS	Gel Bead-in-EMulsions
GzmA	Granzyme A
GzmB	Granzyme B
GzmC	Granzyme C
GzmH	Granzyme H
HLA	Human leukocyte antigen
HLA-E	Human leukocyte antigen - E

IACUC	Institutional Animal Care and Use Committee
ICB	Immune checkpoint blockade
iCre	Improved Cre recombinase
IFNg	Interferon gamma
IL_1	Innate lymphocyte cluster 1
IL_2	Innate lymphocyte cluster 2
IL-15	Interleukin 15
IL-15Ra	Interleukin 15 receptor alpha
IL-2Rb	Interleukin 1 receptor beta
IL7R	Interleukin 7 receptor
ILC	Innate lymphoid cell
ILC1	Type 1 innate lymphoid cell
ILC2	Type 2 innate lymphoid cell
ILC3	Type 3 innate lymphoid cell
ILCp	Innate lymphoid cell precursor
ITAM	Immunoreceptor tyrosine-based activation motif
ITIM	Immunoreceptor tyrosine-based inhibitory motif
JAK	Janus kinase
KICH	TCGA designation for chromophobe RCC
KIR	Killer immunoglobulin-like receptor
KIRC	TCGA designation for clear cell RCC
LSL	Lox-stop-lox
MACS	Magnetic-activated cell sorting

MAPK	mitogen-activated protein kinase
MHC	Major histocompatibility complex
MICA	MHC class I polypeptide–related sequence A
MMTV	Mouse mammary tumor virus
MTMs	Mammary tissue macrophages
NK	Natural killer
NKC	Natural killer complex
NKG2A	Natural killer cell protein group 2-A
NKp	Natural killer cell progenitor
PD-1	Programmed death 1
PI	Propidium iodide
PI3K	Phosphoinositide 3-kinase
PyMT	Polyoma middle T antigen
Qdm	Qa1 determinant modifier
RPKM	Reads Per Kilobase of transcript, per Million
RPMI	Roswell Park Memorial Institute
SHP1	Src homology region 2 domain-containing phosphatase-1
SKI	Sloan Kettering Institute
ssGSEA	Single sample Gene Set Enrichment Analysis
STAT	Signal transducer and activator of transcription
TAMS	Tumor associated macrophages
TCGA	The Cancer Genome Atlas
TCR	T cell receptor

tdT	Tandem Dimer Tomato
TNFa	tumor necrosis factor alpha
TRAIL	TNF-related apoptosis-inducing ligand
Trm	Resident Memory T cell
tSNE	t-Distributed Stochastic Neighbor Embedding
ULBP	UL-16 binding proteins
gC	Common gamma chain
YFP	Yellow fluorescent protein

Chapter 1: Introduction

1.1 Overview of Immunity

The immune system is a complex network of cells spanning the entire body with the purpose of preventing infection or invasion by foreign entities and maintaining physiological homeostasis. Broadly, the immune system is comprised of innate and adaptive immunity. The innate immune system consists of cells representing the first line of defense with the ability to sense and combat pathogens through germline-encoded receptors and effector molecules. Adaptive immunity is more complex, with Rag-rearranged genes encoding antigen receptors with exquisite specificity and robustness in responding to and eliminating foreign challenges. Furthermore, the adaptive immune response is able to retain memory of infectious challenges, providing long term vigorous protection from reinfection. Cells of the innate immune system also provide help to adaptive immune cells, forming an integrated, beautifully intricate system of host protection.

The immune system has evolved to respond to many challenges of diverse pathogenic nature. Generally, these challenges can be grouped into either extracellular or intracellular threats. Extracellular threats are those such as parasites and extracellular bacteria, commonly occurring at mucosal barrier sites causing damage or disrupting homeostasis. Type 2 and type 3 immunity are equipped to deal with such challenges by calling to arms multiple types of immune cells through recruitment, cell-to-cell communication and cytokine secretion. Intracellular threats encompass pathogens like bacteria and viruses that infect host cells or transformation of “self” cells resulting in

cancer. These threats are addressed by type I immunity, which has the capacity to directly kill cells that have been compromised.

In terms of infection, type I immunity has generally been studied in the context of circulating cells in the blood and lymphatic system that become primed in lymphoid organs and subsequently traffic to tissues. Recently, the presence of immune cells holding residency in peripheral tissues serving as sentinels of tissue homeostasis, already poised in the tissue to encounter threats, has become better appreciated. In the context of cancer, these tissue-resident cells likely represent a first line of defense upon cellular transformation.

1.2 Subsets of Cytotoxic Lymphocytes

1.2.1 Mechanisms of Cytotoxicity

Cytotoxic lymphocytes are able to directly sense and kill target cells. They do so through release of the cytotoxic molecules perforin and granzymes, which results in pore formation in target cells allowing entrance of granzymes to mediate cell death (Fig. 1.1) [1]. They can also induce cell lysis through engagement of death receptors like Fas and TRAIL [2]. Classically, two subsets of cytotoxic lymphocytes exist – adaptive $CD8^+$ T cells and innate natural killer (NK) cells. While the mechanisms of granzyme mediated cytotoxicity are similar for both subsets, the nature in which cells are detected and targeted for cell killing are distinct.

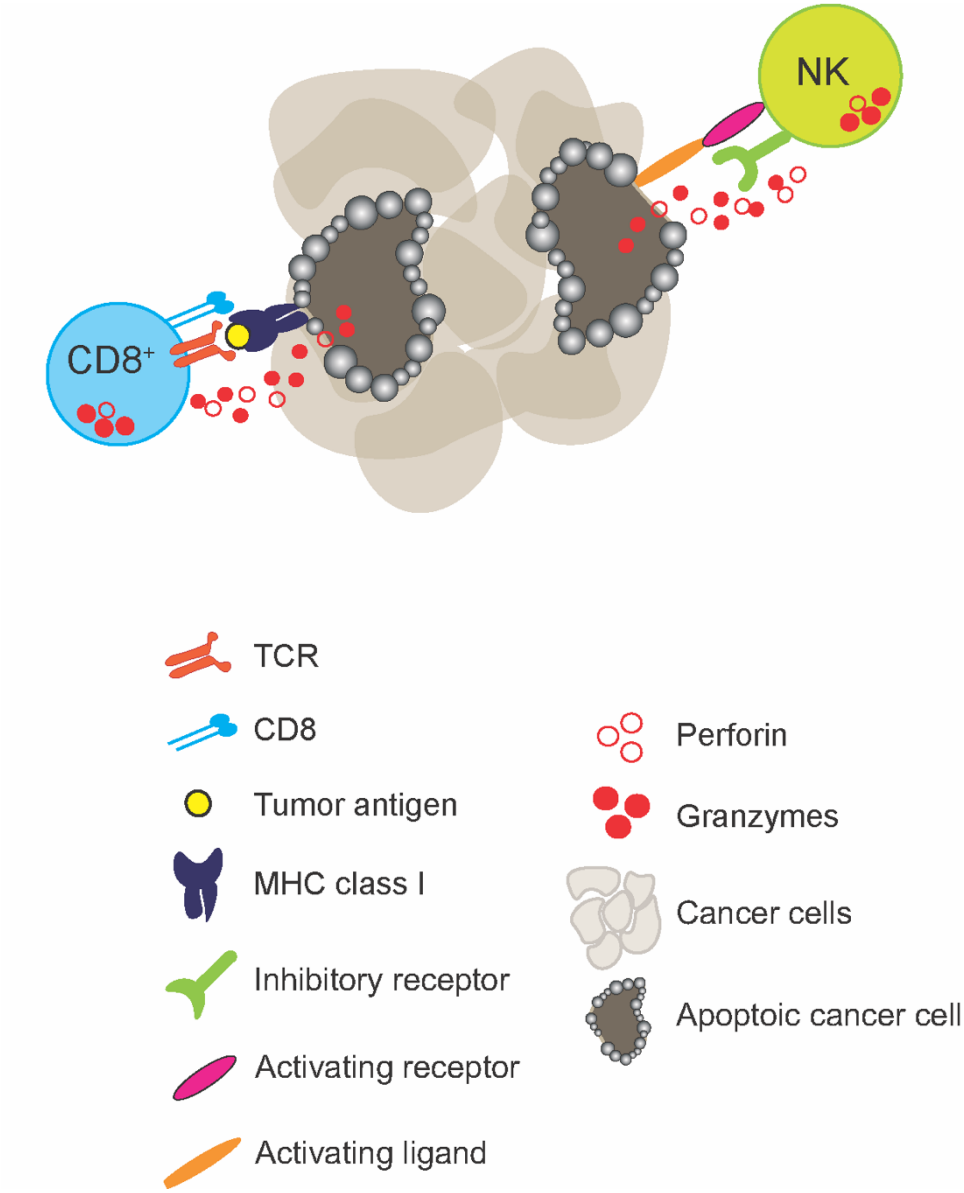

Figure 1.1 CD8$^+$ T cells and NK cells directly kill target cells

CD8$^+$ T cells recognize non-self antigens presented by MHC class I molecules on the surface of target cells, resulting in release of granzymes and perforin to induce cell death. NK cell cytotoxicity is controlled by integration of an array of inhibitory and activating signals. NK cells recognize the loss of MHC class I molecules in a process called "missing self" whereby loss of inhibitory signaling allowing activation signals to dominate, resulting in target cell death via perforin/granzyme release.

1.2.2 CD8$^+$ T Cells

CD8$^+$ T cells are critical effector cells in the context of infection and cancer. In the periphery, the majority of CD8$^+$ T cells express ab T cell receptors (TCRs). Expression of these receptors allows CD8$^+$ T cells to respond to foreign antigen in the form of short peptides presented by major histocompatibility complex (MHC) (human leukocyte antigen or HLA in humans) class I molecules [3]. At the steady state, naïve and memory subsets of CD8$^+$ T cells circulate throughout the blood stream and lymphatic system. During infection, CD8$^+$ T cells undergo robust proliferation and clonal expansion, differentiating into effector CD8$^+$ T cells with the ability to directly lyse target cells and control infection after being recruited into the infected tissue. Here, a subset of CD8$^+$ T cells will persist and can differentiate into antigen-specific tissue-resident memory T cells (Trm) [4]. These Trm cells then remain resident in the tissue even after the infection is cleared, left behind to continuously patrol for cognate antigen. Abundance of tissue resident Trm, often marked by the integrin CD103 or transcription factor Hobit (encoded by the *ZFP683* gene), in tumors frequently correlates with favorable prognosis in many cancer types [5].

The tumor microenvironment is often suppressive in terms of cytotoxic CD8$^+$ T cell responses. CD8$^+$ T cells found in both mouse and human tumors, in particular during late stages of disease, often display hallmarks of T cell exhaustion which includes consistent expression of inhibitory receptors like programmed death 1 (PD-1) and cytotoxic T-lymphocyte-associated protein (CTLA-4) [6]. Exhausted T cells lose operational ability to exert effector function and proliferate, making them dysfunctional and ineffectual. This exhaustion program can be driven by chronic antigen exposure or

other mechanisms that induce an overall tolerogenic immune environment, like soluble factors released by other immune cells or stromal cells that effectually dampen cytotoxic lymphocyte responses [6, 7]. Thorough investigation into the tumor environment and the particular kinds of cytotoxic lymphocytes that are present in tumors will undoubtedly lead to better understanding of the kinds of immune responses that can control cancer, resulting in novel strategies for therapy, or understanding of why the available therapies are not always effective.

1.2.3 Innate Lymphocytes

Natural killer cells are the most widely recognized and studied cytotoxic innate lymphocyte, particularly in viral infections and hematological malignancies [8]. Normal, healthy cells express MHC (HLA in humans) class I molecules on their surface which are recognized by inhibitory molecules on the surface of NK cells, preventing cell lysis. Virally infected or cancerous cells can downregulate MHC class I as an immune evasion mechanism to prevent presentation of mutated or non-self-antigens; these cells are detected as aberrant and killed by NK cells due to lack of inhibitory signaling [9, 10]. Oncogenic transformation can also induce expression of cell surface ligands that are detected by NK cells through activating receptors, resulting in cancer cell lysis [11, 12].

In addition to circulating NK cells, reports over the last decade have revealed previously unappreciated heterogeneity of innate lymphocytes to include innate lymphoid cells (ILCs) [13]. These ILCs are generally considered to be tissue-resident and are grouped based on their transcription factor dependency and effector programs and include ILC1, ILC2, ILC3 and lymphoid tissue inducer (LTi) cells. ILC1 and NK cells

are considered to be group 1 innate lymphocytes and share a dependency on the transcription factor T-bet, encoded by the T-box 1 gene *Tbx21* and their ability to produce type 1 cytokines like IFNg and TNFa [13]. However, NK cells are traditionally circulating and express cytotoxic molecules, while ILC1 reside in peripheral tissues and are generally cytokine producers. Despite this conventional classification, tissue-resident ILC-like cells with cytotoxic activity have been reported in spontaneous models of murine epithelial cancers [14]. The protective effects of group 1 innate lymphocytes have also been established in models of chemically induced and transplantable tumors. Antibody-mediated depletion of NK1.1^{+} cells and loss of NKp46^{+} cells via genetic model systems demonstrate the importance of innate lymphocytes in controlling tumor growth, however as ILC1 and NK cells express both markers, causation cannot be attributed to one or the other [15-17].

In humans, CD56 is used as a marker of innate lymphocytes classically defined as NK cells, generally subset into CD56^{bright} and CD56^{dim} populations that are abundant in tissues and circulation, respectively [18]. A body of evidence suggests that CD56^{bright} NK cells are less mature and are dominantly cytokine producers, while CD56^{dim} NK cells are terminally differentiated and potent killers. However, with the recent description of ILCs and studies that suggest CD56^{bright} cells may be derived from a distinct progenitor, whether these two populations represent linear steps along the NK cell developmental pathway or belong to different lineages remains unclear [19]. Notably, infiltration of CD56^{bright} innate lymphocytes has been reported in several solid tumor types and association of a variety of NK/ILC-related genes is indicative of improved patient

outcome in multiple cancer types [8, 20]. However, the characteristics and function of these tumor-infiltrating innate lymphocytes remain incompletely understood.

1.3 Cancer Immunosurveillance

Throughout the last century, evidence for a role of the immune system in tumorigenesis in both mice and humans has accumulated, spurring multiple avenues of inquiry into immunotherapy approaches for the treatment of cancer. The theory of cancer immunosurveillance originally attributed the protective mechanisms to adaptive immune responses, in particular antigen-specific $CD8^+$ T cells [21]. Studies since then have demonstrated that T cells can indeed play a critical role in restraining tumor growth in carcinogen-induced or virally associated cancers, especially those in which the process of carcinogenesis results in immunogenic antigen expression [22]. However, activation by tumor antigens generally results in robust intrinsic regulatory mechanisms that restrain T cell responses, most notably through engagement of inhibitory checkpoint receptors such as PD-1 and CTLA-4 [6, 7], resulting in T cell exhaustion. The clinical success of immunotherapy approaches that remove these brakes through checkpoint blockade, rendering cytotoxic $CD8^+$ T cells functional again, have produced durable responses in some cancer subtypes including clear cell renal cell carcinoma (ccRCC) [23-25], demonstrating that in certain contexts conventional mechanisms of cancer immunosurveillance can be exploited for therapy.

However, many tumor types lack expression of immunogenic antigens [22]. In such cases it is unlikely that conventional T cell responses will have a major anti-tumor effect. Furthermore, exposure to tumor-associated non-self-antigens in oncogene-induced

tumors does not guarantee induction of a host-protective immune response [26, 27]. The ability of tumor cells to "escape" immunosurveillance as a result of immunological pressure and subsequent mutation also highlights the fact that antigen-specific lymphocyte responses often fail at tumor control [28].

A major outstanding question in the field of cancer immunotherapy is why immunotherapy treatments have proven effective only in a subset of patients and cancer types [29]. The variability in response can be due to a number of factors, including the lack of targetable biomarkers, heterogeneity of cancer cells within tumors, treatment history and other immunosuppressive mechanisms present in the tumor microenvironment [30]. Overall, these truths highlight the need to continue investigating potential immunotherapy approaches and suggests other methods that are independent of, or work in concert with, antigen-specific lymphocytes may provide further benefit.

1.4 Regulation of Innate Lymphocytes by MHC Class I

As alluded to above, NK cell activity is tightly regulated by the integration of signals from inhibitory and activating receptor ligand interactions [31]. As such, NK cells express an array of inhibitory and activating receptors whose genes reside primarily in the natural killer cell (NKC) gene complex [31-33]. These receptors include the C-type lectin-like Ly49 receptors in mouse and killer immunoglobulin-like receptors (KIR) in human that recognize MHC class Ia, as well as the conserved NKG2 family of receptors that engage MHC class Ib molecules or stress induced ligands (Fig. 1.2) [31]. Recognition of normal expression of MHC class Ia and Ib molecules through inhibitory KIR/Ly49 or NKG2A molecules results in inhibition of NK cell effector function (Fig.

1.2). Loss or downregulation of MHC class I molecules is sensed by NK cells through a process termed “missing self”, which removes the inhibitory signal thereby enhancing activation and resulting in target cell death (Fig. 1.3) [34, 35]. The ability to sense changes in the MHC class I environment is the result of “licensing” during NK development and maturation, a process by which NK cells become “educated” in balancing their functional capability with tolerance to self through engagement of NKG2A and Ly49 receptors with MHC class I molecules [36-38].

The Ly49 and KIR receptors directly recognize MHC class Ia molecules on the surface of target cells and are the main receptors responsible for providing NK cell education [39, 40]. The dominant role of the evolutionarily conserved MHC class Ib molecule Qa1 (HLA-E in humans) is to present Qa1 determinant modifier peptide (Qdm), a signature peptide of 9 amino acids derived from the leader sequence of MHC class Ia proteins [41-43]. The inhibitory NKG2A/CD94 heterodimer expressed on NK and CD8 T cells recognizes the beta-2 microglobulin (B2M)-dependent Qa1-Qdm complex [44-46]. Interestingly, the association between Qa1 and Qdm is relatively weak compared to MHC class Ia and peptide, suggesting that NKG2A/CD94 surveillance of MHC class Ia through Qa1 is a dynamic process that allows timely assessment of the MHC class I expression status and functionality of antigen presentation machinery of a cell [47-49]. Mechanistically, inhibition mediated by inhibitory receptor engagement of MHC class I is dictated by the presence of an immunoreceptor tyrosine inhibitory motif (ITIM) in the cytoplasmic tail of the receptor. Upon receptor ligand engagement, ITIMs become phosphorylated by Src family kinases, resulting in recruitment of SH2 domain-containing phosphatases

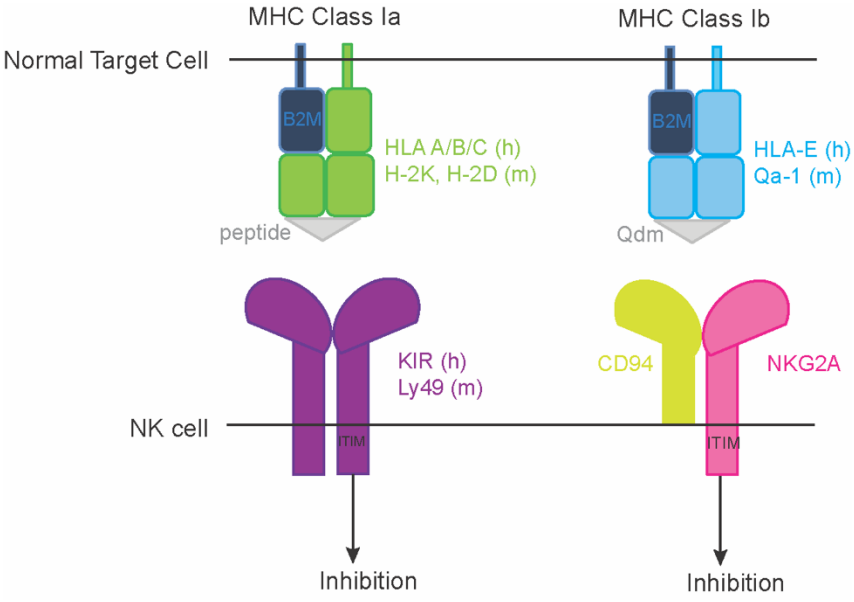

Figure 1.2 MHC class I molecule-induced NK cell inhibition

Healthy cells express normal levels of peptide-MHC class I complexes (HLA-A/B/C in human, H-2K and H-2D in mouse). These complexes are recognized by inhibitory receptors on the surface of NK cells (KIR in human, Ly49 molecules in mouse). A secondary measure of host cell health is achieved through presentation of Qdm, peptides derived from the leader sequence of MHC class Ia molecules, by MHC class Ib (HLA-E in human, Qa-1 in mouse). These complexes are recognized by the inhibitory receptor NKG2A that heterodimerizes with CD94 on the surface of NK cells. Presence of an ITIM motif results in inhibition of NK cell responses.

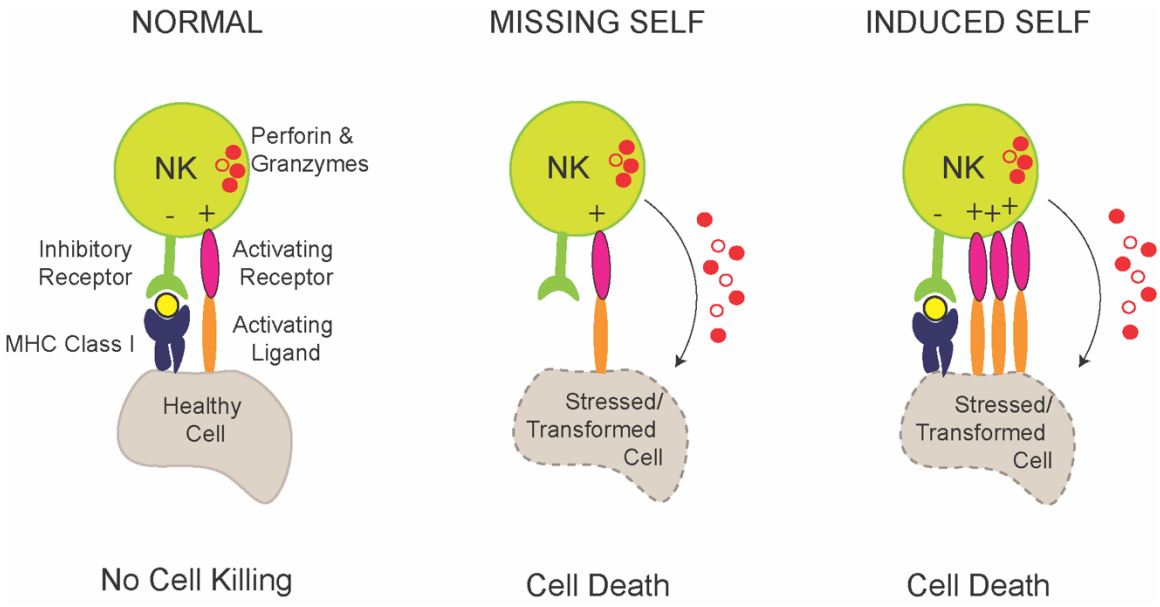

Figure 1.3 Mechanisms of NK cell recognition

NK cell activity is controlled by a balance between activating and inhibitory signaling. (Left) Normal, healthy cells express MHC class I molecules sensed by inhibitory receptors on NK cells. This inhibitory signal is stronger than activating ligands that may be present at low levels on healthy cells, resulting in net inhibition and no cell killing. (Middle) Virally infected or transformed cells often downregulate or lose expression of MHC class I molecules in an effort to evade foreign peptide recognition and subsequent death by $CD8^+$ T cells. However, NK cells sense this loss of MHC class I molecules as "missing self", which relieves the NK cell of its inhibitory signal allowing activation and release of perforin and granzymes to induce target cell death. (Right). NK cells have activating receptors that have evolved to detect evolutionarily conserved molecules upregulated on stressed or damaged cells. Increased expression due to stress or transformation is recognized by NK cell activating receptors, a phenomenon called "induced self". Strong activation signals through these interactions results in net activation and target cell death.

including SHP1 and subsequent inhibition via dephosphorylation of critical activating signaling molecules like Vav1 [31, 50, 51].

MHC class I-like molecules including MHC class I polypeptide–related sequence A (MICA) and the UL16 binding protein (ULBP) family of ligands are indicators of the evolutionarily conserved intracellular stress response [52]. They are rarely present on healthy tissues but can be upregulated upon cellular stress or damage from infection or transformation, a phenomenon termed "induced self" (Fig. 1.3). The presence of activating receptors on NK cells that interact with MHC class I-like molecules suggests that NK cells can recognize and subsequently eliminate stressed or damaged cells. The most well characterized activating receptor NKG2D has been indicated in sensing tissue injury and pathogenic infection as well as mediating tumor control [53, 54]. Activating receptors like NKG2D have a charged residue in their cytoplasmic tail that interacts with the adaptor molecule DAP10 or DAP12 in mice and DAP10 in humans [31]. Ligand engagement results in phosphorylation by Src kinases and subsequent employment of receptor tyrosine kinases Syk and/or Zap70 to mediate downstream activation pathways similar to T cell receptor mediated signaling [31]. In the mouse, NKG2D has been shown to associate with either DAP12 or DAP10 depending on the isoform expressed; DAP10 signaling results in PI3K activation and downstream signaling [31].

1.5 Regulation of Innate Lymphocytes by IL-15

$CD8^+$ T cells and NK cells are dependent on cytokine signaling through the common gamma chain (γc) receptor for various aspects of their development, maturation and/or effector function. During development in the bone marrow, NK cells express IL7R

and IL2Rβ and as such rely on signaling from IL-7 and IL-15, respectively [55]. As NK cells mature, they lose expression of IL7R and gain expression of IL2Rβ and become dependent on IL-15. Loss of this cytokine or IL-15Ra alone is sufficient to significantly abolish the pool of mature NK cells similar to levels seen in $\gamma c^{-/-}$ mice [56, 57].

IL-15 is predominantly trans-presented by IL15Rα on the surface of a presenting cell and signals through the IL-15/IL-2Rβ and γc receptor complex on a receiving cell, making signaling through this unique cytokine generally cell-contact dependent (Fig. 1.4) [58-61]. Signal transduction occurs through Janus-associated kinases (JAK) and signal transducer and activator of transcription (STAT) proteins [62]. Upon IL-15 binding to IL-15/IL-2Rβ and γc receptor complex, JAK1 is activated and phosphorylates STAT3 via the β chain and JAK3 is activated by the γc receptor resulting in STAT5 phosphorylation [62]. Phosphorylated STAT3 and STAT5 proteins dimerize and subsequently traffic to the nucleus for transcriptional activation. The Ras-Raf-MAPK and PI3K-Akt pathways are also induced upon Shc binding to a phosphorylated site on the IL-15/IL-2Rβ chain and subsequent activation of Grb2 [62]. Transcriptional activation by these factors results in immune cell activation and effector function, proliferation, anti-apoptosis and pro-survival cues.

Interestingly, IL-15 is produced by cells of both hematopoietic and non-hematopoietic origin [63-65]. While IL-15 transcript is abundantly available, stringent regulation at the post-transcriptional and translational levels tightly control IL-15 protein expression [66]. Previous studies have established that dendritic cell (DC) and macrophage-expressed IL-15 promotes the homeostasis, maturation and effector differentiation of adaptive and innate lymphocytes in secondary lymphoid organs

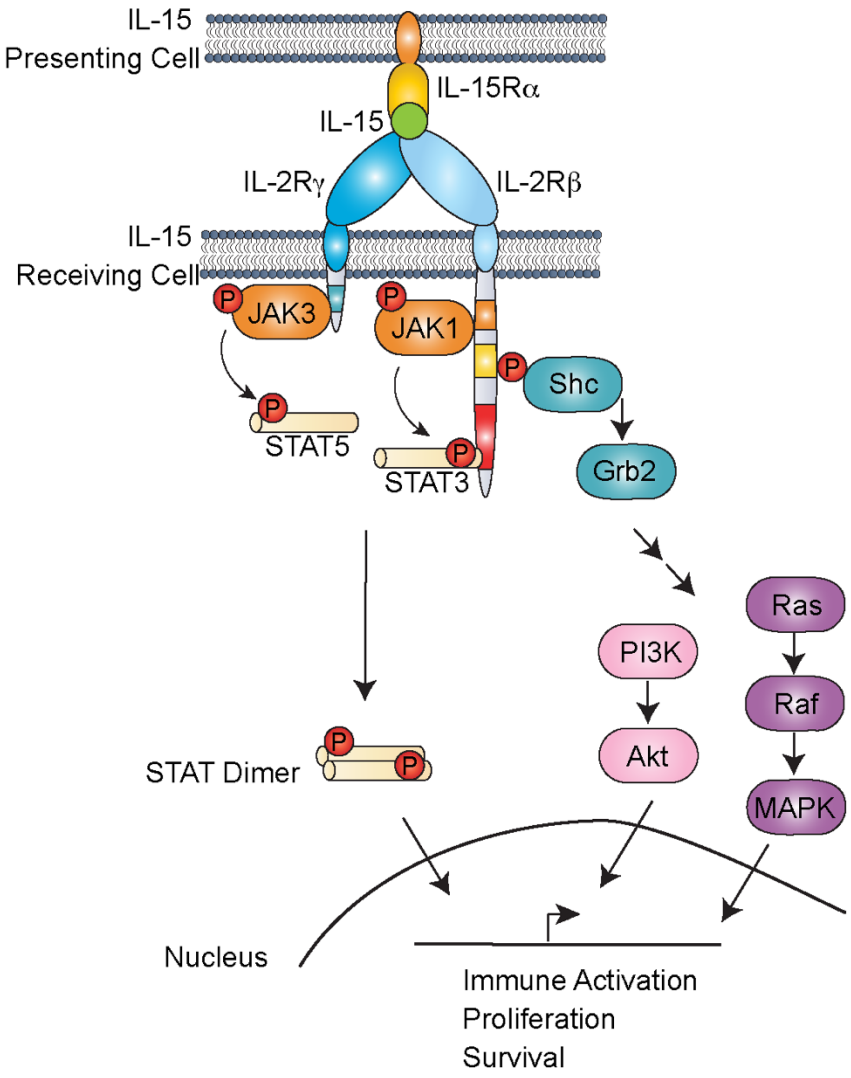

Figure 1.4 IL-15 signaling pathway

[66-70]. Following viral infection or bacterial lipopolysaccharide stimulation, IL-15 is induced in DCs and macrophages and promotes activation and differentiation of circulating effector and memory NK cells [69, 71, 72]. Non-hematopoietic cell sources of IL-15 include fibroblastic reticular cells in secondary lymphoid organs as well as parenchymal cells in peripheral tissues such as enterocytes, adipocytes, and the hair follicle epithelium [63-65, 67, 73, 74].

Tissue-resident cells provide a first line of defense against local challenges, including infections and tumorigenesis. IL-15 has a well-established role in supporting tissue-resident populations, including $CD103^+$ Trm in non-lymphoid tissues such as the skin [75]. The integrin CD103 binds E-Cadherin and signaling as a result of this interaction has been shown to regulate positioning and release of cytotoxic granules during cancer cell killing [76]. Furthermore, the presence of $CD103^+$ lymphocytes in various human tumor types including bladder urothelial cell carcinoma, non-small cell lung carcinoma, ovarian cancer, and endometrial adenocarcinoma is associated with favorable outcome [77-80].

Tissue-resident ILC-like innate lymphocytes were also shown to be fully dependent on IL-15 in a mouse model of breast cancer, as IL-15 knockout mice were completely devoid of $CD49a^+$Granzyme B^+ innate lymphocytes [14]. On the other hand, overexpression of IL-15 resulted in a significant increase in abundance of $CD49a^+$Granzyme B^+ innate lymphocytes [14]. Studies using mouse models of transplantable melanoma demonstrated that IL-15/IL-15Ra complexes in the tumor stroma regulated tumor-infiltrating lymphocyte numbers, and induction of IL-15 promotes anti-tumor responses [81]. Importantly, higher expression of the *IL15* gene is

correlated with better outcomes in a few different cancer types in human, although the exact mechanism is unknown [20]. Overall, IL-15 is a critical regulator of tissue-resident cytotoxic lymphocyte responses in the context of cancer.

1.6 Models of Cancer

In this dissertation, studies to investigate the cytotoxic immune cell repertoire in cancer involved primary human tissue samples. Tumor tissue, tumor-adjacent normal kidney tissue and peripheral blood samples from renal cell carcinoma patients were provided to us through collaboration with Dr. A. Ari Hakimi and urological surgeons at Memorial Sloan Kettering Cancer Center. We were able to characterize the distinct cytotoxic lymphocyte responses present in clear cell RCC (ccRCC) and chromophobe RCC (chRCC), the most common and rarest forms of RCC, respectively. We identified abundant $CD49a^{+}CD103^{+}$ tissue resident, granzyme-expressing $CD56^{bright}$ innate lymphocytes in both RCC subtypes, and further identified IL-15 as a crucial regulator of this response.

Our lab previously described tissue-resident cytotoxic innate lymphocytes that expanded upon cellular transformation in the MMTV-PyMT murine model of breast cancer [14, 82]. These cells express CD49a, CD103, granzyme B, and depend on IL-15 for their survival and/or maintenance in the tumor, and thus closely mimic the tissue-resident innate lymphocytes described in RCC tumors [14]. In this model, the polyoma middle T (PyMT) oncogene is driven by the mammary epithelial cell specific MMTV promoter to induce oncogenic Ras and AKT signaling pathways, leading to spontaneous transformation with 100% penetrance in female mice, affecting all 10 mammary glands

[82]. Mammary tumors closely recapitulate human breast cancer, and progress from early hyperplasia to early and late carcinoma stages starting at about 12 weeks of age to 20-25 weeks of age [83]. Although originally generated on the FvB mouse strain, previous members of the Li lab backcrossed the PyMT allele onto C57BL/6 mouse strain background. This allowed for combined usage of the PyMT model with other genetically modified alleles, a majority of which exist on the C57BL/6 background, in order to mechanistically investigate the regulation of tumor-infiltrating cytotoxic innate lymphocytes.

1.7 Dissertation Research Aims

While it is increasingly appreciated that the immune system plays pivotal roles in the control of cancer, the kinds of cytotoxic immune responses elicited during tumorigenesis remain incompletely understood. The mechanisms by which tumor-elicited immune responses sense and detect cancer cells, and how these signals regulate anti-tumor effector mechanisms are similarly less well known. In this dissertation, we aim to investigate the kinds of tumor-elicited immune mechanisms capable of tumor control that are present in human and murine solid tumors. Furthermore, we aim to uncover the mechanisms by which anti-tumor immune responses sense and detect cancer cells. A deeper understanding of these aspects of cancer immunology will allow for exploration into alternative approaches to immunotherapy.

Chapter 2: Cytotoxic Lymphocyte Responses in Renal Cell Carcinoma

2.1 Introduction

Renal cell carcinoma represents greater than 90% of all kidney cancers and is among the top 10 most common cancers in both men and women. The average age at diagnosis is 64 years old, and risk factors include smoking, obesity, family history and genetics, with subtype specific molecular characteristics and response to treatment [84]. The most common subtype, clear cell (ccRCC), accounts for ~75% of all RCC cases and is an aggressive disease with a 5-year survival rate of only 12% if the patient presents with distant metastases [85]. Clear cell RCC tumors originate in the proximal nephron or tubular epithelium [84]. More than 90% of ccRCC are associated a mutation in the *VHL* tumor suppressor gene, which is the hallmark of the hereditary disease Hippel-Lindau syndrome [86]. Chromophobe (chRCC) is the rarest subtype of RCC, accounting for ~5% of all RCC cases but is associated with interesting clinical and molecular characteristics [87, 88]. Despite often growing to a large size, chRCC tumors are relatively indolent, with a positive prognosis (10-year survival rate of 90%) unless the patient presents with metastasis [89, 90]. ChRCC tumors form in the distal nephron or intercalated cells of the distal tubule and are often associated with Birt-Hogg-Dube syndrome, caused by germline mutation in the *FLCN* gene [91-93], or Cowden syndrome which presents upon germline mutation of the *PTEN* gene [94]. Intriguingly, concurrent loss of heterozygosity of multiple chromosomes, including chromosome 1, 2, 6, 10, 13 and 17, is present in 86% of cases [87]. In addition, *TP53* is mutated in about 30% of chRCC cases [87].

Notably, ccRCC and chRCC have disparate responses to treatment. While immune checkpoint blockade (ICB) therapy has significantly increased survival of

ccRCC patients, chRCC patients are generally refractory to the treatment [95]. Combination therapy of ipilimumab (anti-PD-1) and nivolimumab (anti-CTLA-4) significantly increased overall survival compared to sunitinib (a receptor tyrosine kinase inhibitor) in a cohort of clear cell RCC patients in a phase III clinical trial, a success that has now become standard of treatment for many ccRCC patients [96-98]. The efficacy of ICB in non-clear cell patients is less established. An ongoing phase II clinical trial focused on evaluating non-clear cell RCC patient response to pembrolizumab (anti-PD-1) included 21 chRCC patients; 9.5% or about 2 patients saw improved overall survival, suggesting that only a minority of chRCC patients may benefit from ICB [99]. This distinct response to ICB therapy potentially underscores distinct mechanisms of tumor control.

Our work aimed to understand the classes of immune responses capable of tumor control that are present in ccRCC and chRCC tumors. Using single cell RNA-sequencing, flow cytometric analysis, and *in vitro* assays we profiled patient tumor tissue, adjacent normal kidney tissue and peripheral blood samples towards characterizing the cytotoxic lymphocyte repertoire. We show that ccRCC tumors have both a conventional, phenotypically exhausted PD-1^{+} $CD8^{+}$ T cell response and a cytotoxic tissue-resident $CD56^{bright}$ innate lymphocyte response while chRCC tumors are populated by only the latter.

2.2 Results

2.2.1 ccRCC, but not chRCC, tumors are abundantly infiltrated by $PD1^+CD8^+$ T cells

In an effort to characterize and probe the regulation of the cytotoxic immune cell repertoire within chRCC and ccRCC patients, we collected tumor tissue, normal adjacent kidney tissue and peripheral blood from drug treatment-naïve patients directly from the operating room to be utilized in various downstream assays (Fig. 2.1). First, to understand the heterogeneity of immune cells within the tumor tissue of chRCC and ccRCC patients, we performed single-cell RNA sequencing experiments on $CD45^+$ cells isolated from tumors. Pooled data revealed 10 major clusters defined by lineage marker plots (Fig. 2.2A-B) and differential gene analysis (Fig. 2.3). Of note, the overall abundance of the different immune cell clusters was markedly different between the two cancer subtypes (Fig. 2.2C).

We were particularly interested in investigating the cytotoxic lymphocyte response in these tumors and as such began our inquiry looking at $CD8^+$ T cells. Among the three $CD8^+$ T cell clusters defined by tSNE, cluster CD8_1 and clusters CD8_2A and 2B contained cells mostly from chRCC and ccRCC patients, respectively (Fig. 2.4A). Notably, cluster CD8_1 had a 'passenger' gene expression profile as exemplified by high expression of *S1PR5* and *KLF2* (Fig. 2.4B), molecules implicated in mediating cell egress into the blood and lymphatic system [100]. Clusters CD8_2A and 2B showed highly similar gene expression profiles and expressed exhaustion markers *PDCD1* and *TOX* (Fig. 2.4B and 2.3) but clustered separately based on differences in the expression

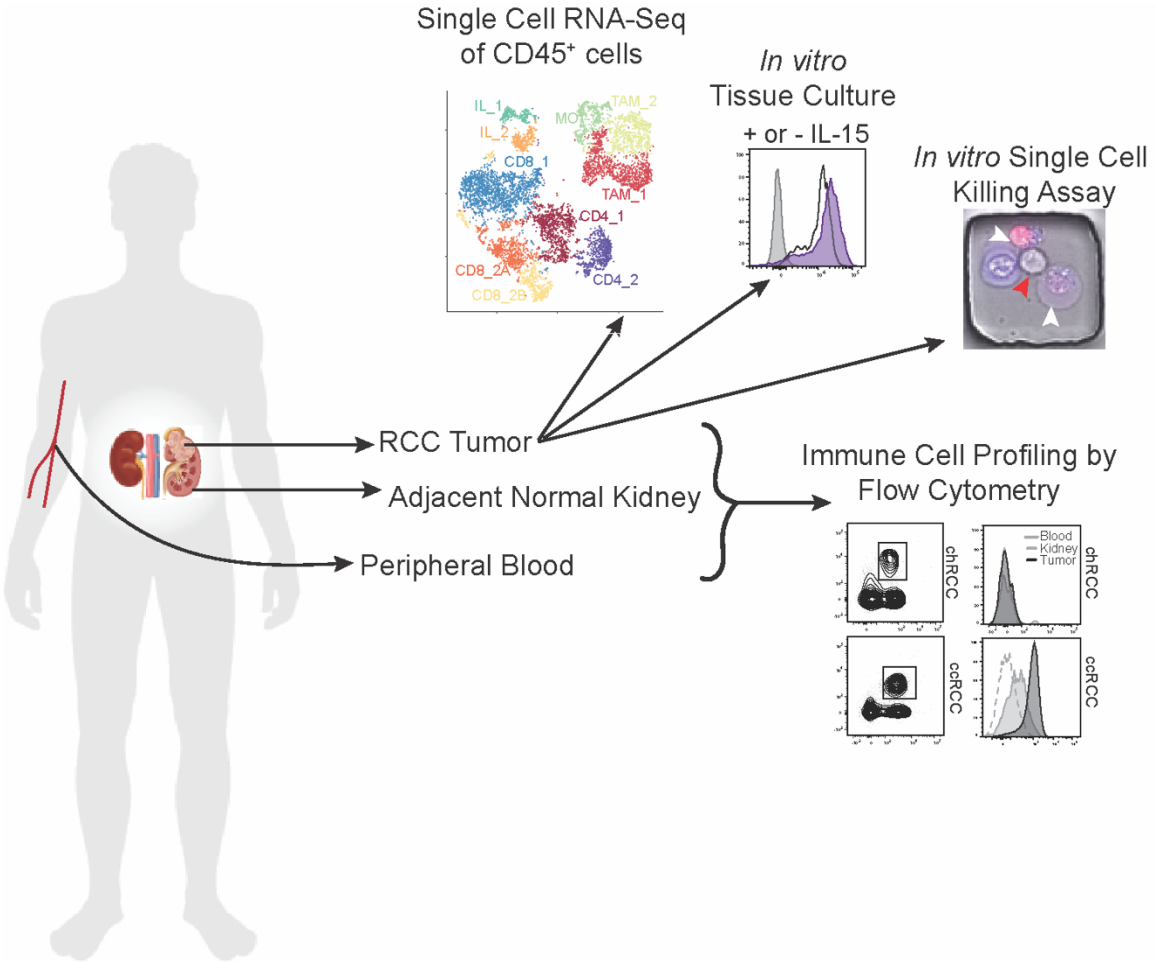

Figure 2.1 Schematic workflow of tissues collected from RCC patients and their designation for downstream applications

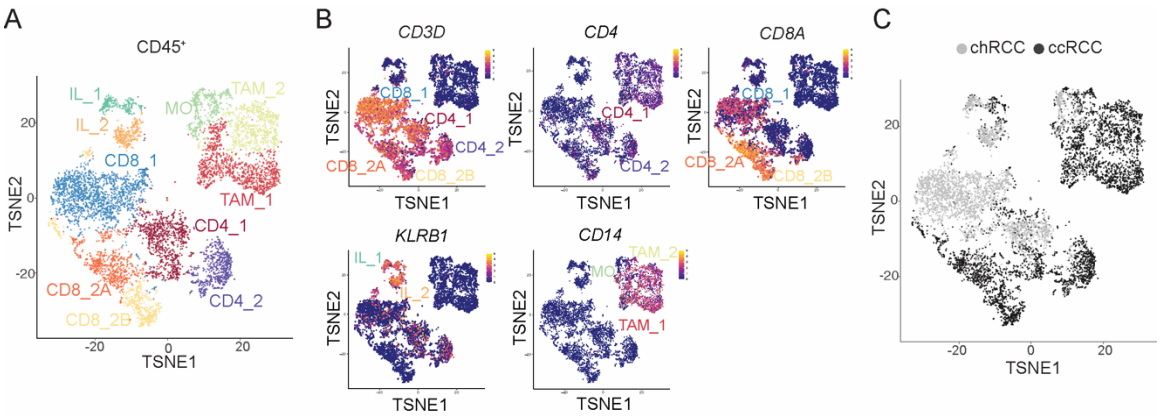

Figure 2.2 Single cell RNA sequencing analysis of CD45$^+$ immune cells in chRCC and ccRCC tumors

A. t-distributed Stochastic Neighbor Embedding (tSNE) embedding of transcriptional profiles from two RCC patient tumors, one chRCC and one ccRCC. Each dot represents a single CD45$^+$ cell, and colors represent clusters denoted by cell type inferred from lineage markers and differential gene expression. **B.** Marker plots showing normalized expression of selected common markers for lymphoid and myeloid populations (*CD3D* – T cells, *CD4* – CD4$^+$ T cells, *CD8A* – CD8a$^+$ T cells, *KLRB1* – innate lymphocytes, *CD14* – myeloid cells). **C.** tSNE plot as in **A**, colored by histology (chromophobe or clear cell).

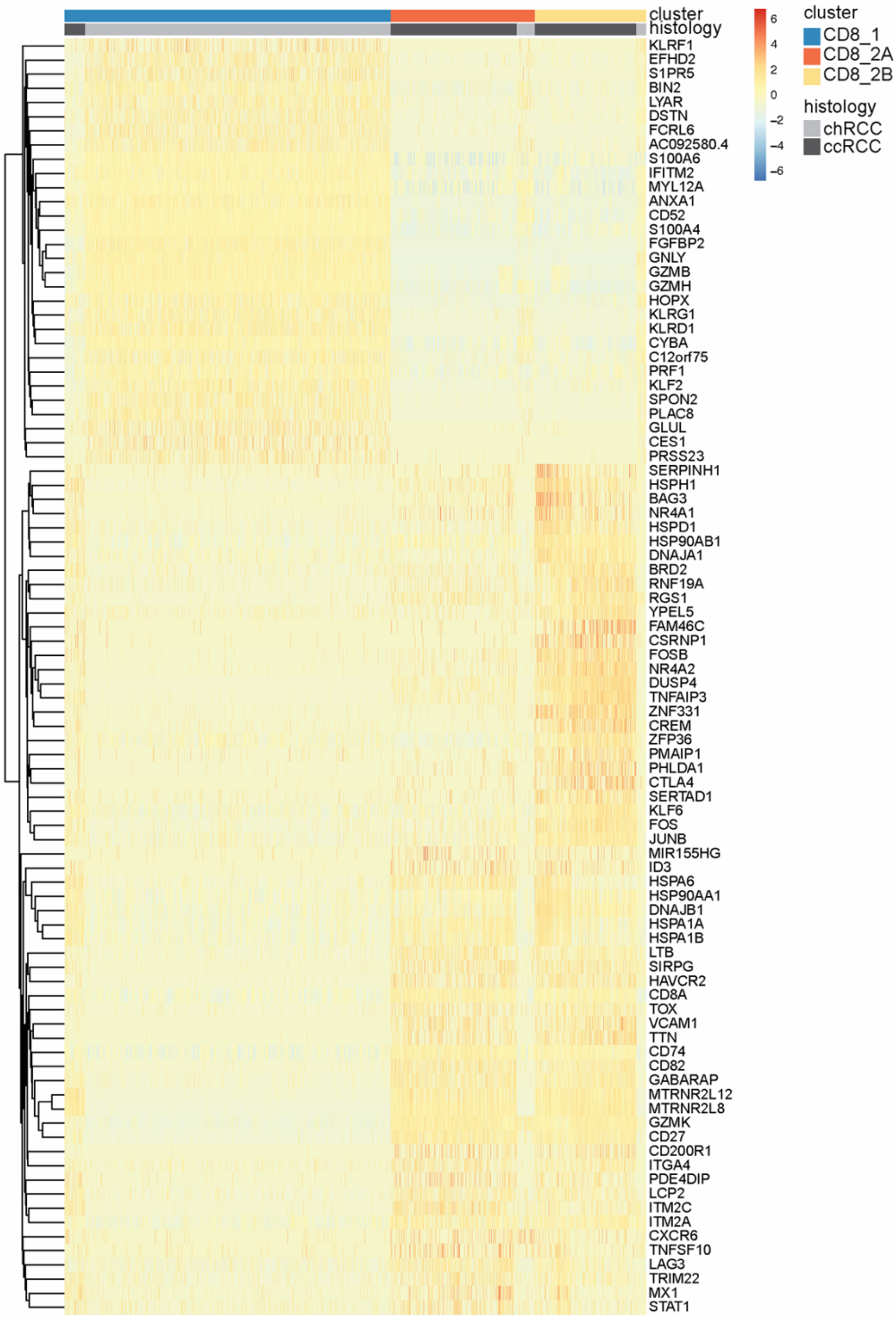

Figure 2.3 Phenotypically distinct CD8$^+$ T cells in chRCC and ccRCC

Heatmap of expression of the top 30 differentially expressed (FDR P <0.05) genes by log fold change across the three CD8$^+$ T cell clusters within the chRCC and ccRCC patients. Each column represents an individual cell.

of immediate early genes induced by T cell receptor signaling including *FOSB* and *NR4A1* (Fig. 2.4B and 2.3)

Upon uncovering these intriguing differences in $CD8^+$ T cell abundance and phenotype by single-cell RNA sequencing, we sought to substantiate these findings and as such performed flow cytometric analyses on an extensive cohort of RCC patient tumor, tumor-adjacent normal kidney and blood samples collected directly from the operating room. Across this patient cohort, we observed that ccRCC tumors had significantly more $CD8^+$ T cells compared to adjacent normal kidney and blood, reflecting either infiltration or expansion in the tumor (Fig. 2.5A). chRCC patients, however, had no significant difference in $CD8^+$ T cell abundance across tissues (Fig. 2.5A). In addition, quantification of PD-1 expression revealed that higher percentages of $CD8^+$ T cells from ccRCC tumors expressed PD-1 than their normal kidney and blood counterparts (Fig. 2.5B). With rare exception, chRCC $CD8^+$ T cells were practically PD-1-negative across tissues suggesting that like the $CD8^+$ T cells profiled by single-cell RNA sequencing in the chRCC patient, these cells were bystanders (Fig. 2.5B). Overall, these data suggest that contrary to ccRCC patients, chRCC patients generally do not have a conventional PD-1^+CD8^+ T cell response in tumors, revealing a potential mechanism for the failed response to anti-PD-1 therapy.

2.2.2 chRCC tumors are highly enriched for $CD56^{bright}CD49a^+CD103^+$ innate lymphocytes

In addition to three clusters of $CD8^+$ T cells, two clusters of group 1 innate lymphocytes defined by high expression of *KLRB1* were detected by single-cell RNA

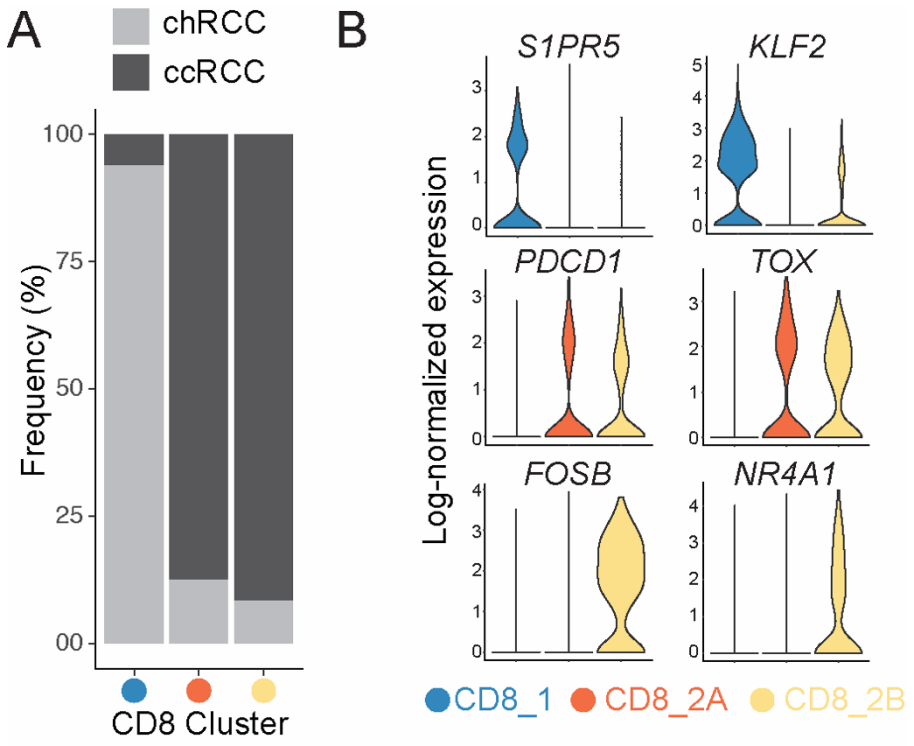

Figure 2.4 chRCC and ccRCC tumors have different abundances of phenotypically distinct CD8$^+$ T cells

A. For each CD8$^+$ cluster, the frequency out of all CD8$^+$ clusters at which it is found in chRCC and ccRCC tumors. **B.** Violin plots showing log-normalized expression of selected differentially expressed genes between the three CD8$^+$ clusters.

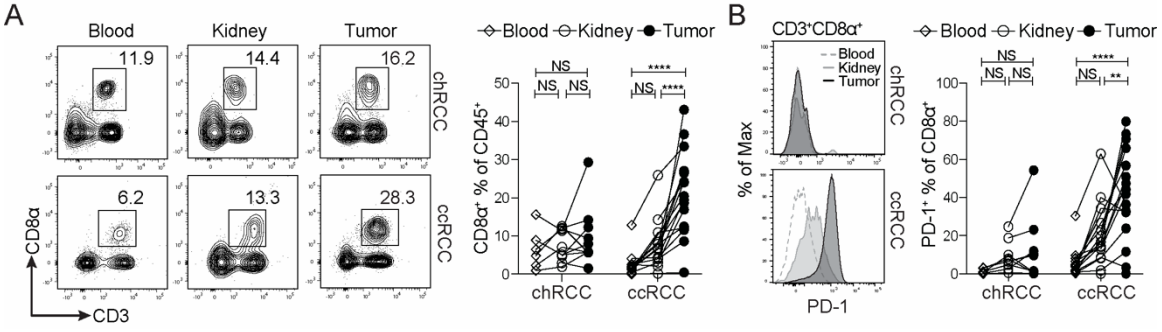

Figure 2.5 PD-1$^+$ CD8$^+$ T cells infiltrate ccRCC, but not chRCC, tumors

A. Representative plots of flow cytometric analysis of the percentage of CD3$^+$CD8$^+$ T cells out of the lymphocyte gate (CD45$^+$SSC^{Low}) in blood, adjacent normal kidney and tumor samples from one patient of the indicated histology. Quantification is CD3$^+$CD8$^+$ T cells out of total CD45$^+$ immune cells. **B.** Representative histograms of PD-1 expression in CD8$^+$ T cells from blood, adjacent normal kidney and tumor tissues from a single patient of the indicated histology. Quantification of flow cytometric analysis of percentage of total PD-1$^+$ CD8$^+$ T cells in blood, adjacent normal kidney and tumor samples from the indicated histology. **A, B.** Each pair of symbols connected by a line denotes an individual patient (chRCC n = 5-10, ccRCC n = 14-16). One-way ANOVA with Tukey's multiple comparison test was used for statistical analysis, NS = non-significant, **p<0.01, ***p<0.001, ****p<0.0001.

sequencing (Fig. 2.2). Both innate lymphocyte 1 (IL_1) and IL_2 clusters were present in each histology, but cluster IL_2 was more abundant in chRCC than ccRCC (Fig. 2.6A). Their phenotypes were distinct in terms of their expression of surface molecules, transcription factors and cytotoxic molecules. Cluster IL_1, like cluster CD8_1, had generally high expression of *S1PR5* and *KLF2* (Fig. 2.6B and 2.7). Additionally, this cluster had high expression of *CX3CR1* (Fig. 2.7), a chemokine receptor that supports leukocyte trafficking in the vasculature [101], together suggesting this population is predominantly circulating. Conversely, cluster IL_2 expressed high levels of *ITGA1*, encoding the CD49a integrin that promotes lymphocyte retention in epithelial niches [102], and *ZNF683*, the transcription factor HOBIT that regulates tissue-residency programs [75] (Fig. 2.6B and 2.7). Both clusters displayed potential for cytotoxicity but interestingly had differences in granzyme expression, such as *GZMH* and *GZMA* expressed in cluster IL_1 and cluster IL_2, respectively (Fig. 2.7). These data suggest that two distinct populations of innate lymphocytes with cytotoxic potential exist in RCC tumors – one predominantly circulating and the other tissue-resident.

To confirm these findings, we analyzed an extensive RCC patient cohort by flow cytometry, as performed for the $CD8^+$ T cell analysis. There was a significant increase in total $CD56^+$ innate lymphocytes in chRCC, but not ccRCC, tumors compared to adjacent normal kidney and blood (Fig. 2.8A) Based on the phenotypes uncovered by single-cell RNA sequencing regarding trafficking and localization, we probed the $CD56^+$ population for expression of the integrins CD49a as well as CD103, another commonly used marker of epithelial tissue retention [103], towards quantifying the tissue-resident and circulating

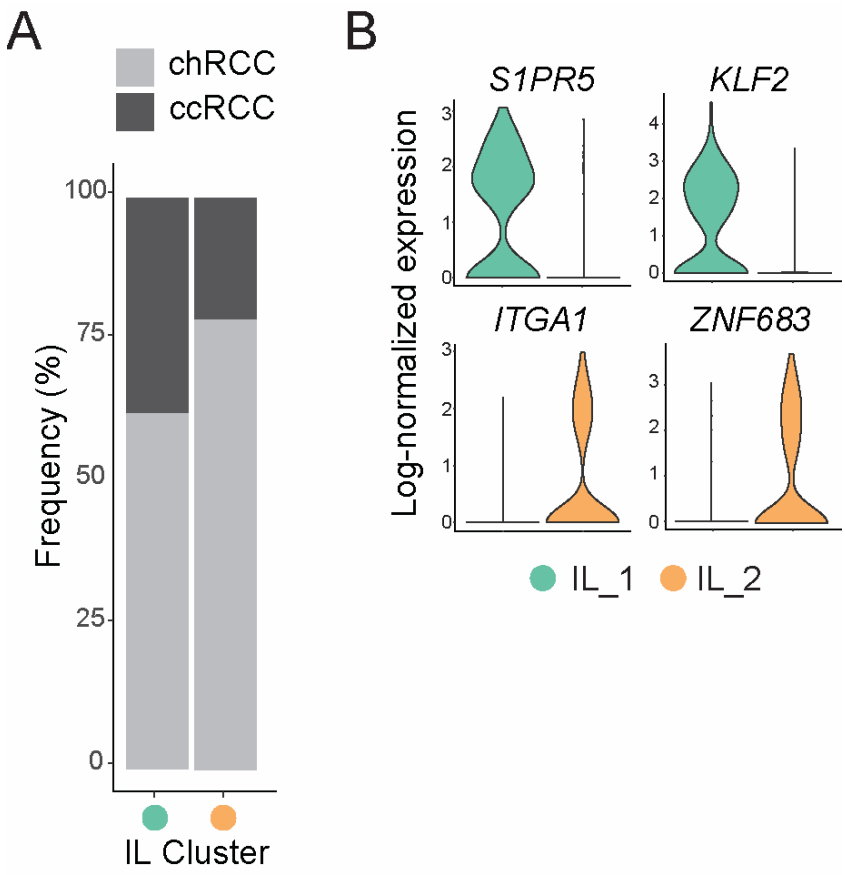

Figure 2.6 Two clusters of innate lymphocytes with distinct gene expression profiles infiltrate chRCC and ccRCC tumors

A. For each innate lymphocyte (*KLRB1*$^{+}$) cluster, the frequency out of all *KLRB1*$^{+}$ clusters at which it is found in chRCC and ccRCC tumors. **B.** Violin plots showing log-normalized expression of differentially expressed genes between the two innate lymphocyte clusters.

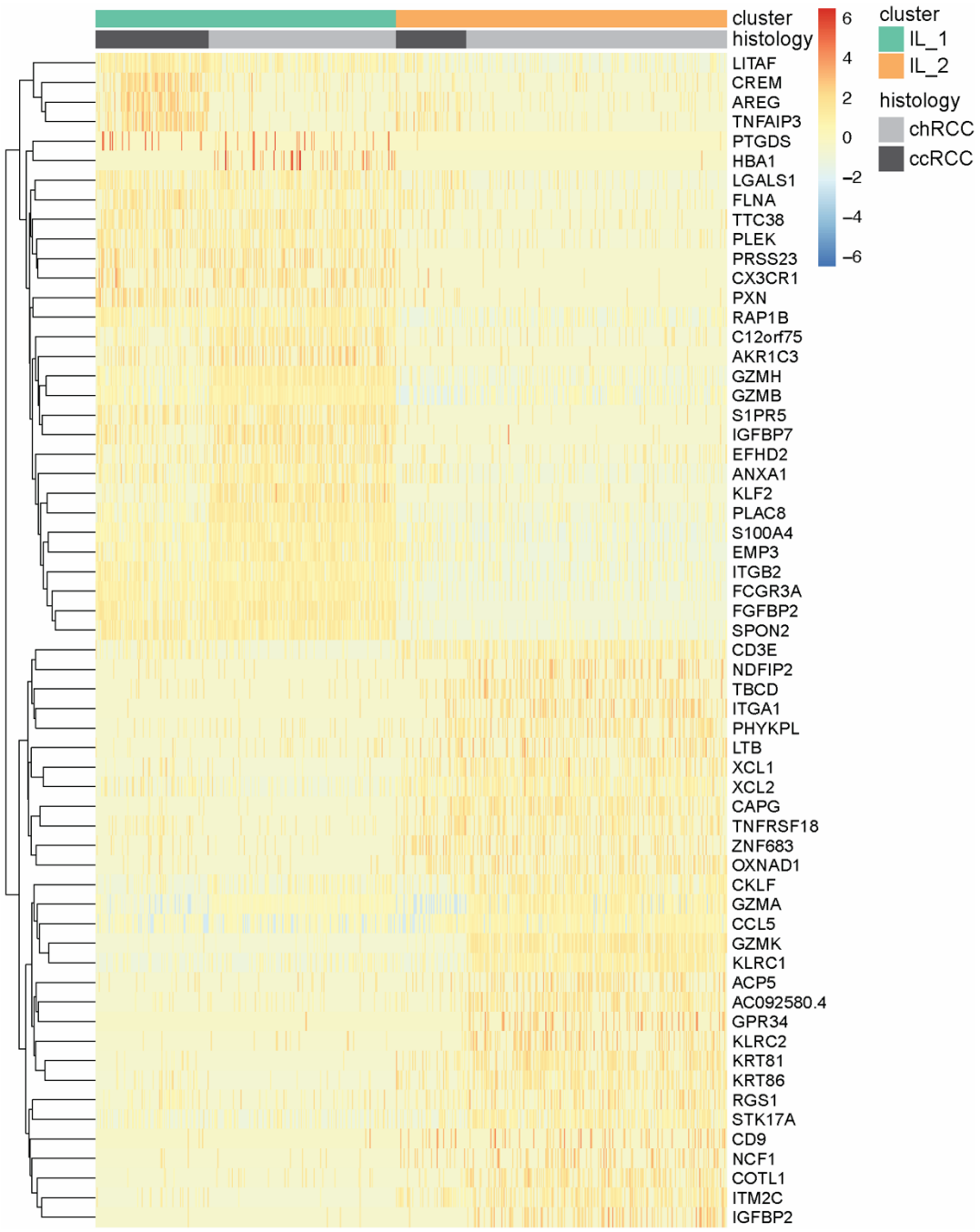

Figure 2.7 Two distinct subsets of innate lymphocytes in chRCC and ccRCC tumors

Heatmap of expression of the top 30 differentially expressed (FDR P <0.05) genes by log fold change across the two innate lymphocyte clusters in the chRCC and ccRCC patients. Each column represents an individual cell.

populations of innate lymphocytes in RCC tumors. As expected, the vast majority of $CD56^+$ cells in the blood and adjacent normal kidney were $CD49a^-CD103^-$ (Fig. 2.8B). There was a substantial increase in $CD49a^+CD103^+$ cells in tumor tissues of both histologies, however the magnitude of the response was significantly higher in chRCC compared to ccRCC (Fig. 2.8B). Immunofluorescence of chRCC tumors showed $CD103^+$ cells of lymphoid morphology in direct contact with E-Cadherin$^+$ cancer cells (Fig. 2.9). As $CD8^+$ T cells were of low abundance and $CD103^+$ expression on $CD8^+$ T cells virtually non-existent in chRCC tumors (data not shown), we can reasonably conclude these cells to be innate lymphocytes. Such localization highlights their tissue-residency and proximity to cancer cells in the tumor niche.

To further characterize these two innate lymphocyte populations in RCC tumors, we measured the level of CD56 expression in the $CD49a^-CD103^-$ and $CD49a^+CD103^+$ subsets and noted that the $CD49a^+CD103^+$ population consistently expressed higher levels of CD56 than the $CD49a^-CD103^-$ subset (Fig. 2.8C). CD16 is often used in conjunction with CD56 to describe stages of NK cell maturation. We noted that cluster IL_1 had higher expression of *FCGR3A* (encoding CD16) compared to cluster IL_2 (Fig. 2.10A). We therefore also probed the expression level of CD16 on $CD49a^-CD103^-$ and $CD49a^+CD103^+$ subsets from our flow cytometry cohort and noted that the $CD49a^-CD103^-$ population consistently expressed higher levels of CD16 than the $CD49a^-CD103^-$ subset (Fig. 2.10B). These differences could either reflect that the circulating and tissue-resident subsets have distinct levels of maturation along the same differentiation pathway or perhaps represent discrete innate lymphocyte populations.

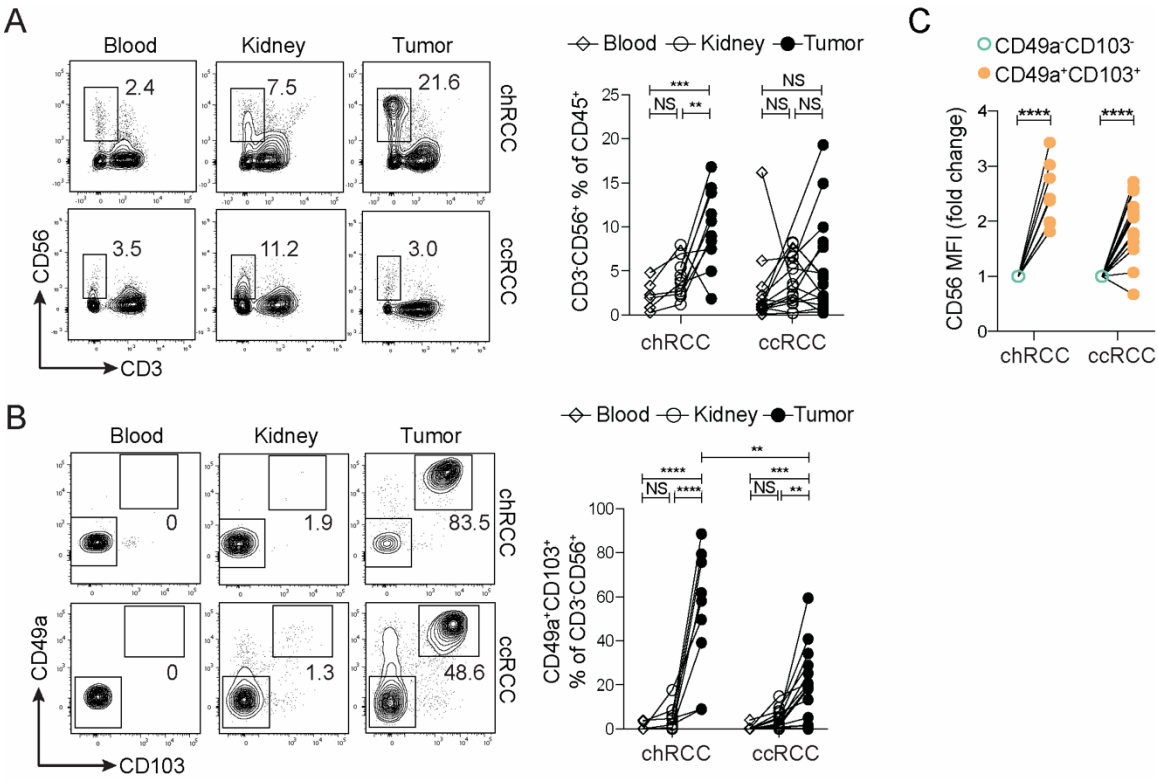

Figure 2.8 chRCC tumors are highly infiltrated by CD56^{bright} CD49a^{+}CD103^{+} innate lymphocytes

A. Representative plots of flow cytometric analysis of percentage of CD3^{-}CD56^{+} innate lymphocytes out of the lymphocyte gate (CD45^{+}SSC^{Low}) in blood, adjacent normal kidney and tumor samples from one patient of the indicated histology. Quantification is CD3^{-}CD56^{+} innate lymphocytes out of total CD45^{+} immune cells. **B.** Representative plots and quantification of CD49a and CD103 expression in CD3^{-}CD56^{+} innate lymphocytes from blood, adjacent normal kidney and tumor tissue from one patient of the indicated histology. **A, B.** Each pair of symbols connected by a line denotes an individual patient (chRCC n = 5-9, ccRCC n = 14-15). One-way ANOVA with Tukey's multiple comparison test was used for statistical analysis. Two-tailed unpaired t test was used to analyze significance of CD49a^{+}CD103^{+} abundance in chRCC versus ccRCC tumors. NS = non-significant, **p<0.01, ***p<0.001, ****p<0.0001. **C.** Fold change of CD56 MFI in CD49a^{+}CD103^{+} innate lymphocytes (orange) compared to CD49a^{-}CD103^{-} innate lymphocytes (green, set as 1) in the indicated histology. Each pair of symbols connected by a line denotes an individual patient. Two-tailed unpaired t test was used for statistical analysis, ****p<0.0001.

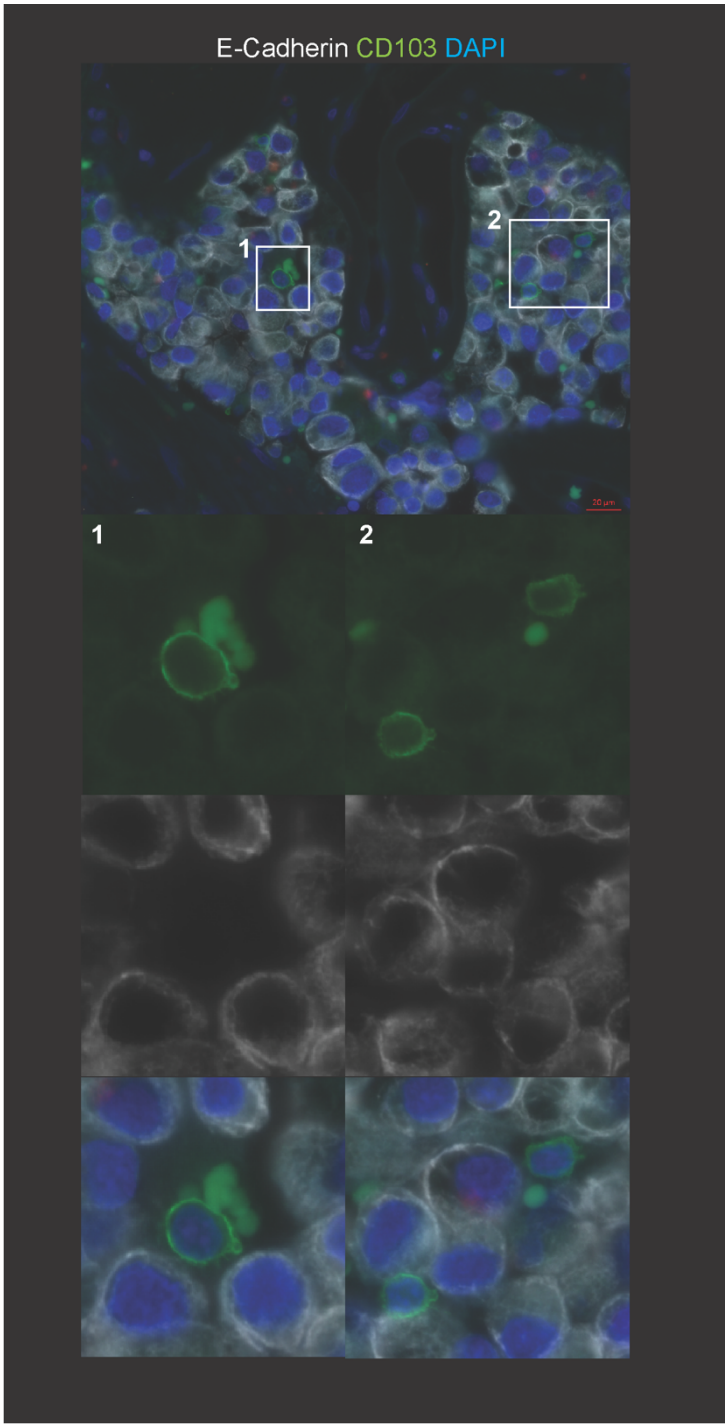

Figure 2.9 CD103^{+} innate lymphocytes are in direct contact with tumor cells

chRCC tumor tissue was stained with anti-CD103 (green), anti-ECadherin (white) and DAPI (blue). Scale bar = 20 mM.

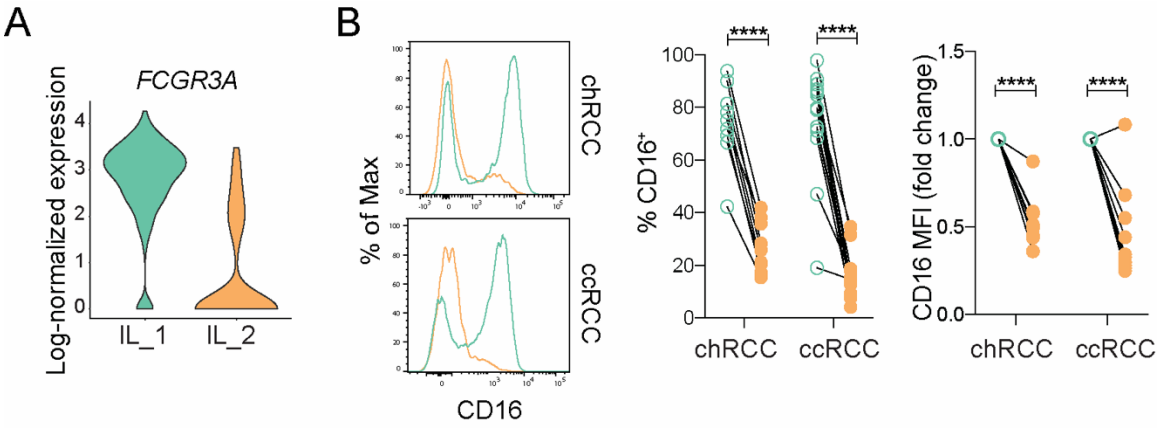

Figure 2.10 CD49a^{+}CD103^{+} and CD49a^{-}CD103^{-} innate lymphocytes are phenotypically distinct in terms of CD16 expression

A. Violin plot showing *FCGR3A* expression in the indicated clusters. **B.** (Left) Representative histograms of CD16 expression in CD49a^{-}CD103^{-} (green) and CD49a^{+}CD103^{+} (orange) CD3^{-}CD56^{+} innate lymphocytes from the same patient of the indicated histology. (Center) Quantification of CD16^{+} cells within the indicated cell type and histology. (Right) Relative MFI of CD16 in CD16^{+}CD49a^{+}CD103^{+} innate lymphocytes compared to CD16^{+}CD49a^{-}CD103^{-} (set as 1) in tumor samples. Each pair of symbols connected by a line denotes an individual patient. Two-tailed unpaired t test was used for statistical analysis, ***p<0.001, ****p<0.0001.

Overall, these findings reveal that the cytotoxic lymphocyte repertoire in chRCC tumors is characterized by induction of tissue-resident group 1 innate lymphocytes, with almost a complete lack of a conventional $CD8^+$ T cell response.

2.2.3 Tissue-resident innate lymphocyte response predicts better overall survival in chRCC

Thus far our data imply that ccRCC tumors have an antigen-experienced and exhausted $CD8^+$ T cell response as well as a population of tissue-resident innate lymphocytes with cytotoxic potential, while chRCC tumors are populated by only the latter. To explore the functional relevance of these tumor-elicited responses, we generated signatures of $CD8^+$ T cell and innate lymphocyte clusters discovered in our single cell analysis. Given the overall similarities of clusters CD8_2A and CD8_2B, we combined them into one cluster and performed pairwise differential gene expression (DEG) analysis relative to every other cluster retrieved from single-cell RNA sequencing experiments. The resulting gene set included genes significantly upregulated in CD8_2A and CD8_2B in every comparison, and included the exhaustion markers *PDCD1, LAG3 and TOX* (Fig. 2.11A). Application of the CD8_2 gene signature to the ccRCC and chRCC TCGA cohorts showed a negative association of enrichment of this signature and overall survival for both histologies (Fig. 2.11B), likely a reflection of an ineffectual $CD8^+$ T cell response that tracks with disease progression.

Similarly, we generated a signature for cluster IL_2, which included the tissue residency marker gene *ITGA1* (Fig. 2.12A). Interestingly, high expression of the IL_2 gene signature was associated with better and worse overall survival in chRCC and

ccRCC patients, respectively (Fig. 2.12B). Of note, all chRCC patients that fell in the top quartile for IL_2 expression had a 100% survival rate, suggesting the potential for a prognostic marker as well as a mechanism of effective tumor control.

The opposing predictive values of the IL_2 gene signature on ccRCC and chRCC patients' survival suggested phenotypic and functional heterogeneity of tissue-resident innate lymphocytes. One noticeable difference was the trend of higher CD56 expression in $CD49a^{+}CD103^{+}$ innate lymphocytes from chRCC patients than those from ccRCC patients (Fig. 2.8C). CD56 was recently reported to promote cytotoxicity in human NK cells [104]; however, CD56 was not a signature gene and thus it's activity is unlikely to explain the histology-specific prognosis of the IL_2 gene signature.

A potentially functional IL_2 signature gene was *GZMA* (Fig. 2.12A), which encodes a cytotoxic molecule involved in lytic granule-mediated noncanonical apoptosis and pyroptosis [105, 106]. Of note, *GZMA* was among the least enriched signature genes in cluster IL_2 compared to cluster IL_1 (Fig. 2.12A), suggesting that its expression could be dynamically regulated in the tumor environment. Examination of granzyme A protein among a cohort of chRCC and ccRCC patients revealed that $CD49a^{+}CD103^{+}$ innate lymphocytes consistently expressed more granzyme A than matched $CD49a^{-}CD103^{-}$ counterparts, but only in chRCC tumors (Fig. 2.13A).

In fact, the $CD49a^{+}CD103^{+}$ subset had lower granzyme A expression than the $CD49a^{-}CD103^{-}$ subset in ccRCC tumors (Fig. 2.13A). In addition, $CD49a^{+}CD103^{+}$ innate lymphocytes from tumor tissue expressed higher levels of granzyme A than cells from adjacent normal kidney, again only in chRCC tumors (Fig. 2.13B). Thus, despite induction of $CD49a^{+}CD103^{+}$ tissue-resident innate lymphocytes in both chRCC and

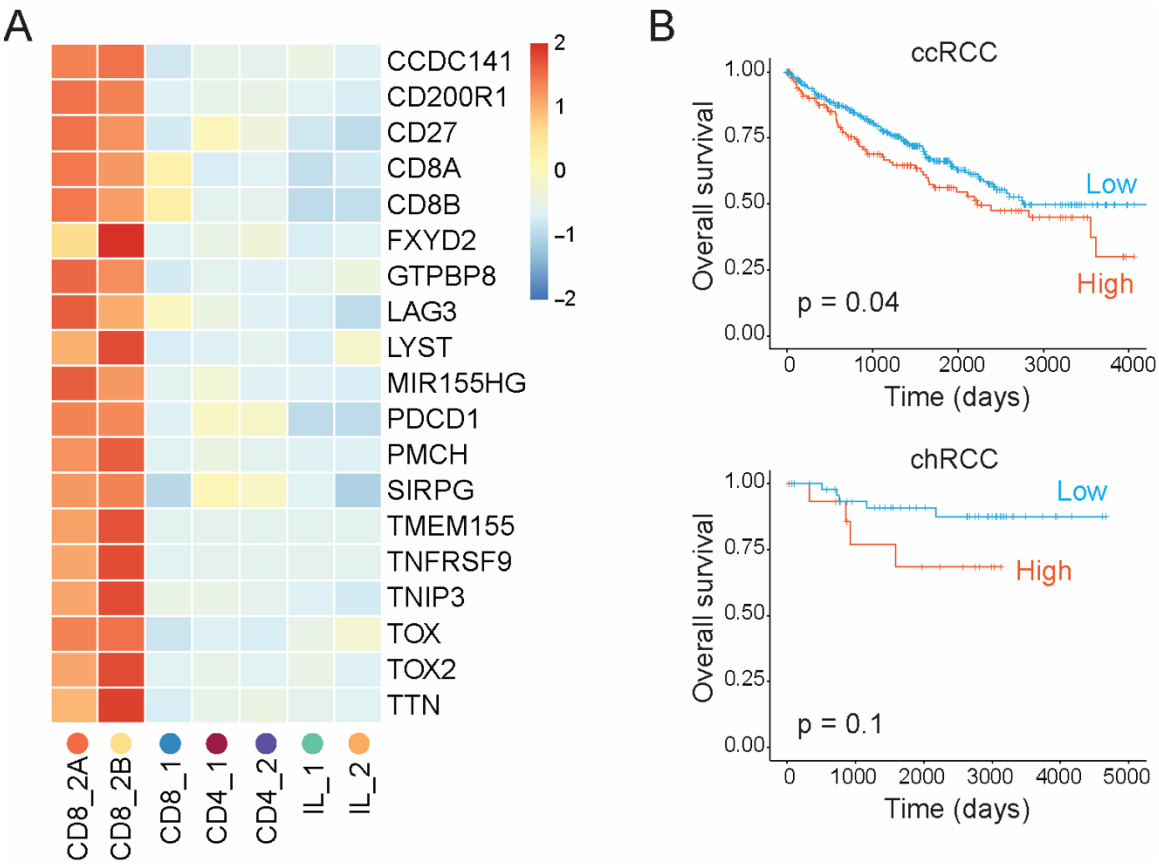

Figure 2.11 Enrichment of CD8_2 signature predicts worse overall survival in ccRCC

A. Heatmap showing enrichment of the CD8_2 signature genes in the indicated clusters. **B.** Survival analysis demonstrating association of the CD8_2 signature across the TCGA ccRCC (top) and chRCC (bottom) cohorts. High represents the top quartile of the distribution of signature scores, low represents the bottom 3 quartiles. Statistical p values calculated using Spearman's correlation.

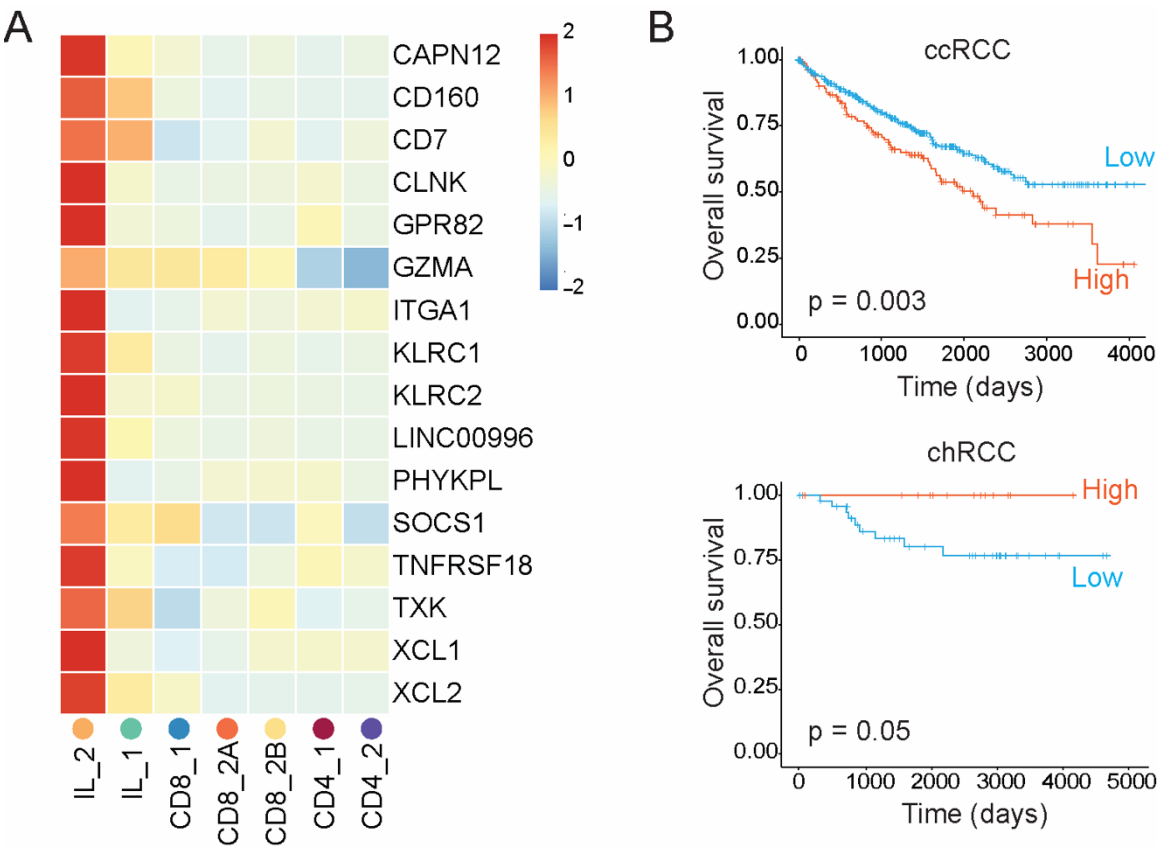

Figure 2.12 Enrichment of IL_2 signature predicts better overall survival in chRCC

A. Heatmap showing enrichment of the IL_2 signature genes in the indicated clusters. **B.** Survival analysis demonstrating association of the IL_2 signature across the TCGA ccRCC (top) and chRCC (bottom) cohorts. High represents the top quartile of the distribution of signature scores, low represents the bottom 3 quartiles. Statistical p values calculated using Spearman's correlation.

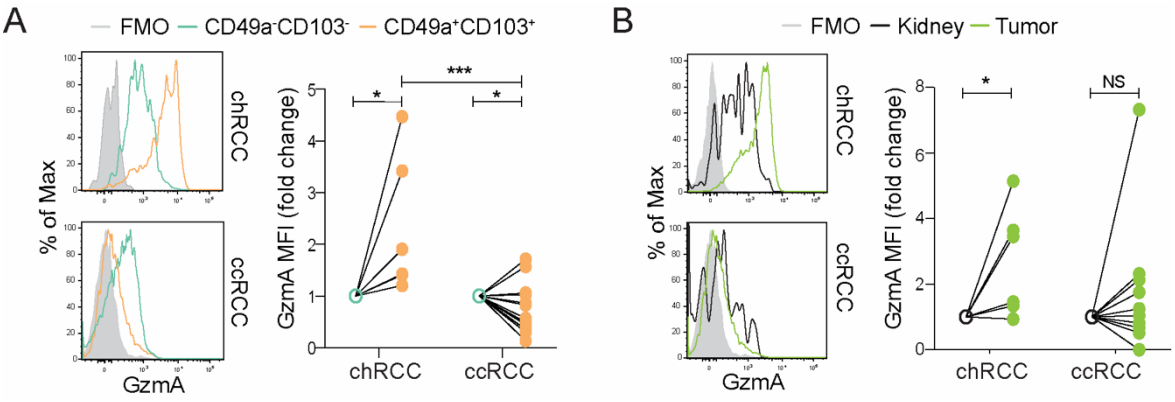

Figure 2.13 CD49a$^+$CD103$^+$ express higher granzyme A than CD49a$^-$CD103$^-$ innate lymphocytes, GzmA expression is specifically induced in chRCC tumors

A. (Left) Representative histograms of granzyme A expression in CD49a$^-$CD103$^-$ (green) and CD49a$^+$CD103$^+$ (orange) CD3$^-$CD56$^+$ innate lymphocytes from the same patient of the indicated histology. FMO = fluorescence minus one control. (Right) Relative mean fluorescence intensity (MFI) of granzyme A in CD49a$^+$CD103$^+$ innate lymphocytes compared to CD49a$^-$CD103$^-$ (set as 1) in tumor samples. **B.** (Left) Representative histograms of granzyme A expression in CD49a$^+$CD103$^+$ innate lymphocytes in adjacent normal kidney (black) and tumor (green) of the same patient of the indicated histology. (Right) Relative MFI of granzyme A in CD49a$^+$CD103$^+$ innate lymphocytes in tumor (green) compared to adjacent normal kidney (black, set as 1) of the same patient of the indicated histology.

ccRCC tumors, they exhibit disparate patterns of granzyme A expression, which likely accounts for histology-specific prognosis of the IL_2 gene signature.

2.2.4 Signaling through the inhibitory receptor NKG2A does not regulate tissue-resident innate lymphocyte function

We next wished to define how tissue-resident innate lymphocyte responses were differentially regulated in RCC tumors. Inhibitory signaling through NKG2A interaction with HLA-E acts as a checkpoint to dampen NK cell activation [31]. Cluster IL_2 was enriched for *KLRC1* transcripts, which encodes for NKG2A (Fig. 2.14A). Flow cytometry experiments revealed that compared to $CD49a^{-}CD103^{-}$ innate lymphocytes, $CD49a^{+}CD103^{+}$ innate lymphocytes had a higher fraction of cells expressing NKG2A as well as higher levels of protein expression within the $NKG2A^{+}$ subset (Fig. 2.14B) and was also an IL_2 signature gene (Fig. 2.12A). We wondered if signaling via this pathway may explain the differential prognosis between ccRCC and chRCC and hypothesized that perhaps tissue-resident innate lymphocytes from ccRCC tumors expressed higher levels of NKG2A compared to chRCC tumors. However, both chRCC and ccRCC tumors displayed similar enrichment of NKG2A among the $CD49a^{+}CD103^{+}$ and $CD49a^{-}CD103^{-}$ subsets of innate lymphocytes, respectively (Fig. 2.14B), implying that differential histology-associated responses are unlikely caused by differential expression of this receptor.

To probe the functional consequence of NKG2A signaling further, we plotted expression of its ligand, HLA-E, within the chRCC TCGA cohort against the IL_2 signature but saw no significant correlation, suggesting that level of HLA-E expression

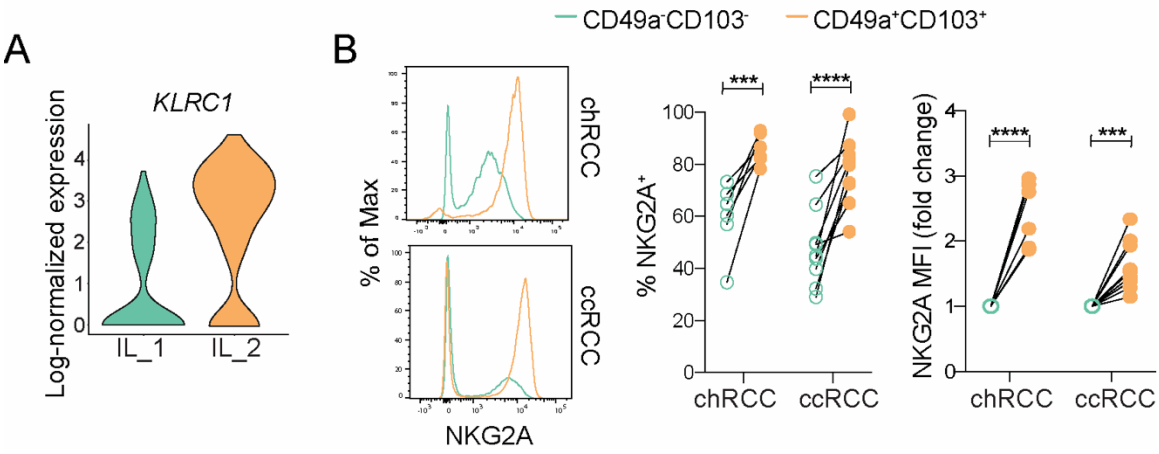

Figure 2.14 CD49a$^+$CD103$^+$ and CD49a$^-$CD103$^-$ innate lymphocytes are phenotypically distinct in terms of expression of NKG2

A. Violin plot showing *KLRC1* expression in the indicated clusters. **B.** (Left) Representative histograms of NKG2A expression in CD49a$^-$CD103$^-$ (green) and CD49a$^+$CD103$^+$ (orange) CD3$^-$CD56$^+$ innate lymphocytes from the same patient of the indicated histology. (Center) Quantification of NKG2A$^+$ cells within the indicated cell type and histology. (Right) Relative MFI of NKG2A in NKG2A$^+$CD49a$^+$CD103$^+$ innate lymphocytes compared to NKG2A$^+$CD49a$^-$CD103$^-$ (set as 1) in tumor samples. Each pair of symbols connected by a line denotes an individual patient.

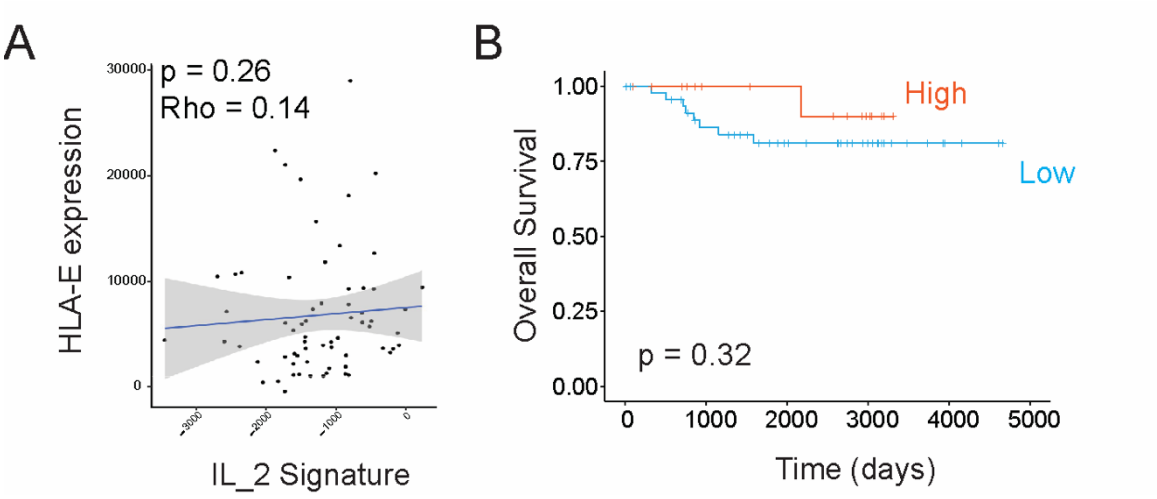

Figure 2.15 HLA-E expression does not correlate with IL_2 signature or patient outcome in chRCC

A. Correlation between level of HLA-E expression and IL_2 signature in chRCC cases from the TCGA database. **B.** Association of HLA-E expression and overall survival across the TCGA chRCC cohort. High represents the top quartile and low represents the bottom 3 quartiles of HLA-E expression level. Statistical p values calculated using Spearman's correlation.

does not influence the enrichment of the IL_2 signature (Fig. 2.15A). Moreover, there was no association between the level of HLA-E expression and overall survival in the TCGA chRCC cohort (Fig. 2.15B). Therefore, inhibitory signaling through the NKG2A/HLA-E axis is likely inconsequential to tissue-resident innate lymphocyte function in chRCC tumors.

2.2.5 IL-15 is a crucial regulator of tissue-resident innate lymphocyte phenotype and function

The cytokine IL-15 in complex with IL-15 receptor α chain (IL-15Rα) promotes the development, maintenance and effector function of lymphocytes with cytotoxic potential [56, 57, 107]. Previous studies have shown that brief priming with IL-15 markedly enhances the antitumor response of $CD56^{bright}$ NK cells isolated from blood [108]. As $CD49a^{+}CD103^{+}$ innate lymphocytes from RCC tumors phenotypically resembled $CD56^{bright}$ NK cells (Fig. 2.8C), we explored whether IL-15 played a role in their regulation. Indeed, clusters IL_1 and IL_2 both showed high expression of *IL2Rß* (Fig. 2.16A), encoding the shared signaling IL-2/IL-15 receptor α chain. Notably, chRCC tumors from the TCGA cohort had substantially higher expression of *IL15* transcripts than ccRCC tumors (Fig. 2.16B), implying that IL-15 in the tumor microenvironment may regulate tissue-resident innate lymphocyte responses in a dose-dependent manner.

To explore the potential role of IL-15 in control of $CD49a^{+}CD103^{+}$ innate lymphocytes, we isolated these cells from RCC tumors and cultured them with two different doses of IL-15/IL-15Rα complex, 10 and 100 ng/ml, both of which maintained survival of the cells (data not shown). The higher dose of IL-15/IL-15Rα complex

induced greater expression of CD56 and granzyme A (Fig. 2.17A-B), two proteins enriched in chRCC innate lymphocytes. In addition, the higher dose of IL-15/IL-15Rα substantially enhanced the cytotoxicity of $CD49a^{+}CD103^{+}$ innate lymphocytes against target cells in a single cell killing assay (Fig. 2.17C). Of note, there was a positive correlation of level of IL-15 expression and enrichment of the IL_2 signature across the chRCC TCGA patient cohort (Fig. 2.18A). Moreover, patients with higher expression of IL-15 trended towards better overall survival than patients with lower expression (Fig. 2.18B). Collectively, these findings demonstrate that IL-15 regulates the cytotoxic program of tissue-resident innate lymphocytes and enhances their ability to kill target cells in a dose-dependent manner, which may represent a critical mechanism for tumor control in chRCC patients.

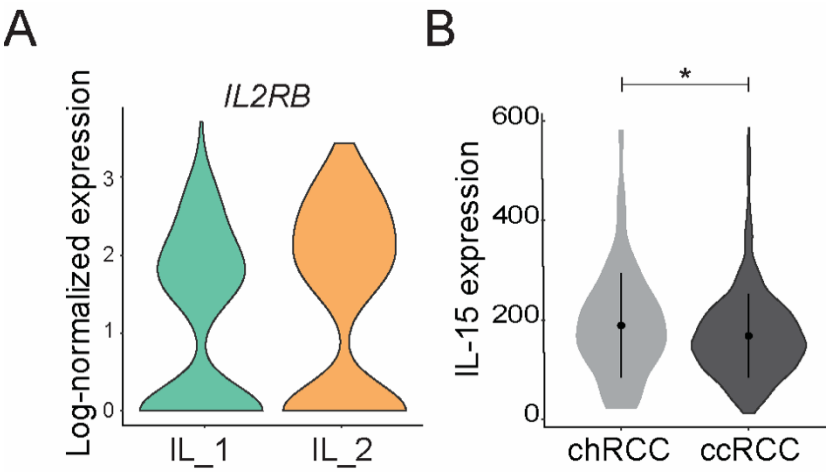

Figure 2.16 Clusters IL_1 and IL_2 express *IL2Rb*, IL-15 expression is higher in chRCC tumors compared to ccRCC tumors within TCGA

A. Violin plot showing log-normalized expression of *IL2Rß* in the indicated innate lymphocyte clusters. **B.** Box plot showing level of IL-15 expression across chRCC and ccRCC patients in the TCGA cohort. One-sided Wilcoxon was used for statistical analysis, *p<0.05.

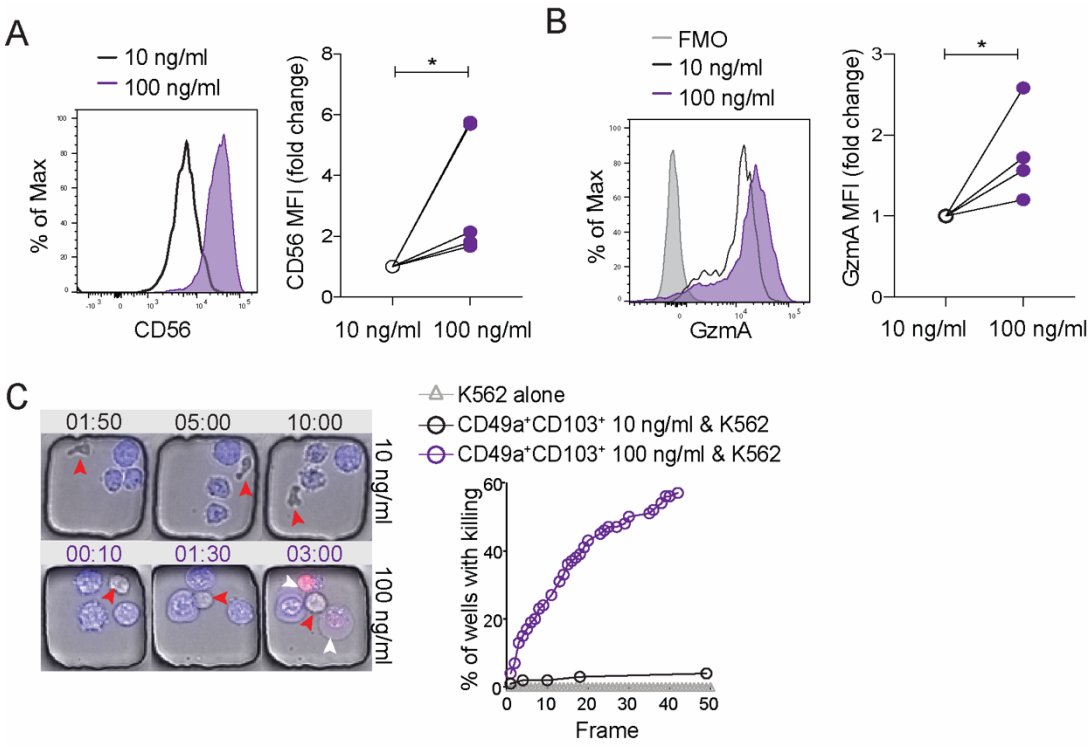

Figure 2.17 IL-15 governs the effector function of CD49a$^+$CD103$^+$ innate lymphocyte

A. (Left) Representative histograms of CD56 expression in CD49a$^+$CD103$^+$ innate lymphocytes treated with the indicated level of IL-15/IL-15Rα complex. (Right) Relative MFI of CD56 in CD49a$^+$CD103$^+$ innate lymphocytes isolated from tumors treated with 100 ng/mL IL-15/IL-15Rα complex compared to 10 ng/mL IL-15/IL-15Rα complex (set as 1). Each pair of symbols connected by a line denotes cells isolated from an individual patient (n = 4). Two-tailed unpaired t test was used for statistical analysis, *p<0.05.**B.** (Left) CD49a$^+$CD103$^+$ innate lymphocytes were sorted from RCC tumors and cultured in the indicated concentrations of IL-15/IL-15Rα complex and analyzed by flow cytometry for granzyme A expression. Plot is representative of 4 independent experiments. (Right) Fold change of granzyme A MFI of CD49a$^+$CD103$^+$ innate lymphocytes cultured with 100 ng/ml versus 10 ng/ml (set as 1) of IL-15/IL-15Rα complex. Each pair of symbols denotes cells isolated from an individual patient (n = 4). Two-tailed unpaired t test was used for statistical analysis, *p<0.05. **C.** CD49a$^+$CD103$^+$ innate lymphocytes were sorted and cultured either with 10 ng/ml or 100 ng/ml of IL-15/IL-15Rα complex and subject to single cell killing assays (See methods). (Left) Representative still images from the imaging time course. Times are in format of hour:minute. Blue cells are cell trace violet (CTV)-stained K562 target cells. Red arrows indicate CD49a$^+$CD103$^+$ effector cells and white arrows indicate a dead (propidium iodide, PI$^+$) K562 target cell. (Right) The plot shows the percentage of wells with target cell killing events out of total wells containing both target and innate lymphocyte effector cells over time. Plot is representative of 3 independent experiments.

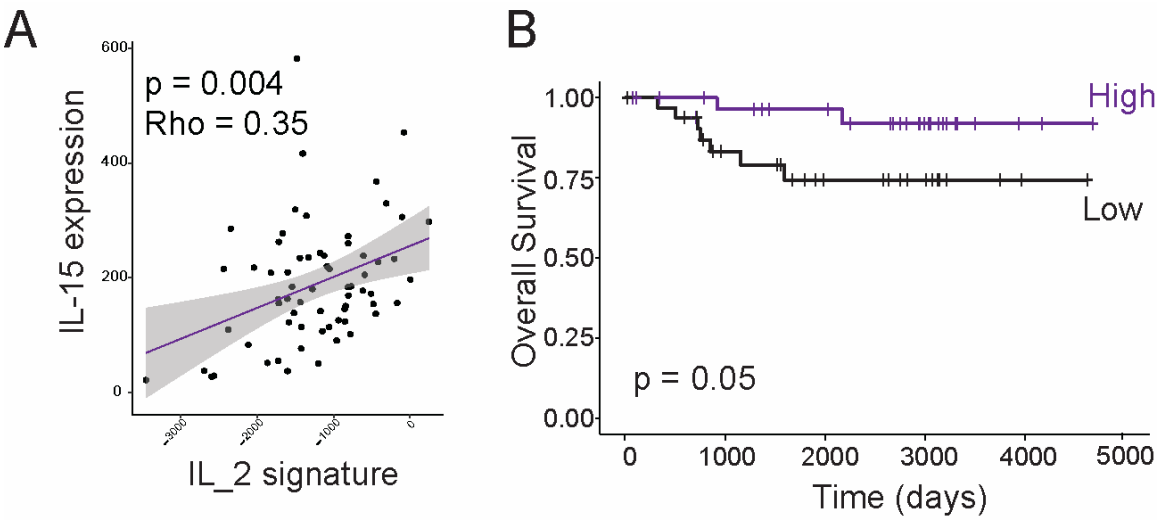

Figure 2.18 IL-15 expression correlates with IL_2 signature and overall survival in chRCC patients from the TCGA cohort

A. Correlation between level of IL-15 expression and IL_2 signature in chRCC cases from the TCGA database. **B.** Association of IL-15 expression and overall survival across the TCGA chRCC cohort. High represents the top quartile and low represents the bottom 3 quartiles of IL-15 expression level. P values calculated using Spearman's correlation.

2.3 Discussion

Renal cell carcinoma is a complex disease comprising multiple subtypes with unique clinical features, cellular origins, molecular characteristics and outcomes. In this study, we performed an in-depth comparative analysis of the immune cell repertoire of clear cell and chromophobe RCC. Using single cell RNA sequencing and extensive flow cytometry, we found that while antigen-experienced phenotypically exhausted $CD8^+$ T cells accumulated selectively in ccRCC tumors, tissue-resident group 1 innate lymphocytes were induced in both ccRCC and chRCC tumors (Fig. 2.19). We show that across the patient cohort analyzed, clear cell RCC tumors have a substantial infiltration of $CD8^+$ T cells compared to adjacent normal kidney and blood, with a significant increase in PD-1 expression. However, there was considerable variation in the abundance of $CD8^+$ T cells and amount of PD-1 expression between ccRCC patients. Currently, the response to immunotherapy in ccRCC patients in terms of overall survival after 2.5 years is ~50% with combination therapy [24]. Our data suggests that there is a correlation between the magnitude of PD-1^+ $CD8^+$ T cell responses and responsiveness to checkpoint blockade, partial or non-responders perhaps being patients with mid to low range abundance of PD-1^+CD8^+ T cells. Chromophobe RCC tumors, on the other hand, generally have a minimal $CD8^+$ T cell response with no difference in abundance compared to adjacent normal kidney and blood and virtually no checkpoint receptor expression, suggesting a potential mechanism for the overall unsuccess of checkpoint blockade in chRCC.

Intriguingly, we found that the major relevant cytotoxic lymphocyte population in chRCC tumors were $CD49a^+CD103^+$ $CD56^{bright}$ innate lymphocytes (Fig. 2.19). This response could effectively restrain chRCC, but not ccRCC, cancer progression. Previous

studies of group 1 innate lymphocytes in RCC have been limited to the ccRCC subtype with no clear ramification on patient outcome [109-111]. In addition, although $CD56^{bright}CD49a^{+}CD103^{+}$ innate lymphocytes have been found in human colorectal and lung tumors, their role in modulating cancer progression is unclear [112]. Thus, our findings are the first to reveal a tumor suppressor function of tissue-resident group 1 innate lymphocytes in human cancer.

A common molecular characteristic present in >93% of chRCC cases is loss of chromosomes 2, 6, 10, 13, 17, 21 [87]. The HLA locus is located on the short arm of chromosome 6, meaning that the vast majority of chRCC cases do not have HLA class I molecules that would inhibit NK cell activity through inhibitory receptors. Along with potentially explaining why chRCC tumors do not have an antigen-experienced $CD8^{+}$ T cell response, loss of HLA class I molecules suggests that high expression of NKG2A, the inhibitory receptor that interacts with HLA-E, on $CD49a^{+}CD103^{+}$ innate lymphocytes is not functional in the sense that an NK cell response will not be dampened by interaction of NKG2A and HLA-E. Interestingly, the level of NKG2A expression was similar on $CD49a^{+}CD103^{+}$ innate lymphocytes from chRCC and ccRCC tumors, suggesting that inhibition through this receptor is unlikely to account for the differential histology-specific survival prediction outcomes.

The differential prediction outcomes of the tissue-resident innate lymphocyte signature on ccRCC and chRCC tumors imply tumor-type specific regulation. Of note, compared to tissue-resident innate lymphocytes from adjacent normal kidney, granzyme A expression was specifically induced in $CD56^{bright}CD49a^{+}CD103^{+}$ innate lymphocytes from chRCC, but not ccRCC, tumors. These findings imply that the cytotoxic potential of

tissue-resident group 1 innate lymphocytes is a critical determinant of their anti-tumor function, which is in agreement with our previous report of the cytolytic granule-mediated cancer immunosurveillance function of tissue-resident innate lymphocytes in transgenic models of murine epithelial cancers [14]. Notably, in a carcinogen-induced murine fibrosarcoma model, constitutive activation of TGF-ß signaling promotes the generation of tissue-resident group 1 innate lymphocytes, causing accelerated cancer progression as a likely consequence of increased production of pro-angiogenic molecules [113]. Thus, heterogeneous or even opposing functional programs can be elicited by tissue-resident innate lymphocytes in tumors. It remains to be determined whether negative prognosis of the tissue-resident innate lymphocyte signature on ccRCC patients reflects a pro-tumor function as suggested by a recent study [114]. Alternatively, the innate lymphocyte response may be inconsequential, and the adverse association is simply because it tracks with disease progression.

An important regulator of the cancer immunosurveillance function of tissue-resident innate lymphocytes was IL-15 expressed in the chRCC tumor tissue. *In vitro* cell culture experiments showed that IL-15 promoted the cytotoxic activities of tissue-resident innate lymphocytes in a dose-dependent manner. IL-15 promoted expression of granzyme A and CD56, two markers enriched in $CD49a^{+}CD103^{+}$ innate lymphocytes from chRCC tumors, as well as their cytotoxic activities against cancer cells (Fig. 2.19). In the TCGA chRCC patient cohort, IL-15 expression was positively associated with the tissue-resident innate lymphocyte signature and stratified patients for survival probability. While both ccRCC and chRCC had increased abundance of $CD49a^{+}CD103^{+}$ innate lymphocytes compared to normal kidney and blood, expression of IL-15 trended higher in chRCC

tumors compared to ccRCC tumors. Prominent infiltration of antigen-experienced phenotypically exhausted $CD8^+$ T cells that express high levels of the IL-15 receptor complex might also compete with innate lymphocytes for IL-15 in ccRCC tumors.

Together, these data imply that there is a mechanism of quantitative sensing for IL-15 in which low levels may allow for expansion of tissue-resident innate lymphocytes, as in the case of ccRCC, but high levels are required for the activation and induction of a cytotoxic effector program with potential functional impact on tumor control as observed for chRCC.

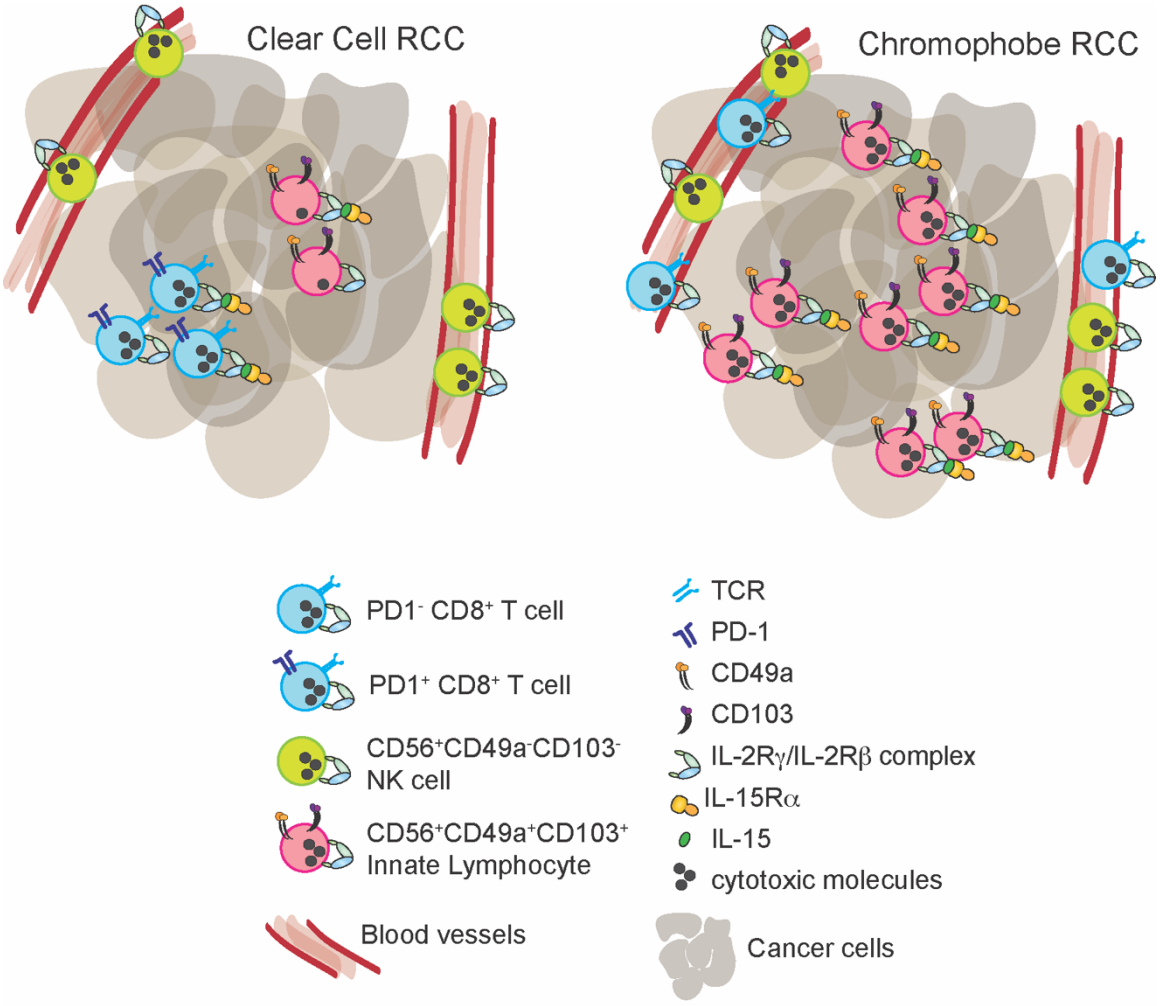

Figure 2.19 Model of tumor-elicited immune responses in ccRCC and chRCC

2.4 Experimental Procedures

Human subjects and tissue collection

All research activities were preapproved by the Institutional Ethics Review Board at Memorial Sloan Kettering Cancer Center and individuals were required to provide written informed consent to participate in the study. All histological diagnoses were confirmed by expert genitourinary pathologists. After institutional review board approval and patient consent, blood samples were collected in cellular preparation tubes (CPT) just prior to surgery. Tumor and adjacent normal kidney samples were directly obtained from the operating room during nephrectomy. Tissue samples were placed in separate labeled containers containing Roswell Park Memorial Institute (RPMI) medium and transported in regular ice to the laboratory. The CPTs were transported at room temperature. Overall transit time in all cases was less than 1 hour (from specimen extraction to cell dissociation) and the tissue samples were kept in this medium at all times. The cohort of ccRCC patients from which tissues were analyzed were 73.3% male, mean age 58.6, median age 58. The cohort of chRCC patients from which tissues were analyzed were 40% male, mean age 53.7, median age 58. For single-cell RNA sequencing, only tumor tissue was collected. The ccRCC patient was a 57-year-old female with stage IV disease and was treatment-naïve at the time of sample collection. The chRCC patient was an 84-year-old female with stage I disease and was treatment-naïve at the time of sample collection.

Immune cell isolation from human and mouse tissues

Human blood was transferred from CPT tubes to 50 ml conical tubes containing red blood cell (Ammonium-Chloride-Potassium, ACK) lysis buffer and incubated for 10 minutes at room temperature. Tubes were spun at 2,400 RPM for 3 minutes, pellets were resuspended in FACS buffer (1x PBS with 1% FBS, 2mM EDTA and 0.02% sodium azide) and stored on ice until staining procedure. Human tumor and adjacent normal kidney tissues were prepared by mechanical disruption via mincing with a razor blade followed by treatment with 280 U/ml Collagenase Type 3 (Worthington Biochemical) and 4 μg/ml DNase I (Sigma) in HBSS medium at 37°C for 1 hour with periodic short vortexing. Digested tissues were mashed through 70-μm filters and collected by centrifugation. Cell pellet was resuspended in 44% Percoll, layered on top of 66% Percoll (Sigma), and centrifuged at 1,900 g for 30 minutes without brake. Cells at the Percoll interface were collected, washed and resuspended in FACS buffer for downstream assays.

Preparation of single cell RNA-seq libraries

A suspension of 10,000 FACS sorted live cells in 1X PBS (calcium and magnesium free) containing 0.04% BSA (Sigma) were used as input to the 10X chromium controller system (10x Genomics Inc., product code 120223). Cells were barcoded using the 10x™ GemCode™ Technology to separately index each cell's transcriptome by partitioning them into Gel Bead-in-EMulsions (GEMs). GEMs were generated by combining barcoded Single Cell 5' Gel Beads, RT Master Mix with cells, and Partitioning Oil on a microfluidic chip. The GEM RT reaction was performed in thermocycler (53°C for 45 minutes, 85°C for 5 minutes, 4°C hold overnight). After RT incubation, the GEMs were

broken, and the first strand of cDNA was recovered using DynaBeadsR MyOne™ Silane beads. 2 ng – 50 ng of amplified cDNA and the target enriched product respectively were used as input for library construction. Fragmentation, end repair and A tailing were performed to obtain final libraries containing the P5 and P7 priming sites used in IlluminaR sequencing. High sensitivity DNA chips and the Agilent 2100 bioanalyzer (Agilent Technologies) were used for 5' gene expression quality control and quantification. Quality control was performed twice before sequencing. The 5' gene expression library was sequenced on NovaSeq 6000 S1 with sequencing depth of approximately 300-500 million reads per sample.

Batch effect correction and single cell count matrix processing

Pre-processing of single-cell RNA sequencing fastq files was conducted using Cell Ranger v3.0.2 (10x genomics). Single-cell RNA sequencing reads were aligned to the hg19 reference genome (ref-version 3.0.0). The count matrix used for downstream analysis was generated using the Cell Ranger count function with parameter –expect-cells=3000 (filter_matrix output). Cells with > 20% of transcripts derived from mitochondrial genes were considered apoptotic and were thus excluded, and all mitochondrial genes were removed from the final count matrix. Ribosomal genes and the noncoding RNAs NEAT1 and MALAT1 were excluded [115]. Genes with mean raw count < 3.0 were removed from the analysis, resulting in a final count matrix of 7402 cells and 14362 genes for downstream analysis. We used Seurat v2.3.4 to perform standard library size and log-normalization. The mean library size was 2240 transcripts per cell.

To mitigate potential batch effects, we used the mutual nearest neighbors method [116]. Log-normalized counts for each of the samples were used as input to the fastMNN() function from the R scran package [117] in Bioconductor with default parameters. The resulting batch-corrected PCA matrix was then input into Seurat using the SetDimReduction() function. The top 10 principal components were used as input for Louvain clustering using the FindClusters() function in Seurat at resolution 0.5 [118, 119]. tSNE was used for cluster visualization. We computed differentially expressed genes using the Wilcox test in the FindMarkers() function in Seurat, and genes with log fold change > 0 and FDR $P < 0.05$ were considered significantly differentially expressed. Log-normalized counts were used for tSNE marker plots, violin plots and heatmaps.

Derivation of cell type signatures from single-cell RNA sequencing data

To interrogate TCGA bulk RNA sequencing data using single-cell RNA sequencing clusters, we sought to derive robust gene signatures from our single-cell RNA sequencing data. We generated two signatures- one for the innate lymphocyte cluster IL_2, and one for phenotypically exhausted T cells (clusters CD8_2A and CD8_2B). We first performed a pairwise differential expression analysis- i.e., for cluster IL_2, we compared cluster IL_2 to each other cluster, and took the set of genes upregulated in cluster IL_2 in all 7 comparisons (excluding myeloid clusters). We repeated this analysis for the combined clusters CD8_2A and CD8_2B. To ensure that signatures were comprised only of genes associated with immune cells and to enable robust application to TCGA data, we used the data from the Cancer Cell Line Encyclopedia to filter out genes expressed in any cancer cell line using a cutoff of 4 RPKM. Signatures were then applied

to the TCGA KICH and KIRC cohorts using single-sample Gene Set Enrichment Analysis (ssGSEA), and patients were considered to be in the high group for each signature if the ssGSEA score exceeded the top quartile within each cancer type. The significance of each signature was calculated using a log-rank test. For the correlation of the IL2_signature and IL-15 expression, the signature was applied to TCGA bulk RNA-seq data using ssGSEA, and the resulting score was plotted against the normalized expression of IL-15.

Flow cytometry

For flow cytometry experiments, cells were pre-incubated with 2.4G2 mAb (Biolegend) to block FcγR binding and then stained with panels of cell surface marker antibodies for 20 min on ice. Fluorochrome conjugated antibodies against human CD45 (clone H130), CD49a (SR84), CD16 (3G8), and CD14 (M5E2) were purchased from BD Biosciences. Antibodies against human CD3 (OKT3), PD-1 (EH12.2H7), Granzyme A (CB9), CD56 (HCD56), CD49a (TS2/T), CD103 (Ber-ACT8), and CD16 (3G8) were purchased from Biolegend. Anti-human CD15 (MMA) was purchased from eBioscience, now Thermo Scientific, and anti-human NKG2A (REA110) was purchased from Miltenyi Biotec. Anti-human CD8a (RPA-T8) and biotinylated anti-human CD3 (UCHT1) were purchased from Tonbo Biosciences. Cells were washed 2x with FACS buffer and stained with LIVE/DEAD kit (Invitrogen) or Zombie Live/Dead kit (BioLegend) to exclude dead cells. Intracellular staining was carried out using the FoxP3/Transcription factor Fix/Perm Kit (Tonbo). All samples were acquired with a LSRII flow cytometer (Becton Dickinson) and analyzed with FlowJo software version 9.6.2 or 10.6.1 (Tree Star).

Immunofluorescence staining

Tumor tissues were paraffin embedded and sliced by the Molecular Cytology Core Facility at MSKCC. Tumor slices were de-paraffinized and rehydrated as following: three 5-minute washes in HistoClear, two 10-minute washes in each of the following ethanol concentrations – 100%, 90%, 70%, and 50% followed by two 5-minute washes in distilled water. Antigen retrieval was performed by bringing slides to a boil in 10mM sodium citrate buffer (pH 6.0) and maintained at sub-boiling temperature for 10 minutes in the microwave, then cooled at room temperature for 30 minutes. Slides were washed twice for 5 minutes in distilled water. Endogenous peroxidase activity was quenched with 3% hydrogen peroxide in methanol for 30 minutes at room temperature then washed twice for 5 minutes in distilled water. Tissues were permeabilized by washing twice for 10-minutes in 1% animal serum in PBS with 0.4% Triton X-100 (PBS-T) followed by blocking for non-specific binding by incubating the tissue sections with 5% animal serum in PBS-T for 30 minutes at room temperature. Primary antibodies against CD103 (clone EPR4166, Abcam catalog number ab29202, concentration 1:100) and E-Cadherin-AF647 (clone EP700Y, Abcam catalog number ab194982, concentration 1:100) were added in PBS-T and incubated overnight at 4°C in a humidified chamber. Slides were washed twice in PBS-T and stained with secondary antibody (goat anti-rabbit AF488, Life Technologies catalog number A11034, 1:1000) for 1 hour at room temperature. Slides were washed twice in PBS-T and stained with DAPI then mounted with OmniMount (National Diagnostics catalog number HS-110). Slides were imaged with an upright widefield microscope with a 40X objective. Images were pseudocolored and processed with FIJI software.

FACS cell sorting

Immune cells isolated from tissues were resuspended in MACS buffer (1x PBS with 1% FBS and 100 U/ml Penicillin G and 0.1 mg/ml Streptomycin) with appropriate cell surface marker antibodies and incubated for 20 minutes on ice. Cells were washed 2x in MACS buffer and stained with LIVE/DEAD kit (Invitrogen) or Zombie Live/Dead kit (BioLegend) to exclude dead cells. Cells were sorted using the BD FACS Aria Cell Sorter. Refer to figure legends for sorting strategy. Samples were collected in RPMI with 10% FBS and processed immediately after sorting.

In vitro cell culture

Sorted cells were pelleted and resuspended in T cell medium (RPMI supplemented with 10% FBS, 1 mM sodium pyruvate, non-essential amino acids (Gibco), 10 mM Hepes, 55 μM 2-Mercaptoethanol, 100 U/ml Penicillin G and 0.1 mg/ml Streptomycin) with the indicated amount of IL15/IL15Rα complex (provided by Dr. Naikong Cheung, MSKCC). Cells were cultured for 7 days in U-bottom plates in a 37°C humidified incubator prior to downstream analysis.

Single cell killing assay

Sorted innate lymphocyte populations were cultured for 7 days to recover from stress associated with cell sorting in T cell medium (RPMI supplemented with 10% FBS, 1 mM sodium pyruvate, non-essential amino acids (Gibco), 10 mM Hepes, 55 μM 2-Mercaptoethanol, 100 U/ml Penicillin G and 0.1 mg/ml Streptomycin). Cells were

supplemented with either 10 ng/ml or 100 ng/ml human IL-15/IL-15Rα complex for the duration of culture. Polydimethylsiloxane grids containing 50x50x50 μm^3 wells were applied to the bottom of an 8-well chamber plate which was then heated at 60°C for 30 minutes, cooled and the appropriate medium was added to each chamber (T cell media supplemented with 10 ng/ml or 100 ng/ml human IL-15/IL-15Rα complex). 1 μg/ml propidium iodide (PI) was added to the medium to enable real-time labeling of dead cells. K562 cells were labeled with Cell-trace Violet (CTV) dye to facilitate their identification. Once labeled, K562 cells and effector innate lymphocytes were combined at a 1:1.5 ratio, mixed well and added to the appropriate chamber well, which was then briefly spun down to place the cells within the wells. In general, individual wells contained 1 to 3 K562 cells. The chambers were imaged using a 20x objective lens (ZEN microscope) at 10-minute intervals for 12 hours. Brightfield, CTV and PI images were collected at each time point. Quantification was restricted to wells containing one effector cell in presence of at least one K562 cell in the same well. Only a single killing event per well was scored.

Statistical analysis

Spearman's correlation, log-rank and Wilcoxon tests were used to calculate statistical significance where appropriate. Two tailed unpaired t tests and one-way ANOVA were conducted using Prism 7 software. A value of $P<0.05$ was considered statistically significant.

2.5 Acknowledgements

We would like to thank Dr. Naikong Cheung (MSKCC) for providing us with the human IL-15/IL-15Ra complex reagent, and the laboratory of Dr. Morgan Huse for help with the single cell killing microwell assay. Thank you to the Molecular Cytology Core Facility for help with the microscopes and experimental set up. Thank you to Dr. Ari Hakimi and Dr. Chirag Krishna for their collaboration on the human RCC project and computational analysis.

Chapter 3: Cancer Cell-Expressed IL-15 is Sensed by and Governs the Immunosurveillance Function of Tissue-Resident Innate Lymphocytes

3.1 Introduction

The tumor environment is complex and consists of multiple cell types of both hematopoietic and non-hematopoietic origin. Cells from both lineages, as well as tumor cells themselves, have the ability to modulate immune cells through expression or secretion of a wide array of factors. Thus, it is important to understand the ways in which immune cells can be regulated in the context of all environmental cues. Due to the limitations of human studies, only few manipulations can be done and requires the isolation of cells from tissues and downstream culturing or processing. It is therefore difficult to study immune cells in the *in vivo* context of the tumor microenvironment, as *in vitro* culture conditions do not fully recapitulate all signals and cues present in the tissue. As one of our main goals was to investigate how tissue-resident innate lymphocytes are regulated in tumor tissues and understand how these cells may sense or detect cancer cells, we turned to the MMTV-PyMT (PyMT) mouse model of breast cancer, a well-studied and established epithelial cancer model, to investigate their mechanisms in a physiologically complete context.

Our lab previously published a report of tissue-resident cytotoxic innate lymphocytes that expand upon transformation in PyMT breast cancer and prostate cancer [14]. Compared to normal, non-transformed mammary tissue, transformed tumor tissue in the PyMT model of breast cancer had a significant accumulation or expansion of

$CD49a^{+}CD103^{+}$ cells within the $CD3^{-}TCR^{-}$ innate lymphocyte subset (Fig. 3.1A). These cells express high levels of granzymes and can exert potent cytotoxicity on target cells [14]. Furthermore, like the human $CD56^{bright}CD49a^{+}CD103^{+}$ innate lymphocytes, IL-15 was a crucial signal regulating their survival and/or maintenance in the tumor tissue [14].

Single cell RNA-sequencing of murine immune cells isolated from PyMT tumors revealed, like human, two clusters of NK1.1+ innate lymphocytes (Fig. 3.1B). While both human and murine tissue-resident innate lymphocytes have cytotoxic capability, there was notable differences in the granzymes expressed (Fig. 3.1C). In human RCC tumors, the $CD56^{bright}CD49a^{+}CD103^{+}$ innate lymphocytes express high levels of granzyme A. In mouse, $CD3^{-}TCR^{-}$ $CD49a^{+}CD103^{+}$ innate lymphocytes have the highest expression of granzyme B (Fig. 3.1C). The reason for this distinction is not clear, but perhaps simply represents human and murine differences or is the result of differential signals or cues in human RCC compared with mouse breast cancer. While their mechanisms of inducing cell death are distinct, both granzymes are lethal and potently induce target cell killing. Despite this difference, expression of other molecules like *S1pr5, Itga1 and Itgae* were highly conserved between mouse and human tissue-resident innate lymphocytes (Fig. 3.1C). The $CD3^{-}TCR^{-}$ tissue-resident innate lymphocyte subset therefore represents the murine equivalent of $CD56^{bright}CD49a^{+}CD103^{+}$ innate lymphocytes found in human RCC tumors.

Our work aimed to understand what signals regulate the phenotype and function of tissue-resident innate lymphocytes and to uncover their mode of tumor cell sensing. By utilizing Qa1 mutant and NKG2A knockout mice, we show that signaling through this

inhibitory axis does not affect the phenotype or function of tissue-resident innate lymphocytes in PyMT tumors. By preforming loss of function studies whereby IL-15 was deleted in a cell type specific manner, we were able to demonstrate that while hematopoietic and stromal cell sources of IL-15 are dispensable, cancer cell-expressed IL-15 is crucial for their maintenance and/or survival in the tumor as well as level of granzyme expression. These cellular defects were associated with accelerated tumor growth, suggesting that IL-15 was directly sensed on tumor cells to induce an anti-tumor immune response mediated by tissue-resident innate lymphocytes.

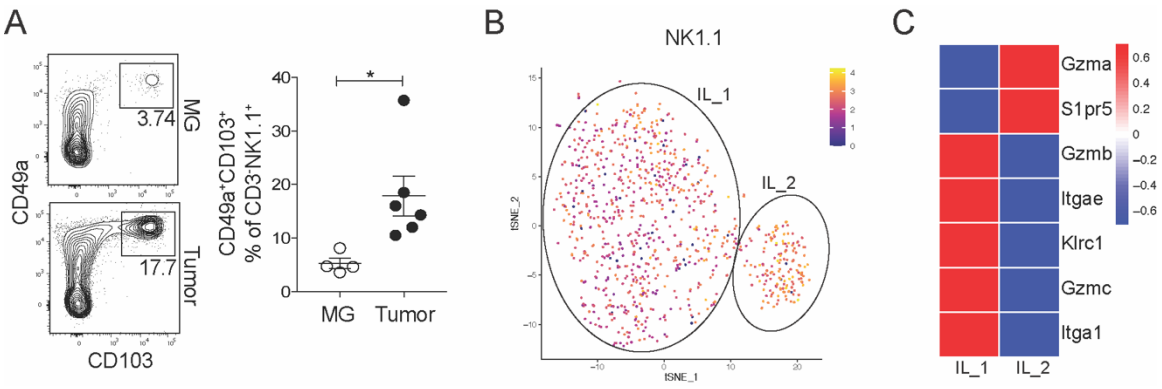

Figure 3.1 Evolutionarily conserved tissue-resident cytotoxic innate lymphocyte response in epithelial tumors

A. Representative plot and quantification of CD49a and CD103 expression within $CD3^-$ $NK1.1^+$ cells in virgin mammary gland and transformed mammary tissue. All error bars represent the mean ± SEM. Two-tailed unpaired t test was used for all statistical analyses, * $p<0.05$. **B**. tSNE plot showing two clusters of $NK1.1^+$ cells from single cell RNA-sequencing of immune cells isolated from a PyMT tumor. **C**. Expression of the indicated genes in the two $NK1.1^+$ clusters from single cell RNA-sequencing. IL = innate lymphocyte.

3.2 Results

3.2.1 Tissue-resident innate lymphocyte function is independent of MHC class I-mediated signaling

Further characterization of $CD49a^{+}CD103^{+}$ innate lymphocytes revealed that about 50% of the population expressed high levels of the inhibitory receptor NKG2A (Fig. 3.2). We therefore sought to investigate if $CD49a^{+}CD103^{+}$ innate lymphocyte function in PyMT tumors is regulated by expression of NKG2A. We utilized a mutant mouse model generated by the laboratory of Dr. Harvey Cantor whereby the interaction of NKG2A and Qa1 is disrupted by a point mutation in the Qa1 gene, conversion of an arginine into alanine at position 72 ($Qa1^{R72A}$) [120]. This mutation specifically abolishes signaling through the Qa1/NKG2A axis but leaves $CD8^{+}$ T cells the ability to directly interact with Qa1. Therefore, this model can be used to observe specific phenotypic and functional differences when signaling between NKG2A and Qa1 is lost.

We crossed the $Qa1^{R72A}$ mutant to the PyMT background and analyzed the tissue-resident innate lymphocyte response in tumors. There was no difference in abundance of total $CD3^{-}NK1.1^{+}$ innate lymphocytes (Fig. 3.3A) or the $CD49a^{+}CD103^{+}$ innate lymphocyte subset (Fig. 3.3B). In addition, the level of granzyme B expression within $CD49a^{+}CD103^{+}$ innate lymphocytes and tumor volume over time was comparable between PyMT and $Qa1^{R72A}$PyMT mice (Fig. 3.3C-D).

In order to confirm the lack of phenotype observed in the Qa1 mutant model, we bred the whole-body NKG2A knockout mouse (*Klrc1*$^{-/-}$, generated on the C57BL/6 background) with PyMT and performed the same analysis [121]. Again, there was no

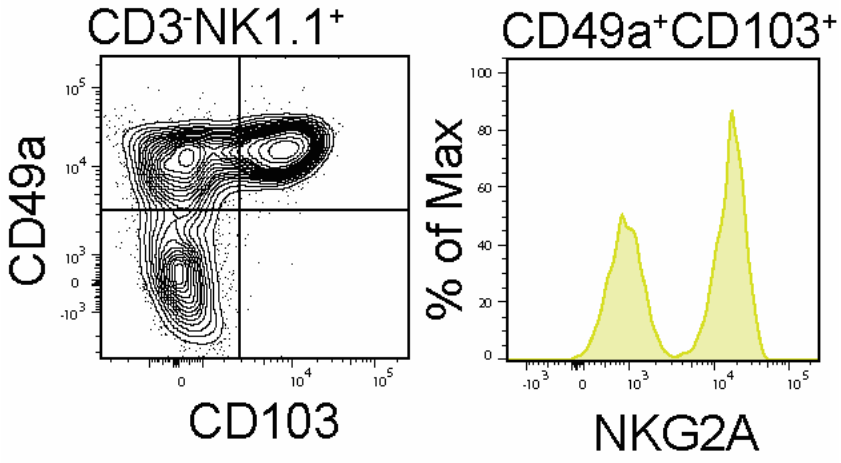

Figure 3.2 CD49a$^+$CD103$^+$ innate lymphocytes in PyMT tumors express NKG2A

Representative histogram of NKG2A expression (right) in the CD49a$^+$CD103$^+$ subset of CD3$^-$NK1.1$^+$ cells (shown in the representative plot on the left).

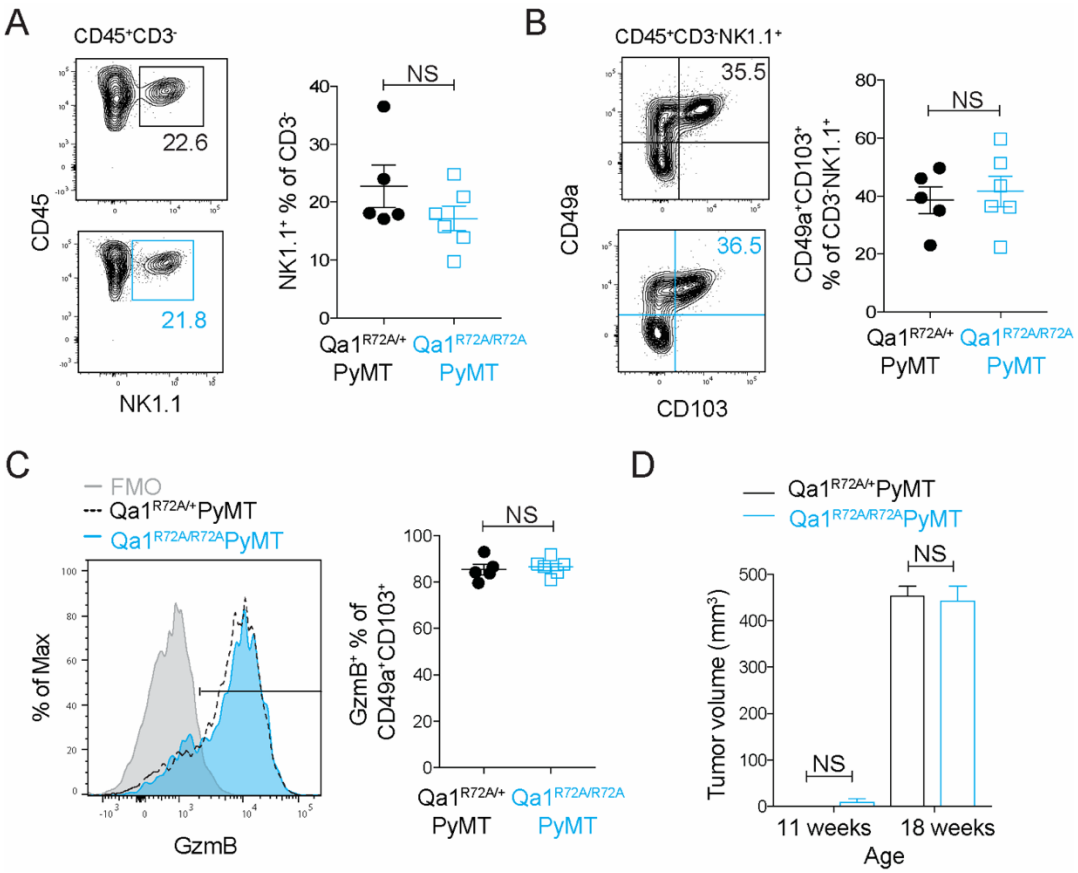

Figure 3.3 Tissue-resident innate lymphocytes function independently of NKG2A/Qa1 signaling

A. Representative plot and quantification of NK1.1^{+} cells out of total CD45^{+}CD3^{-} cells isolated from pooled tumors of 20-24-week-old Qa1$^{R72A/+}$PyMT or Qa1$^{R72A/R72A}$PyMT mice. Each dot represents an individual mouse (n = 5-6 for each genotype). Data are pooled from 3 or more independent experiments. **B.** Representative plot and quantification of percentage of CD49a^{+}CD103^{+} cells out of total CD45^{+}CD3^{-}NK1.1^{+} cells isolated from pooled tumors of 20-24-week-old Qa1$^{R72A/+}$PyMT or Qa1$^{R72A/R72A}$PyMT mice. Each dot represents an individual mouse (n = 5-6 for each genotype). Data are pooled from 3 or more independent experiments. **C.** (Left) Representative histogram of granzyme B expression in CD49a^{+}CD103^{+} innate lymphocytes from pooled tumors of 20-24-week-old Qa1$^{R72A/+}$PyMT or Qa1$^{R72A/R72A}$PyMT mice. (Right) Quantification of percentage of granzyme B^{+} CD49a^{+}CD103^{+} innate lymphocytes. Each dot represents an individual mouse (n = 5-6 for each genotype). Data are pooled from 3 independent experiments. **D.** Total tumor burden of Qa1$^{R72A/+}$PyMT or Qa1$^{R72A/R72A}$PyMT mice monitored between 11 and 18 weeks of age (n = 2-7). All error bars represent the mean ± SEM. Two-tailed unpaired t test was used for all statistical analyses, NS = non-significant.

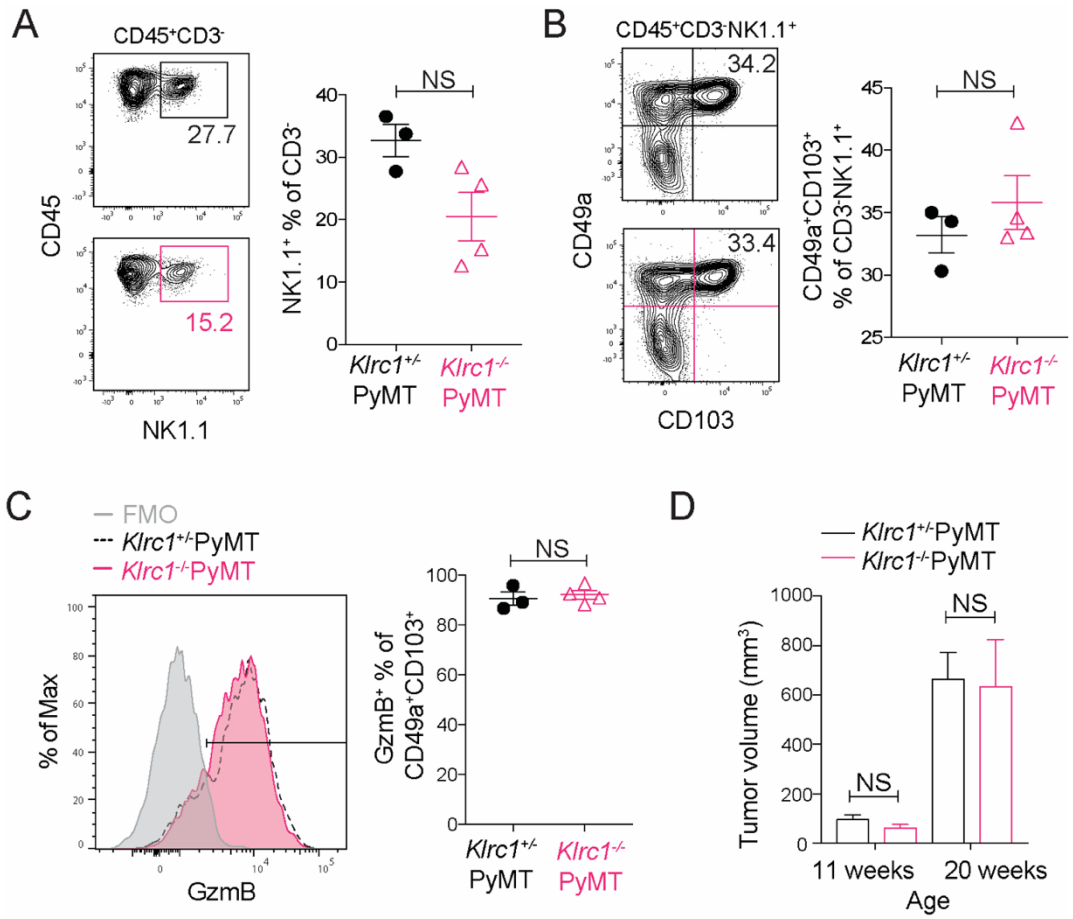

Figure 3.4 Tissue-resident innate lymphocytes function independently of NKG2A signaling

A. Representative plot and quantification of NK1.1$^+$ cells out of total CD45$^+$CD3$^-$ cells isolated from pooled tumors of 20-24-week-old *Klrc1*$^{+/-}$PyMT or *Klrc1*$^{-/-}$PyMT mice. Each dot represents an individual mouse (n = 3-5 for each genotype). Data are pooled from 3 or more independent experiments. **B.** Representative plot and quantification of percentage of CD49a$^+$CD103$^+$ cells out of total CD45$^+$CD3$^-$NK1.1$^+$ cells isolated from pooled tumors of 20-24-week-old *Klrc1*$^{+/-}$PyMT or *Klrc1*$^{-/-}$PyMT mice. Each dot represents an individual mouse (n = 3-4 for each genotype). Data are pooled from 3 or more independent experiments. **C.** (Left) Representative histogram of granzyme B expression in CD49a$^+$CD103$^+$ innate lymphocytes from pooled tumors of 20-24-week-old *Klrc1*$^{+/-}$PyMT or *Klrc1*$^{-/-}$PyMT mice. (Right) Quantification of percentage of granzyme B$^+$ CD49a$^+$CD103$^+$ innate lymphocytes. Each dot represents an individual mouse (n = 3-4 for each genotype). Data are pooled from 3 independent experiments. **D.** Total tumor burden of *Klrc1*$^{+/-}$PyMT or *Klrc1*$^{-/-}$PyMT mice monitored between 11 and 20 weeks of age (n = 9-16). All error bars represent the mean ± SEM. Two-tailed unpaired t test was used for all statistical analyses, NS = non-significant.

difference in overall abundance of total $CD3^{-}NK1.1^{+}$ innate lymphocytes or the $CD49a^{+}CD103^{+}$ innate lymphocyte subset (Fig. 3.4A-B), and no change in granzyme B expression or total tumor volume measured over time (Fig. 3.4C-D). Overall, these data suggest that lack of inhibition through NKG2A does not significantly alter the cytotoxic capabilities of tissue-resident innate lymphocytes in PyMT tumors.

We next sought to investigate if the phenotype and function of tissue-resident innate lymphocytes was dependent upon the detection of any MHC class I molecules expressed on tumor cells. To target cancer cells in the PyMT model, we utilized Mrp8-Cre transgenic mice that marked more than 80% of transformed mammary epithelial cells as read out by crossing the Mrp8-Cre line to a *Rosa26*$^{LSL\text{-}YFP}$ on the PyMT background (Fig. 3.5). To delete MHC class I molecules specifically from tumor cells, we crossed the Mrp8-Cre line on the PyMT background to beta-2 microglobulin (B2M) floxed mice. B2M is required for MHC class I molecule expression on the cell surface, thus deletion of B2M in Mrp8-Cre positive cells prevents cancer cells from expressing all MHC class I molecules (Ia and Ib). Interestingly, we saw no change in abundance of total $CD3^{-}NK1.1^{+}$ cells or $CD49a^{+}CD103^{+}$ innate lymphocytes in PyMT tumors (Fig. 3.6A-B). Additionally, there was no difference in granzyme B expression or total tumor volume in Mrp8-Cre*B2M*$^{fl/fl}$PyMT mice compared to control mice (Fig. 3.6C-D). These data suggest that tissue-resident innate lymphocyte function is not regulated by signaling via interaction with MHC class I molecules on the surface of cancer cells.

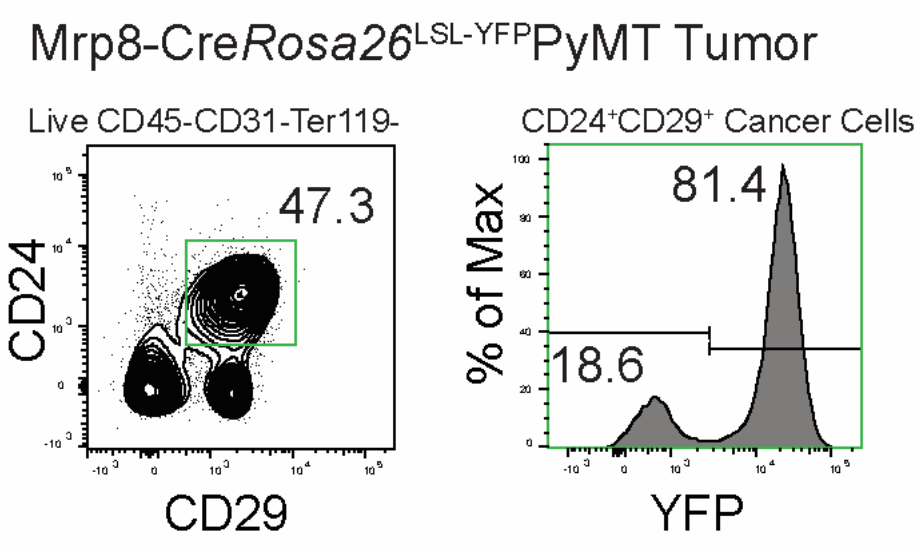

Figure 3.5 Mrp8-Cre targets PyMT cancer cells

Gating strategy and YFP expression in $CD24^{+}CD29^{+}$ cancer cells from pooled tumors of a 20-week-old Mrp8-Cre*Rosa26*$^{LSL\text{-}YFP}$PyMT mouse.

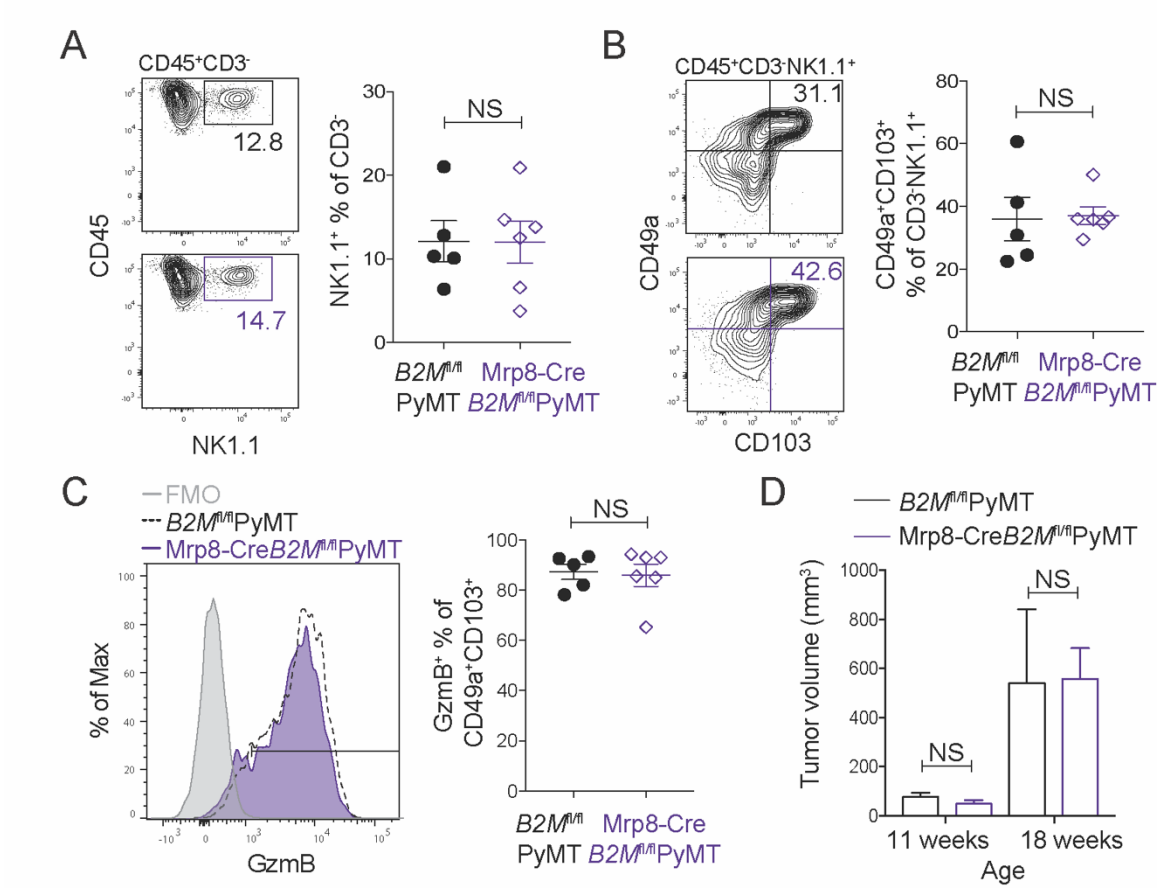

Figure 3.6 Tissue-resident innate lymphocytes function independently of MHC class I expressed by tumor cells

A. Representative plot and quantification of NK1.1^{+} cells out of total CD45^{+}CD3^{-} cells isolated from pooled tumors of 20-24-week-old *B2M*$^{fl/fl}$PyMT or Mrp8-Cre*B2M*$^{fl/fl}$PyMT mice. Each dot represents an individual mouse (n = 5-6 for each genotype). Data are pooled from 3 or more independent experiments. **B.** Representative plot and quantification of percentage of CD49a^{+}CD103^{+} cells out of total CD45^{+}CD3^{-}NK1.1^{+} cells isolated from pooled tumors of 20-24-week-old *B2M*$^{fl/fl}$PyMT or Mrp8-Cre*B2M*$^{fl/fl}$PyMT mice. Each dot represents an individual mouse (n = 5-6 for each genotype). Data are pooled from 3 or more independent experiments. **C.** (Left) Representative histogram of granzyme B expression in CD49a^{+}CD103^{+} innate lymphocytes from pooled tumors of 20-24-week-old *B2M*$^{fl/fl}$PyMT or Mrp8-Cre*B2M*$^{fl/fl}$PyMT mice. (Right) Quantification of percentage of granzyme B^{+} CD49a^{+}CD103^{+} innate lymphocytes. Each dot represents an individual mouse (n = 5-6 for each genotype). Data are pooled from 3 independent experiments. **D.** Total tumor burden of *B2M*$^{fl/fl}$PyMT or Mrp8-Cre*B2M*$^{fl/fl}$PyMT mice monitored between 11 and 18 weeks of age (n = 4-10). All error bars represent the mean ± SEM. Two-tailed unpaired t test was used for all statistical analyses, NS = non-significant.

3.2.2 Tissue-resident innate lymphocytes function independently of DC- and macrophage-expressed IL-15

We next sought to decipher the cellular mechanism by which IL-15 regulates tissue-resident innate lymphocytes in the tumor environment. Dendritic cells (DCs) and macrophages express IL-15 and regulate aspects of the development, maturation and homeostasis of adaptive and innate cytotoxic lymphocytes in secondary lymphoid organs [67-70]. We sought to investigate if macrophages and DCs in PyMT tumors also expressed IL-15 and thus employed an IL-15 translational reporter mouse harboring eGFP under the control of the *Il15* gene locus, (IL-15$^{2a\text{-}eGFP}$) [70], bred to the PyMT background. As previously reported [122], two prominent macrophage populations, tumor-associated macrophages (TAMs) and mammary tissue macrophages (MTMs), were detected in PyMT tumors (Fig. 3.7A). Two conventional DC1 and DC2 subsets were also present in PyMT tumors, albeit at lower frequencies (Fig. 3.7A). Reporter analysis revealed that MTMs and XCR1$^+$ DC1s expressed the highest level of IL-15, followed by TAMs and CD11b$^+$ DC2s (Fig. 3.7B).

To determine whether these myeloid populations may represent a critical source of IL-15 supporting tissue-resident cytotoxic innate lymphocyte responses in tumors, we bred mice harboring a conditional allele of the *Il15* gene (*Il15*^{fl}) with CD11c-CrePyMT transgenic mice that effectively target DCs, TAMs and a fraction of MTMs [122]. Surprisingly, there was no effect on the abundance of total CD3$^-$NK1.1$^+$ cells or CD49a$^+$CD103$^+$ innate lymphocytes in CD11c-Cre*Il15*$^{fl/fl}$PyMT tumors (Fig. 3.8A-B).

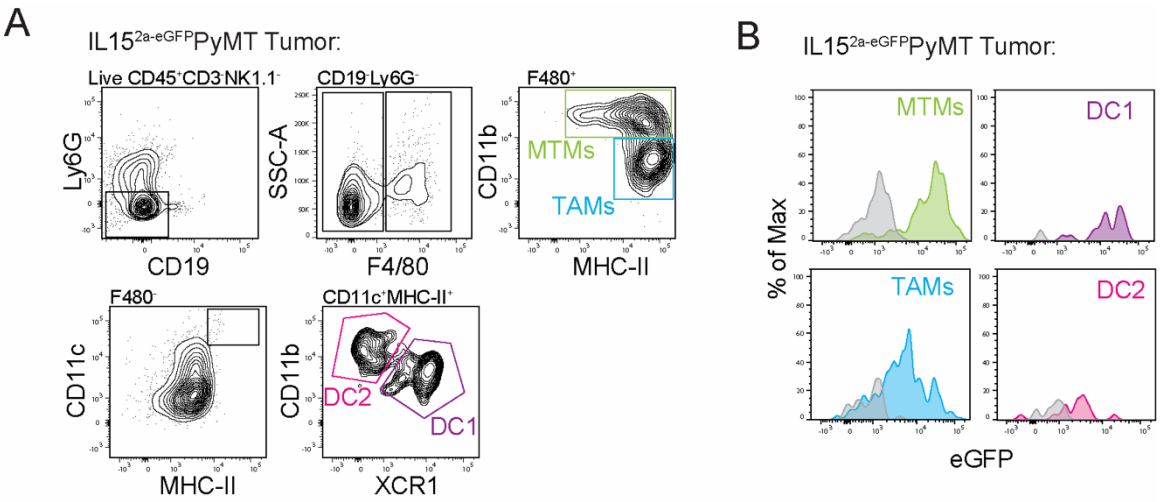

Figure 3.7 Macrophages and DCs express IL-15 in PyMT tumors

A. Gating strategy for determining eGFP expression in the indicated myeloid populations isolated from pooled tumors of a 20-week-old IL15$^{2a\text{-}eGFP}$PyMT mouse in Figure 5A. **B.** Flow cytometric analysis of eGFP expression in the indicated myeloid populations from pooled tumors of a 20-week-old IL15$^{2a\text{-}eGFP}$PyMT (colored) or PyMT mouse (gray). Representative of 3 independent experiments.

Furthermore, there was no difference in level of granzyme B expression, suggesting that loss of IL-15 from myeloid cells had no effect on their effector program (Fig. 3.8C). Moreover, there was no difference in tumor volume measured over time in CD11c-Cre*Il15*$^{fl/fl}$PyMT mice compared to controls (Fig. 3.8D). In line with previous studies [69], splenic NK cells, in particular the mature DX5^{+}CD27^{-}CD11b^{+} NK cell subset, were reduced in CD11c-Cre*Il15*$^{fl/fl}$PyMT mice (Fig. 3.9A-B). These findings demonstrate that IL-15 derived from CD11c^{+} myeloid populations is dispensable for the induction of CD3^{-}NK1.1^{+}CD49a^{+}CD103^{+} innate lymphocytes in PyMT tumors.

3.2.3 Tissue-resident innate lymphocytes function independently of hematopoietic and stromal cell sources of IL-15

IL-15 mRNA is widely expressed in many cell types of both hematopoietic and non-hematopoietic origin [63-65]. We wished to expand IL-15 depletion with the FSP1-Cre line that targets various mesenchymal and hematopoietic cell lineages in adult tissues [123, 124]. Using a *Rosa26*$^{LSL\text{-}YFP}$Cre reporter line bred to the FSP1-CrePyMT background, we observed YFP expression in approximately 94% CD45^{+} leukocytes, the majority of CD29^{+}EpCAM^{-} stromal cells and a subset of CD31^{+} endothelial cells, but minimally in Ter119^{+} erythrocytes or EpCAM^{+} cancer cells in PyMT tumors (Fig. 3.10). IL-15$^{2a\text{-}eGFP}$ reporter analysis revealed that in addition to myeloid subsets including DCs and macrophages (Fig. 3.7), CD29^{+}EpCAM^{-} stromal cells and CD31^{+} endothelial cells in PyMT tumors expressed substantial amounts of IL-15 (Fig. 3.11A-B).

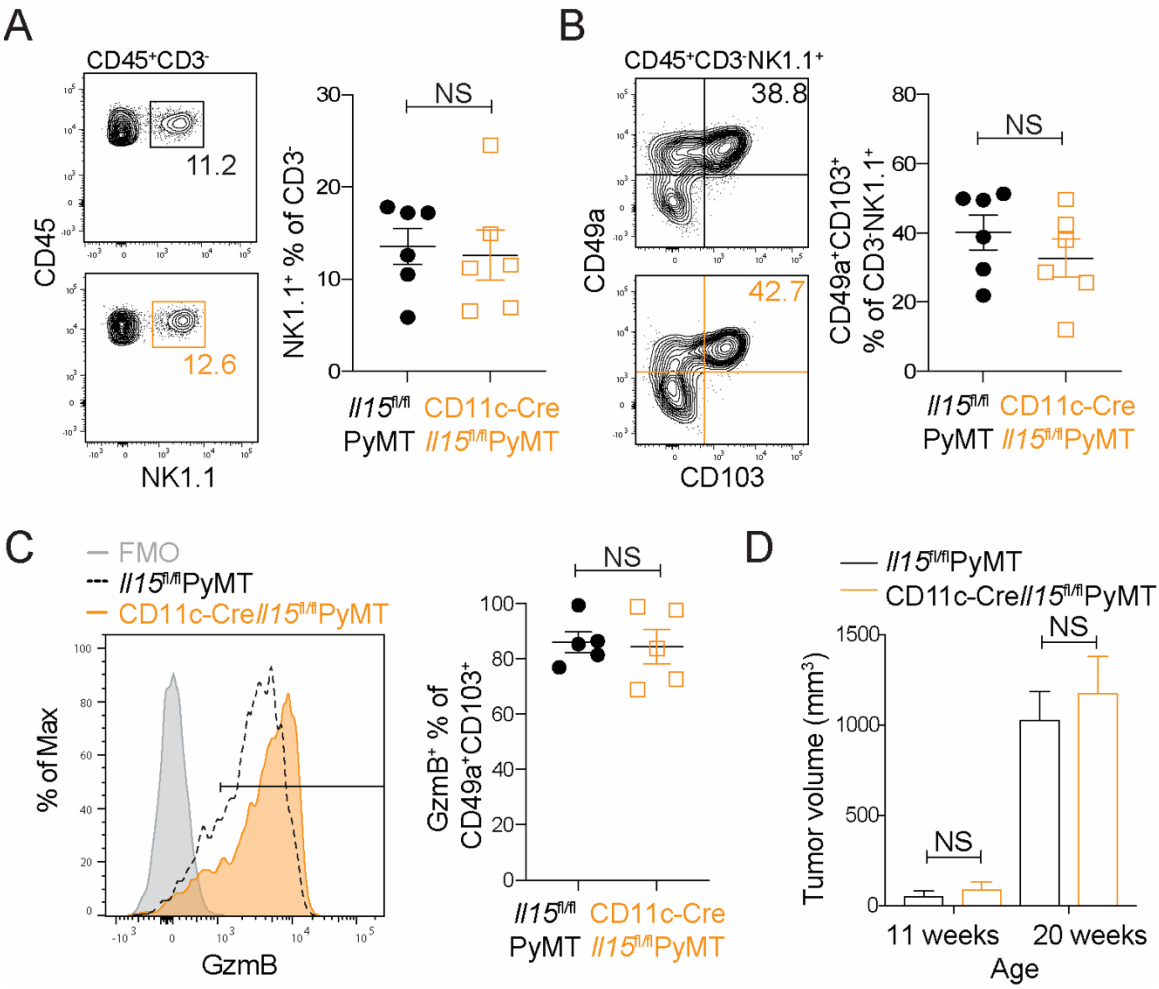

Figure 3.8 Tissue-resident innate lymphocytes function independently of DC- and macrophage-expressed IL-15

A. Representative plot and quantification of NK1.1^{+} cells out of total CD45^{+}CD3^{-} cells isolated from pooled tumors of 20-24-week-old *Il15*$^{fl/fl}$PyMT or CD11c-Cre *Il15*$^{fl/fl}$PyMT mice. Each dot represents an individual mouse (n = 6 for each genotype). Data are pooled from 3 or more independent experiments. **B.** Representative plot and quantification of percentage of CD49a^{+}CD103^{+} cells out of total CD45^{+}CD3^{-}NK1.1^{+} cells isolated from pooled tumors of 20-24-week-old *Il15*$^{fl/fl}$PyMT or CD11c-Cre *Il15*$^{fl/fl}$PyMT mice. Each dot represents an individual mouse (n = 6 for each genotype). Data are pooled from 3 or more independent experiments. **C.** (Left) Representative histogram of granzyme B expression in CD49a^{+}CD103^{+} innate lymphocytes from pooled tumors of 20-24-week-old *IL15*$^{fl/fl}$PyMT or CD11c-Cre*IL15*$^{fl/fl}$PyMT mice. (Right) Quantification of percentage of granzyme B^{+} CD49a^{+}CD103^{+} innate lymphocytes. Each dot represents an individual mouse (n = 5 for each genotype). Data are pooled from 3 independent experiments. **D**. Total tumor burden of *Il15*$^{fl/fl}$PyMT and CD11c-Cre*Il15*$^{fl/fl}$PyMT mice monitored between 11 and 20 weeks of age (n = 6-13). All error bars represent the mean ± SEM. Two-tailed unpaired t test was used for all statistical analyses, NS = non-significant.

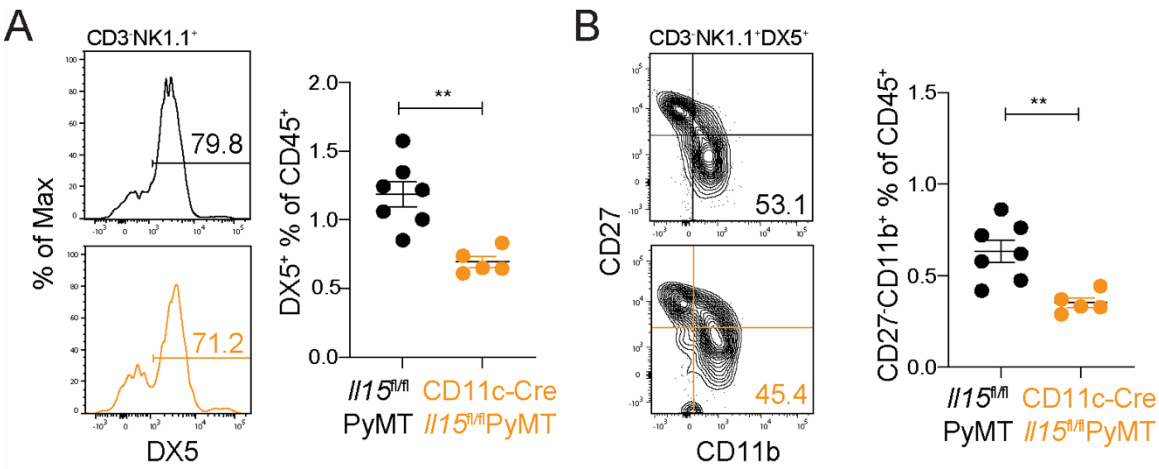

Figure 3.9 Splenic NK cells are reduced in CD11c-Cre*Il15*$^{fl/fl}$PyMT mice

A. (Left) Representative histograms of CD49b (DX5) expression among total CD3$^-$ NK1.1$^+$ cells in spleens of the indicated mouse genotype. (Right) Percentage of DX5$^+$ cells quantified out of total splenic CD45+ immune cells. **B.** (Left) Representative plots of CD27 and CD11b expression among total CD3$^-$NK1.1$^+$DX5$^+$ cells in spleens of the indicated mouse genotype. (Right) Percentage of DX5$^+$CD11b$^+$CD27$^-$ cells quantified out of total splenic CD45$^+$ immune cells. **A, B.** Each dot represents an individual mouse (n = 5-7). Data are pooled from 3 independent experiments. All error bars represent the mean ± SEM. Two-tailed unpaired t test was used for statistical analysis, *p<0.05, **p<0.01.

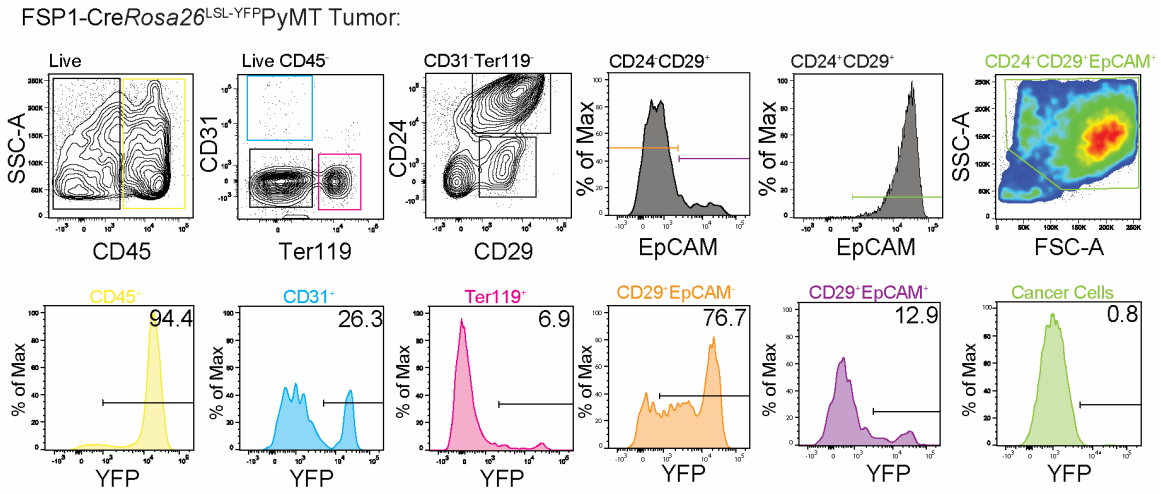

Figure 3.10 FSP1-Cre targets CD45$^+$ cells, CD29$^+$EpCAM$^-$ stromal cells and a subset of CD31$^+$ endothelial cells

Gating strategy and YFP expression in the indicated populations from pooled tumors of a 20-week-old FSP1-Cre*Rosa26*$^{LSL\text{-}YFP}$PyMT mouse.

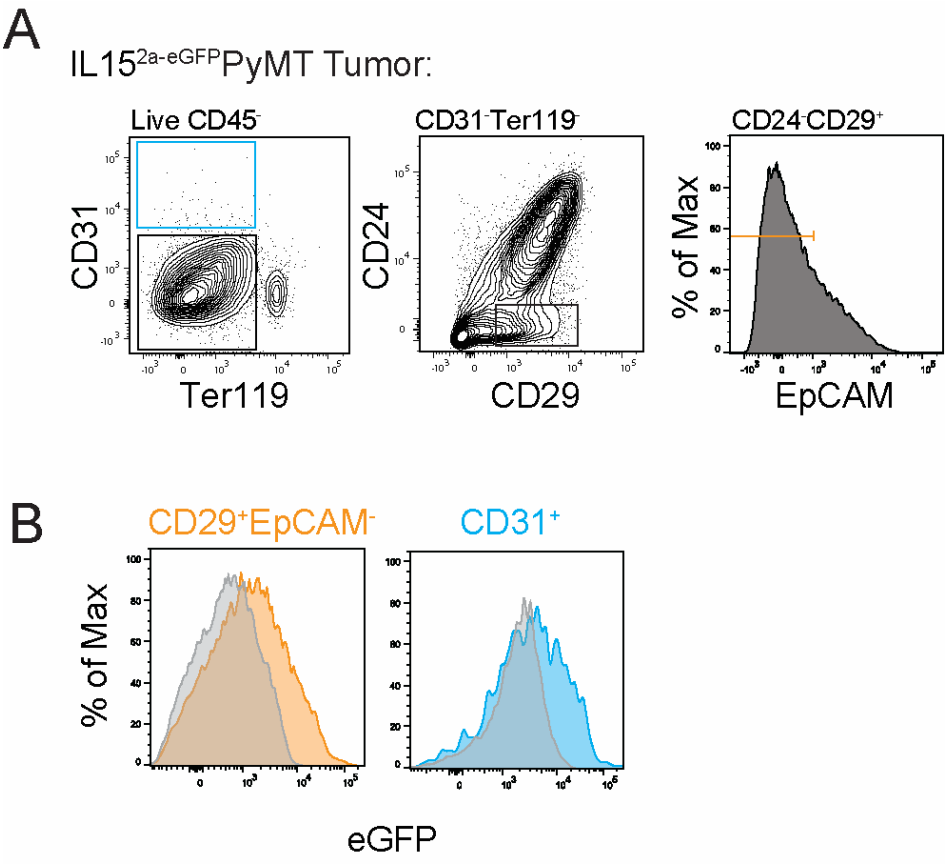

Figure 3.11 CD29$^+$ stromal and CD31$^+$ endothelial cells express IL-15 in PyMT tumors

A. Gating strategy for determining eGFP expression in the indicated stromal cell populations isolated from pooled tumors of a 20-week-old IL15$^{2a\text{-}eGFP}$PyMT mouse. **B.** Flow cytometric analysis of eGFP expression in the indicated stromal cell populations from pooled tumors of 20-week-old IL15$^{2a\text{-}eGFP}$PyMT (colored) or wild-type PyMT (gray) mice. Representative of 3 independent experiments.

To evaluate the function of IL-15 produced by FSP1-Cre-targeted cells, we bred FSP1-Cre mice to the *Il15*$^{fl/fl}$PyMT background. To our surprise, while splenic NK cells and specifically the mature DX5^{+}CD27^{-}CD11b^{+} subset were greatly diminished in FSP1-Cre*Il15*$^{fl/fl}$PyMT mice (Fig. 3.12A-B), neither tumor CD3^{-}NK1.1^{+} cells nor the CD49a^{+}CD103^{+} tissue-resident subset were substantially altered (Fig. 3.13A-B). Granzyme B expression was also comparable in CD49a^{+}CD103^{+} innate lymphocytes in association with similar tumor burden in *Il15*$^{fl/fl}$PyMT and FSP1-Cre*Il15*$^{fl/fl}$PyMT mice (Fig. 3.13C-D). Together, these findings suggest that hematopoietic and stromal sources of IL-15 are of no consequence to the induction and function of tissue-resident innate lymphocytes in PyMT tumors.

3.2.4 Tissue-resident innate lymphocytes are in direct contact with cancer cells

After ruling out hematopoietic and stromal cell sources of IL-15, we turned to immunofluorescence in order to visually investigate the potential IL-15 niche for tissue-resident cytotoxic innate lymphocytes. Unpublished data from our lab revealed that tissue-resident cytotoxic innate lymphocytes are unique in their high levels of expression of the cytotoxic molecule granzyme C (Fig. 3.1C and B. Nixon, manuscript under review). Such specificity enabled us to generate an iCre recombinase reporter mouse in which iCre and tandem dimer of Tomato (tdT) constructs are under the control of the granzyme C locus (Fig. 3.14A). The majority of tdT^{+}NK1.1^{+} lymphocytes in PyMT tumors are TCR^{-}, and in fact GzmC-iCre^{tdT} is expressed exclusively in the CD49a^{+}CD103^{+} subset of TCR^{-}NK1.1^{+} innate lymphocytes (Fig. 3.14B). We therefore used these mice to specifically mark tissue-resident innate lymphocytes in PyMT tumors.

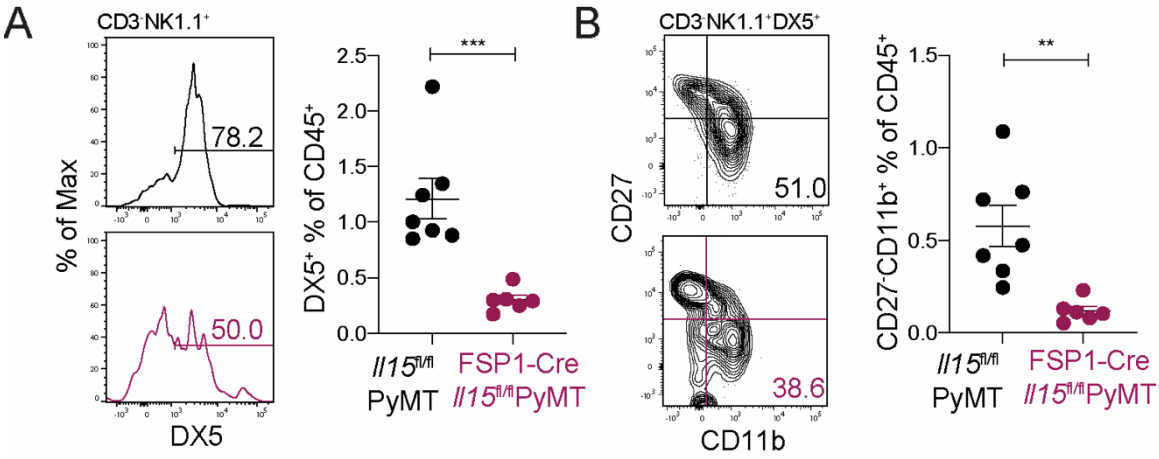

Figure 3.12 Splenic NK cells are reduced in FSP1-Cre*Il15*$^{fl/fl}$PyMT mice

A. (Left) Representative histograms of CD49b (DX5) expression among total CD3$^-$ NK1.1$^+$ cells in spleens of the indicated mouse genotype. (Right) Percentage of DX5$^+$ cells quantified out of total splenic CD45$^+$ immune cells. **B.** (Left) Representative plots of CD27 and CD11b expression among total CD3$^-$NK1.1$^+$DX5$^+$ cells in spleens of the indicated mouse genotype. (Right) Percentage of DX5$^+$CD11b$^+$CD27$^-$ cells quantified out of total splenic CD45$^+$ immune cells. **A, B.** Each dot represents an individual mouse (n = 6-7). Data are pooled from 3 or more independent experiments. All error bars represent the mean ± SEM. Two-tailed unpaired t test was used for statistical analysis, **p<0.01, ***p<0.001.

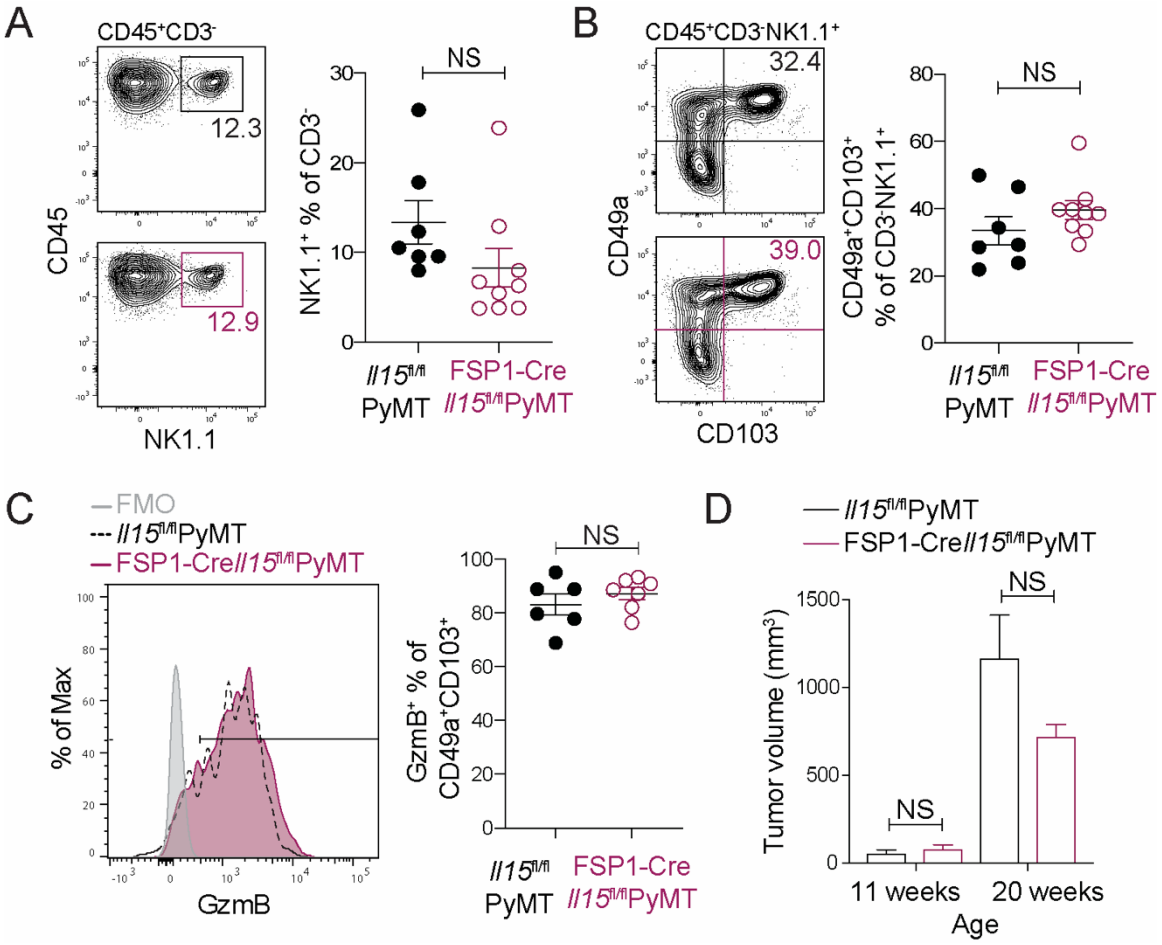

Figure 3.13 Tissue-resident innate lymphocytes function independently of hematopoietic and stromal cell sources of IL-15

A. Representative plot and quantification of percentage of NK1.1$^+$ cells out of total CD3$^-$ cells isolated from pooled tumors of 20-24-week-old *Il15*$^{fl/fl}$PyMT or FSP1-Cre*Il15*$^{fl/fl}$PyMT mice. Each dot represents an individual mouse (n = 7-9). Data are pooled from 3 or more independent experiments. **B.** Representative plot and quantification of percentage of CD49a$^+$CD103$^+$ cells out of total CD45$^+$CD3$^-$NK1.1$^+$ cells isolated from pooled tumors of 20-24-week-old *Il15*$^{fl/fl}$PyMT or FSP1-Cre*Il15*$^{fl/fl}$PyMT mice. Each dot represents an individual mouse (n = 7-9). Data are pooled from 3 or more independent experiments. **C. (**Left) Representative histogram of granzyme B expression in CD49a$^+$CD103$^+$ innate lymphocytes. (Right) Quantification of percentage of granzyme B$^+$ CD49a$^+$CD103$^+$ innate lymphocytes. Each dot represents an individual mouse (n = 6-7). Data are pooled from 3 independent experiments. **D.** Total tumor burden of *Il15*$^{fl/fl}$PyMT and FSP1-Cre*Il15*$^{fl/fl}$PyMT mice monitored between 11 and 20 weeks of age (n = 5-9). All error bars represent the mean ± SEM. Two-tailed unpaired t test was used for all statistical analyses, NS = non-significant.

To mark mammary epithelial cells, we used E-Cadherin reporter mice which harbors and enhanced cyan fluorescent protein (CFP) under the control of the E-Cadherin locus (Fig. 3.14C) [125]. E-Cadherin^{CFP} mice were bred to GzmC-iCre^{tdT}PyMT mice and tissues were taken and stained for PyMT to identify transformed mammary epithelial cells. Intriguingly, GzmC-iCre^{tdT} cells accumulated within PyMT^{+} transformed areas of mammary tissue and were rarely found in PyMT^{-} non-transformed areas (Fig. 3.15). This suggested that GzmC-iCre^{tdT+} innate lymphocytes are in close contact with tumor cells in this model.

To further understand the behavior of cytotoxic innate lymphocytes, we bred E-Cadherin^{CFP}GzmC-iCre^{tdT}PyMT mice to a mouse strain harboring a genetically encoded calcium indicator (GECI) [126]. Briefly, this mouse harbors a calcium responsive element (GCaMP5) along with a tdTomato reporter element located 3' of the gene that encodes the largest subunit of RNA polymerase II (Fig. 3.16A). Crossing this mouse to the GzmC-iCre mouse results in expression of GCaMP5 in GzmC^{+} cells and any activation resulting in calcium flux will cause the cells to flash green (Fig. 3.16A). To analyze these cells in real time, we performed live imaging on a 13-week-old mouse harboring all of these elements. We observed interesting behavior of GzmC-iCre^{tdT+} cells within E-Cadherin^{CFP+} tumors whereby GzmC-iCre^{tdT+} cells were seemingly embedded within the tumor tissue, in very close contact with tumor cells (Fig. 3.16B). Despite being stationary within the tumor tissue, the cells were active as demonstrated by frequent Ca^{2+} flux events (Fig. 3.16B). These data demonstrate functional tissue-resident cytotoxic innate lymphocytes residing within transformed tumor tissue *in vivo*.

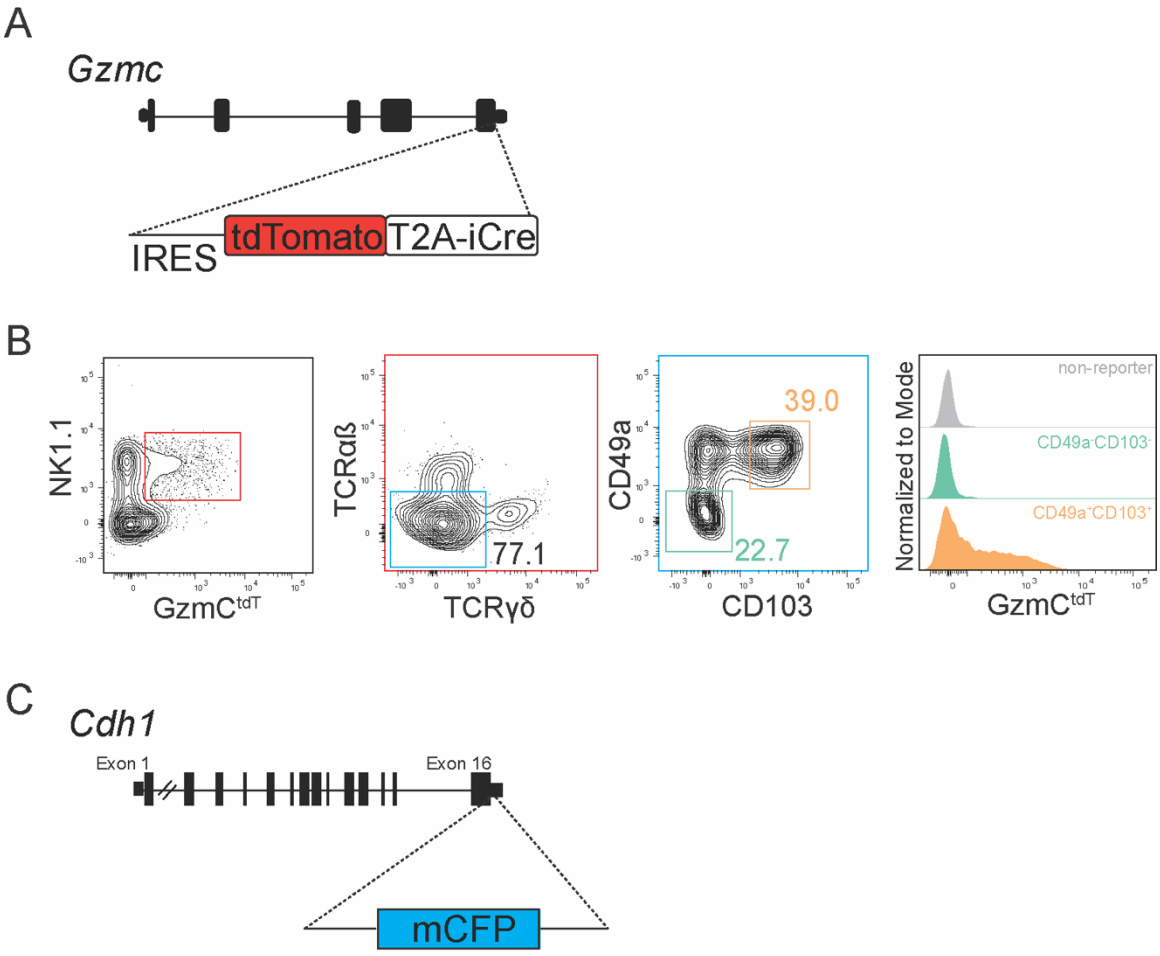

Figure 3.14 GzmC is specifically expressed in CD49a^{+}CD103^{+} innate lymphocytes, diagram of GzmC^{iCre} and E-Cadherin^{CFP} mice

A. Simple diagram denoting the design of the Granzyme C-iCre$^{tdT/+}$ mouse. **B.** Flow cytometric analysis of (top) granzyme C expression as read out by tdTomato staining in NK1.1^{+} cells (left) and the expression of TCRαβ and TCRγδ within that gate (right) and (bottom) granzyme C expression as read out by tdTomato staining in CD49a^{+}CD103^{+} or CD49a^{-}CD103^{-} TCR^{-}NK1.1^{+} innate lymphocytes. **C.** Simple diagram displaying the design of the E-Cadherin^{CFP} reporter mouse.

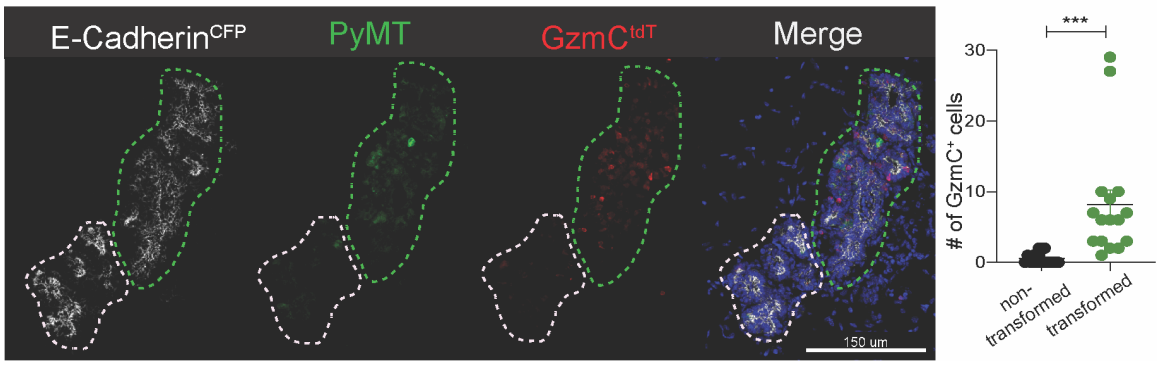

Figure 3.15 Tissue-resident innate lymphocytes expand in transformed mammary tissue

Representative immunofluorescence images of E-cadherin (white), PyMT (green), GzmC-iCre^{tdT} (red) and DAPI (blue) from a tumor section of a 13-week old PyMT mouse. Scale bar, 150 uM. Green outline denotes transformed (PyMT^{+}) area and white outline denotes non-transformed (PyMT^{-}) area. Quantification is of total number of individual GzmC-iCre^{tdT+} cells in non-transformed or transformed areas. Each dot represents discrete, individual E-Cadherin^{+} areas. Error bars represent the mean ± SEM.

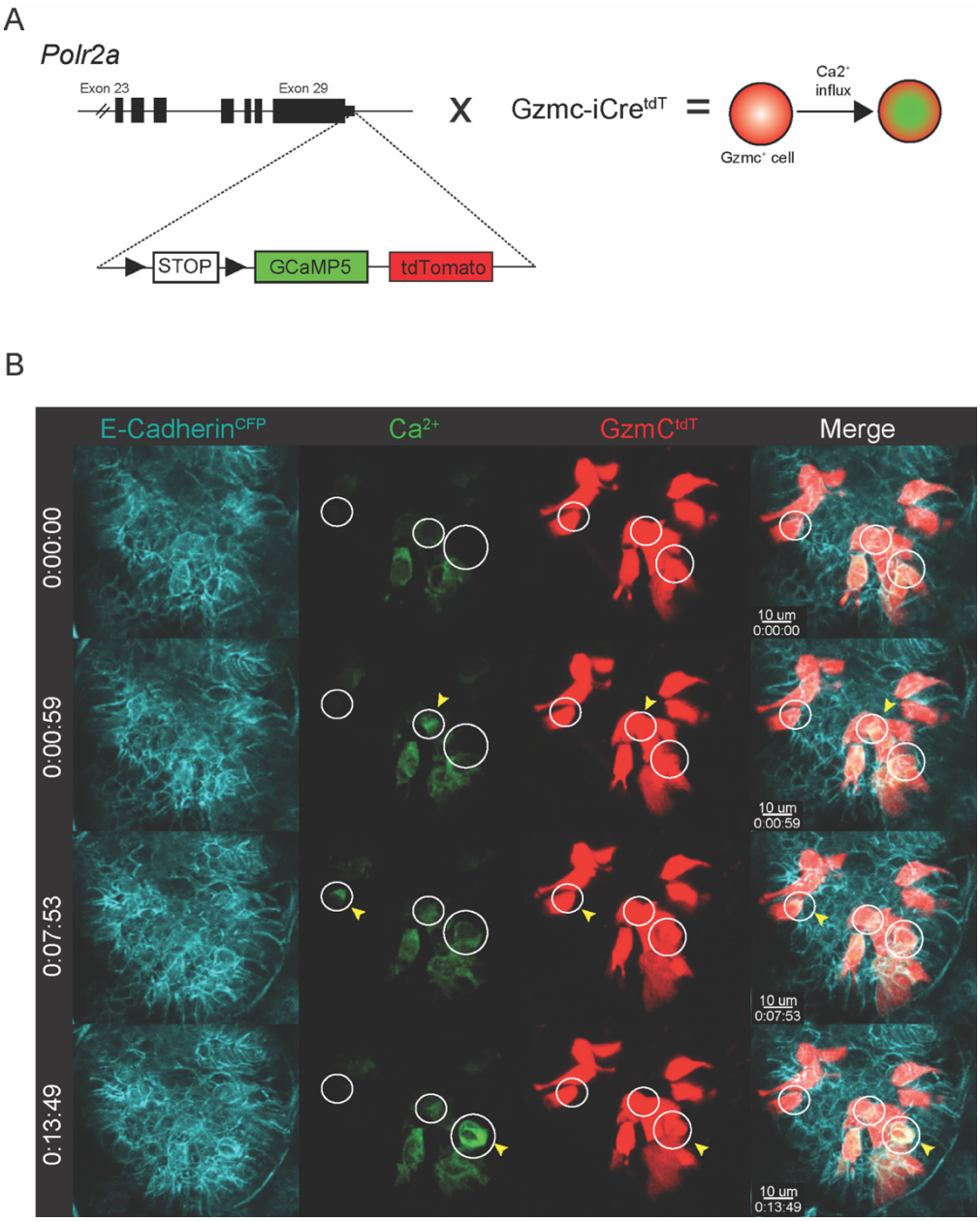

Figure 3.16 Tissue-resident innate lymphocytes are active but stationary within tumor masses

A. Simple diagram describing the calcium reporter mouse crossed to the GzmC-iCre^{tdT} mouse and the resulting fluorescent cellular phenotype that results when calcium signaling is sensed in GzmC-iCre^{tdT+} cells. **B.** Still images of live imaging time lapse of a mammary gland from a 13-week-old PyMT mouse with E-cadherin^{CFP} (teal), Ca^{2+}(green), GzmC-iCre^{tdT} (red) and DAPI (blue). Scale bar, 10 uM. Circles denote cells in which we observe a calcium flux, indicated by a yellow arrow.

3.2.5 Cancer cell-expressed IL-15 dictates tissue-resident innate lymphocyte responses in tumor

Given the close localization of tissue-resident cytotoxic innate lymphocytes with cancer cells, we explored the possibility that cancer cells themselves might be the source of IL-15 driving tissue-resident innate lymphocyte responses in the tumor. To determine whether IL-15 was induced following cell transformation, we analyzed IL-15$^{2a\text{-}eGFP}$ reporter expression in CD24^{+}CD29^{+}EpCAM^{+} mammary epithelial cells from virgin mammary glands and PyMT tumors (Fig. 3.17A). Indeed, a higher level of IL-15 was detected in cancer cells compared to non-transformed mammary epithelia (Fig. 3.17B). To investigate the function of cancer cell-derived IL-15, we crossed Mrp8-Cre mice to the *Il15*$^{fl/fl}$PyMT background. Strikingly, although splenic NK cells were unaffected in Mrp8-Cre*Il15*$^{fl/fl}$PyMT mice (Fig. 3.18A-B), total CD3^{-}NK1.1^{+} innate lymphocytes and the CD49a^{+}CD103^{+} tissue-resident subset were severely reduced in tumors from these mice (Fig. 3.19A-B). In addition, the remaining tissue-resident innate lymphocytes had reduced expression of granzyme B (Fig. 3.19C), suggesting decreased cytotoxic activity. Accompanying these cellular defects, Mrp8-Cre*Il15*$^{fl/fl}$PyMT mice displayed significant acceleration of tumor growth compared to controls (Fig. 3.19D). Collectively, these findings demonstrate that cancer cell-derived IL-15 regulates the expansion and effector function of tissue-resident cytotoxic innate lymphocytes, and that loss of this response is correlated with impaired cancer immunosurveillance.

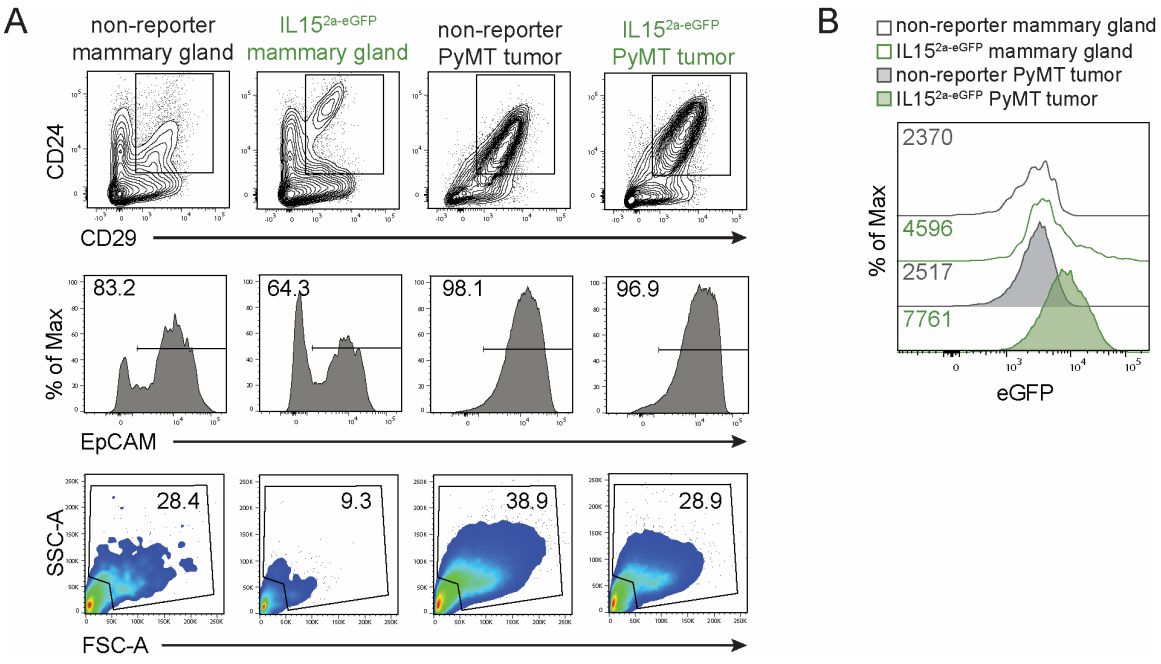

Figure 3.17 IL-15 expression is induced in PyMT cancer cells

A. Gating strategy for determining eGFP expression in $CD24^{+}CD29^{+}EpCAM^{+}$ epithelial cells in the indicated tissues. **B.** Flow cytometric analysis of eGFP expression in $CD24^{+}CD29^{+}EpCAM^{+}$ epithelial cells from pooled mammary tissue of 20-week-old $IL15^{2a\text{-}eGFP}$PyMT (green solid), $IL15^{2a\text{-}eGFP}$ (green empty), PyMT (gray filled) or wild-type mouse (gray empty). Numbers represent MFI. Plot is representative of 2 independent experiments

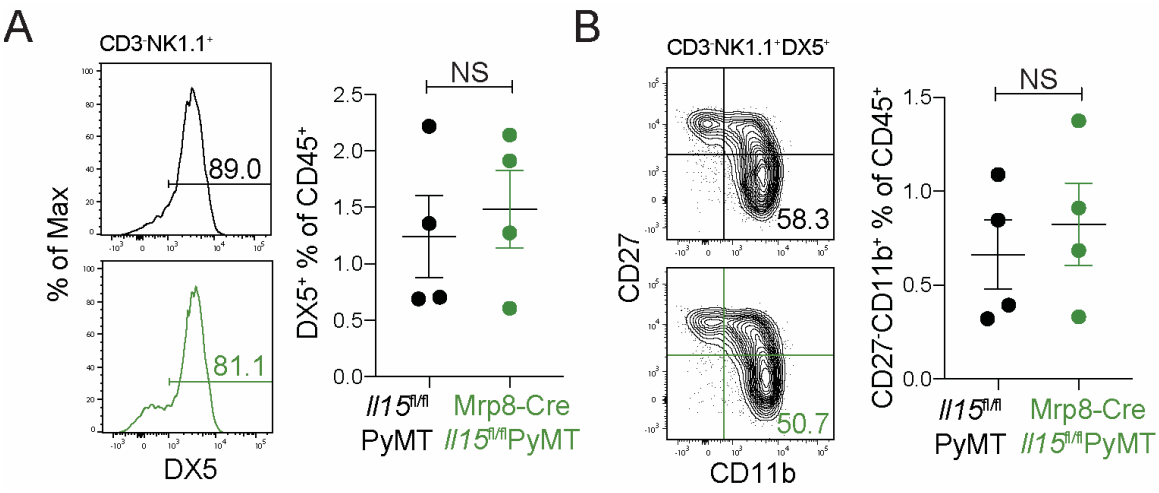

Figure 3.18 Splenic NK cells are unaffected in Mrp8-Cre*Il15*$^{fl/fl}$PyMT mice

A. (Left) Representative histograms of CD49b (DX5) expression among total CD3$^-$ NK1.1$^+$ cells in spleens of the indicated mouse genotype. (Right) Percentage of DX5$^+$ cells quantified out of total splenic CD45$^+$ immune cells. **B.** (Left) Representative plots of CD27 and CD11b expression among total CD3$^-$NK1.1$^+$DX5$^+$ cells in spleens of the indicated mouse genotype. (Right) Percentage of DX5$^+$CD11b$^+$CD27$^-$ cells quantified out of total splenic CD45$^+$ immune cells. **A, B.** Each dot represents an individual mouse (n = 4). Data are pooled from 3 independent experiments. All error bars represent the mean ± SEM. Two-tailed unpaired t test was used for statistical analysis, NS = non-significant.

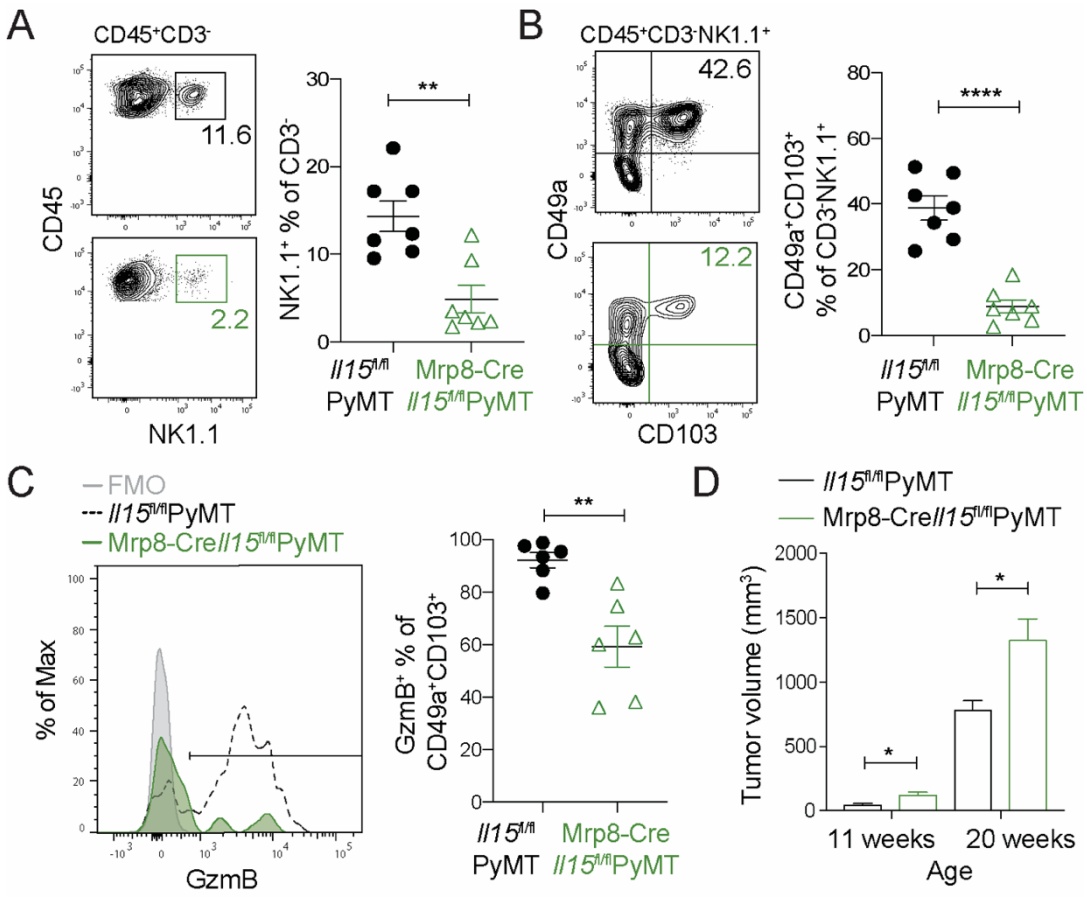

Figure 3.19 Cancer cell-expressed IL-15 dictates tissue-resident innate lymphocyte responses in tumor

A. Representative plot and quantification of percentage of NK1.1^{+} cells out of total CD3^{-} cells isolated from pooled tumors of 20-24-week-old *Il15*$^{fl/fl}$PyMT or Mrp8-Cre*Il15*$^{fl/fl}$PyMT mice. Each dot represents an individual mouse (n = 7 for each genotype). Data are pooled from 3 or more independent experiments. **B.** Representative plot and quantification of percentage of CD49a^{+}CD103^{+} cells out of total CD45^{+}CD3^{-} NK1.1^{+} cells isolated from pooled tumors of 20-24-week-old *Il15*$^{fl/fl}$PyMT or Mrp8-Cre*Il15*$^{fl/fl}$PyMT mice. Each dot represents an individual mouse (n = 7 for each genotype). Data are pooled from 3 or more independent experiments. **C.** (Left) Representative histogram of granzyme B expression in CD49a^{+}CD103^{+} innate lymphocytes from pooled tumors of 20-24-week-old IL15$^{fl/fl}$PyMT or Mrp8-CreIL15$^{fl/fl}$PyMT mice. (Right) Quantification of percentage of granzyme B^{+} CD49a^{+}CD103^{+} innate lymphocytes. Each dot represents an individual mouse (n = 6 for each genotype). Data are pooled from 3 independent experiments. **D.** Total tumor burden of *Il15*$^{fl/fl}$PyMT and Mrp8-Cre*Il15*$^{fl/fl}$PyMT mice monitored between 11 and 20 weeks of age (n = 11-17). All error bars represent the mean ± SEM. Two-tailed unpaired t test was used for all statistical analyses, *p<0.05, **p<0.01, ****p<0.0001

3.3 Conclusions

In this study, we sought to understand the mechanisms of regulation of cytotoxic innate lymphocytes in tumor tissue. MHC class I molecules play an important role in modulating innate lymphocyte effector function as interaction with inhibitory receptors results in suppression of target cell killing. Since both human and mouse tissue-resident innate lymphocytes express the inhibitory NKG2A, we sought to understand if expression of NKG2A on tissue-resident cytotoxic innate lymphocytes had any functional relevance. In addition, we deleted all MHC class I molecules specifically from tumor cells to remove this inhibitory signal and test the NK cell "missing self" process in this PyMT tumor context. Loss of signaling through interaction with MHC class I molecules had no effect on the phenotype or function of tissue-resident cytotoxic innate lymphocytes in PyMT tumors.

However, experiments in both human and mouse suggested that IL-15 is a crucial signal dictating the phenotype and function of tissue-resident cytotoxic innate lymphocytes. We utilized genetic mouse models in which *Il15* could be deleted within specific cellular compartments to uncover the mechanism by which IL-15 regulates these cells of interest.

3.3.1 MHC class I signaling in PyMT tumors

Using a loss of function model whereby the interaction of NKG2A with Qa1 is disrupted by a point mutation in the Qa1 gene, we observed that loss of this inhibitory signaling pathway did not result in any significant changes to the abundance or cytotoxic phenotype of tissue-resident innate lymphocytes. There was also no difference in tumor

growth over time. Similarly, no abundance or phenotypic differences in $CD49a^{+}CD103^{+}$ innate lymphocytes were detected in PyMT tumors on the *Klrc1*$^{-/-}$ background. The lack of phenotype could potentially be due to redundancy of other inhibitory receptors such as the Ly49 family [127, 128].

Intriguingly, we did not observe any significant differences in effector function or tumor growth in the absence of cancer-cell expressed MHC class I molecules. It is interesting that loss of such a strong inhibitory signal did not result in enhanced activation or decreased tumor burden; however, a potential caveat of this experiment is that Mrp8-Cre is expressed in only ~80% of cancer cells. Therefore, the remaining transformed mammary epithelial cells may express sufficient MHC class I molecules to maintain inhibition. Relatedly, lack of phenotype could be explained by "tuning", whereby NK cells that find themselves in a different MHC class I milieu "tune" their responsiveness based on their new environment [129-132]. The integration of activating and inhibitory signals is what dictates NK cell responsiveness to target cells. One intriguing possibility is that in epithelial niches or under conditions of tissue-residency, other inhibitory signals exist and may outweigh the loss of inhibitory signaling from MHC class I molecules.

3.3.2 Regulation of tissue-resident cytotoxic innate lymphocytes by IL-15

As the IL-15-dependent tissue-resident cytotoxic innate lymphocyte-mediated cancer immunosurveillance response is conserved, we sought to define the precise cellular mechanisms of tumor IL-15 sensing in a murine model of breast cancer. IL-15 plays a well-characterized role in the control of steady-state lymphocyte development and homeostasis, involving hematopoietic and non-hematopoietic sources of IL-15, including

DCs, macrophages, fibroblastic reticular cells in secondary lymphoid organs as well as parenchymal cells in peripheral tissues such as enterocytes, adipocytes, and the hair follicle epithelium [63-65, 67, 73, 74]. Following viral infection or bacterial lipopolysaccharide stimulation, IL-15 is induced in DCs and macrophages, and promotes activation and differentiation of circulating effector and memory NK cells [69, 71, 72]. Here, we show that surprisingly, despite their abundant expression, hematopoietic and mesenchymal stromal cell sources of IL-15 were dispensable for the maintenance and activity of tissue-resident cytotoxic innate lymphocytes (Fig. 3.20). Instead, IL-15 specifically from epithelial cancer cells supports tissue-resident cytotoxic innate lymphocytes in terms of abundance and their anti-tumor function (Fig. 3.20). Such a cell type-specific function of IL-15 is likely due to the nature of its trans-presentation by IL15Rα on the surface of a source cell, thus triggering juxtacrine signaling (Fig. 3.20) [58, 59, 61]. As IL-15 is expressed by multiple cell lineages in the tumor microenvironment, it remains to be determined what additional cancer cell-associated molecular features specifically enable cancer cell-expressed IL-15 to be sensed by cytotoxic innate lymphocytes.

IL-15 expression is regulated at transcriptional and posttranscriptional levels [66]. Future studies will unravel how oncogenic pathways modulate its expression in cancer cells, which may help reveal the fundamental nature of such an extrinsic tumor suppressor pathway. Notably, loss of the *IL15* gene in colon cancer has been associated with reduced lymphocyte proliferation and poor patient outcome [133]. A recent study has also revealed that *IL15* loss occurs in colon cancer metastases that are not subject to adaptive lymphocyte-mediated immunoediting [134], raising the intriguing possibility

that innate lymphocyte sensing of cancer cell-expressed IL-15 plays a critical tumor suppressor function not only in primary tumor growth but also in cancer cell dissemination.

Together, our study uncovers an evolutionarily conserved cancer immunosurveillance mechanism whereby cancer cell-expressed IL-15 functions as an alarmin to be directly sensed by tissue-resident cytotoxic innate lymphocytes. As innate lymphocytes and IL-15 are both actively explored in the clinic for cancer treatment, these findings suggest that distinct differentiation states of innate lymphocytes and the method of IL-15 delivery should be taken into consideration for effective cancer immunotherapy.

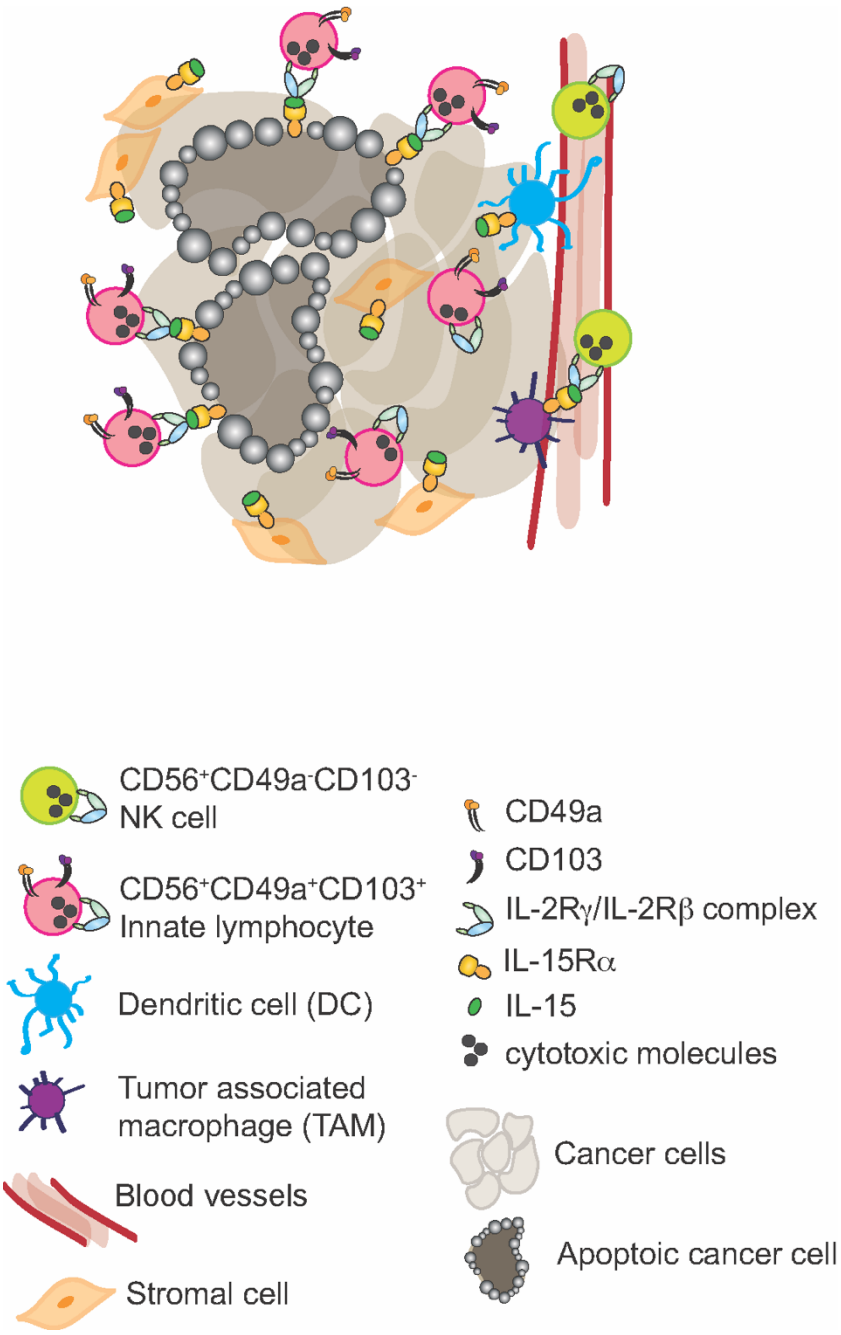

Figure 3.20 Model of tissue-resident innate lymphocyte sensing of and regulation by cancer cell expressed IL-15

3.4 Experimental Procedures

Mice

All in vivo mouse experimental procedures were performed under Sloan Kettering Institute (SKI) Institutional Animal Care and Utilization Committee (IACUC) - approved protocols. Mice were housed in designated specific pathogen-free animal facilities in ventilated cages with at most 5 animals per cage and provided food and water. Only female mice were used in this study. Littermates were used in all experiments when possible, otherwise age-matched cage mates were used. $Qa1^{R72A}$ mice were kindly provided by Dr. Harvey Cantor (Dana-Farber Cancer Institute). *Klrc1*$^{-/-}$ mice were kindly provided by Dr. Marco Colonna (Washington University). CD11c-Cre, FSP1-Cre, Mrp8-Cre, $Rosa26^{LSL-YFP}$ and MMTV-PyMT mice are publicly available (Jackson Laboratories, see Key Resources Table). $IL15^{2a-eGFP}$ mice were generously provided by Dr. Ross Kedl (University of Colorado). $Il15^{fl}$ mice were generated in the Ikuta lab and will be reported elsewhere. Briefly, $Il15^{fl}$ mice were established by flanking exon 5 with two loxP sequences by standard homologous recombination in embryonic stem cells.

Immune cell isolation from mouse tissues

Mouse mammary glands and tumors were prepared by mechanical disruption via mincing with a razor blade followed by treatment with 280 U/ml Collagenase Type 3 (Worthington Biochemical) and 4 μg/ml DNase I (Sigma) in HBSS medium at 37°C for 1 hour with periodic short vortexing. Digested tissues were mashed through 70-μm filters and collected by centrifugation. Cell pellet was resuspended in 44% Percoll, layered on

top of 66% Percoll (Sigma), and centrifuged at 1,900 g for 30 minutes without brake. Cells at the Percoll interface were collected, washed and resuspended in FACS buffer for downstream assays. Spleens were dissected and single cell suspensions were obtained by tissue disruption with glass slides and treated with red blood cell (Ammonium-Chloride-Potassium, ACK) lysis buffer and incubated for 10 minutes at room temperature then washed in PBS prior to staining.

Tumor measurement

Tumors in PyMT mice were measured weekly using a caliper, beginning when a single tumor diameter reached approximately 3-4 mm. Tumor volume was calculated using the equation $[(L \times W^2) \times (\pi/6)]$ where "L"=length and "W"=width. Individual tumor volumes were added together to calculate total tumor burden per mouse.

Flow cytometry

For flow cytometry experiments, cells were pre-incubated with 2.4G2 mAb (Bio X Cell) to block FcγR binding and then stained with panels of cell surface marker antibodies for 20 min on ice. Fluorochrome conjugated antibodies against mouse CD45 (clone 30-F11), CD49a (Ha31/8), CD103 (M290), Ly6G (1A8), F4/80 (T45-2342), CD11b (M1/70), MHC class II A-A/I-E (M5/114/15/2), and CD11c (N418) were purchased from BD Biosciences. Fluorochrome conjugated antibodies against mouse CD3e (17A2), NK1.1 (PK136), CD19 (D1/CD19), XCR1 (ZET), CD49b (DX5), Ter119 (Ter-119), CD29 (HmB1-1) and EpCAM (G8.8) were purchased from BioLegend. Fluorochrome conjugated antibodies against mouse/human granzyme B (GB11) was purchased from

Invitrogen. Fluorochrome conjugated antibodies against mouse CD27 (LG.7F9), CD31 (390) and CD24 (M1/69) were purchased from eBioscience. Cells were washed 2x with FACS buffer and stained with LIVE/DEAD kit (Invitrogen) or Zombie Live/Dead kit (BioLegend) to exclude dead cells. Intracellular staining was carried out using the FoxP3/Transcription factor Fix/Perm Kit (Tonbo). All samples were acquired with a LSRII flow cytometer (Becton Dickinson) and analyzed with FlowJo software version 9.6.2 or 10.6.1 (Tree Star).

Intravital confocal microscopy

At 12 weeks of age, intravital confocal microscopy of mammary tumors was performed as described [135]. Briefly, mice were anaesthetized using a cocktail of ketamine and xylazine. Anaesthesia was maintained by continuous inhalation of 0.5% isoflurane and mice were kept to 37°C and received oxygen (0.5 L/min). The fur from the lower flank region was trimmed and the area sterilized using Betadine solution. The fourth left or right mammary gland was surgically exposed with a ventral skin incision and a skin flap. The mouse was transferred to a stage heated to 37°C. All imaging was done on an Olympus FVMPE-RS upright Multiphoton microscope fitted with a 25x1.05NA Plan water-immersion objective and a Mai-Tai DeepSee Ti-Sapphire laser (Spectraphysics). Imaging was performed using λ = 910 nm excitation and fluorescence emission was collected in three channels, using the following filter sets: a filter (480/40 nm) for CFP, a second filter (540/20 nm) for GFP and a third filter (605/70 nm) for tdTomato detection. Time-lapse images were acquired by scanning at 1024 x 1024 pixels with a z-step size of 3-4 μm and a total z-volume 50-100 μm, at 30 to 60 seconds intervals.

Immunofluorescence

Tumors were harvested from E-Cadherin^{CFP}GzmC-iCre^{tdT}PyMT mice and fixed in Periodate-Lysine-Paraformaldehyde (PLP) for 16-24h, 30% sucrose for 24h, then frozen in OCT. Tissue was sectioned at 20um thickness, blocked for 30 min and stained with Hoechst and a fluorescently conjugated antibody against PyMT (Thermo Fisher Scientific, catalog number MA1-46061) overnight at 4°C. Slides were washed and stained with secondary antibody (goat anti-rat AF488, Life Technologies catalog number A-11006). Images were taken on confocal microscope using 4 color channels.

Statistical analysis

Spearman's correlation, log-rank and Wilcoxon tests were used to calculate statistical significance where appropriate. Two tailed unpaired t tests and one-way ANOVA were conducted using Prism 7 software. A value of $P<0.05$ was considered statistically significant.

3.5 Acknowledgements

We would like to thank Dr. Efstathios Stamatiades, a previous Li Lab member, for the immunofluorescence and intravital imaging data. Thank you to Briana Nixon for generating the GzmC^{iCre} mouse. Thank you to the laboratories of Dr. Harvey Cantor, Dr. Marco Colonna, Dr. Koichi Ikuta and Dr. Ross Kedl for mouse strains critical to this project.

Chapter 4: SUMMARY AND DISCUSSION

The first step in combating a pathogenic challenge is detecting the infected or otherwise aberrant cell as harmful, or as "non-self". Cancer represents a challenge to this notion, as cancer is not a foreign entity. Instead, tumors arise from host cells. Effective elimination therefore depends not only on cancer cells distinguishing themselves from healthy host cells, but cytotoxic lymphocytes sensing and detecting the diseased cells. For adaptive $CD8^+$ T cells, detection and elimination is reliant on expression and presentation of neoantigens by MHC class I molecules. For natural killer cells, germline encoded receptors can detect the loss of MHC class I molecules through "missing self" recognition or can detect the upregulated surface expression of stress-induced molecules through "induced self". Still, the output of NK cell effector function is dictated by the integration of activating and inhibitory signals experienced through receptor engagement of ligands, some of which are more dominant than others [31]. While many of the ligands and the major receptors involved have been identified, the signaling events that lead to activation and the specificity of many receptors remains to be elucidated. On top of that, the nature of and extent to which these mechanisms promote direct NK cell killing in solid tumors is not well understood. Furthermore, little is known about the roles of tissue-resident innate lymphocytes or NK cells in mediating solid tumor destruction, especially in human cancers. This dissertation explored the anti-tumor cytotoxic immune responses induced in human renal cell carcinoma and investigated mechanisms of regulation of tissue-resident cytotoxic innate lymphocytes by MHC class I and IL-15 utilizing a mouse model of breast cancer.

In clear RCC, infiltration of $CD56^+$ NK cells has been reported to correlate with more favorable prognosis [8, 109]. However, the activity of these NK cells leading to better overall survival have not been extensively investigated. In our studies, we identified induction of $CD56^{bright}$ $CD49a^+CD103^+$ innate lymphocytes in tumors of RCC patients. While both clear cell and chromophobe RCC tumors were infiltrated by $CD56^{bright}$ $CD49a^+CD103^+$ innate lymphocytes, their abundance, phenotype and functional relevance were distinct. In ccRCC tumors, this response was induced concurrently with a phenotypically exhausted, functionally irrelevant $CD8^+$ T cell response. Chromophobe RCC tumors, on the other hand, did not have an accumulation of PD-1^+ $CD8^+$ T cells and the $CD56^{bright}$ $CD49a^+CD103^+$ innate lymphocyte response represented the only relevant cytotoxic program. The $CD56^{bright}$ $CD49a^+CD103^+$ innate lymphocyte population expressed high levels of granzyme A in chRCC tumors, but not ccRCC tumors, and the IL_2 signature correlated with better overall survival in chRCC but worse outcome in ccRCC, suggesting histology-specific microenvironmental regulation at play. It is intriguing to imagine the possibility that the presence of a type 1 $CD8^+$ T cell response may inhibit the cytotoxic program of tissue-resident $CD56^{bright}$ innate lymphocytes, either directly or indirectly. Competition for cytokines like IL-2 and IL-15 in the tumor microenvironment could account for the limited accumulation of tissue-resident $CD56^{bright}$ innate lymphocytes in ccRCC tumors, as well as their reduced granzyme expression. As another possibility, dysregulated $CD8^+$ T cells present in ccRCC tumors may directly dampen tissue-resident $CD56^{bright}$ innate lymphocyte expression of granzymes.

In our genetic mouse model studies, we did not find evidence of a functional importance of signaling through MHC class I molecules for the anti-tumor innate lymphocyte response in PyMT tumors. Loss of binding of NKG2A to Qa1, total loss of NKG2A expression and deletion of *B2M* from tumor cells resulting in ablation of all MHC class I molecule expression had no impact on the abundance or effector program of tissue-resident innate lymphocytes, nor did it affect tumor growth in the PyMT model. The concepts of NK cell education and licensing enabled through interaction with MHC class I molecules are complex. While deletion of NKG2A represents loss of one major mode of inhibition, inhibitory Ly49 receptor signaling may compensate, as reports have previously shown NKG2A deficient NK cells are only mildly affected [128]. On the other hand, a recent study demonstrated that education of uterine NK (uNK) cells via NKG2A was required for optimal uNK function in mouse and human [136]. It is therefore possible that *Klrc1*-deficient NK cells were sub-optimally educated and thus hypofunctional in the tumor environment.

In utilizing the Mrp8-Cre line, we targeted deletion of *B2M* specifically to transformed mammary epithelial cells. While we hypothesized that inhibitory receptor positive innate lymphocytes would detect and eliminate MHC class I negative transformed cancer cells as they arise, the possibility remains that the innate lymphocytes were tuned or re-calibrated to the lower MHC class I environment [137]. Another consideration is the ability for cancer cells to escape NK cell mediated immunosurveillance through shedding of ligands or as a result of an overall immunosuppressive tumor microenvironment, both of which have been shown in mouse and human models [138].

Importantly, we found that detection of cancer cells by tissue-resident cytotoxic innate lymphocytes was dependent on cancer-cell expression of IL-15, and this direct sensing was a key determinant of effector function. Transcript levels of IL-15 were higher in chRCC tumors compared to ccRCC tumors, hinting that the magnitude of the innate lymphocyte response is tuned to the level of IL-15 signaling. Why would cancer cells upregulate IL-15? There is evidence for IL-15 operating as a danger signal within distressed tissues, but mainly as a cytokine within the environmental milieu that regulates the functional phenotype of immune cells towards mediating tissue destruction [139]. Interestingly, IL-15 expression in the gut epithelium and lamina propria was necessary for induction of villous atrophy and tissue destruction in a mouse model of coeliac disease [140]. Overexpression of IL-15 in transplantable tumor cells resulted in their elimination by cytotoxic lymphocytes in an antigen-independent manner, suggesting that IL-15 itself or other activating receptors in concert with IL-15 led to tumor cell destruction [141]. These studies lay precedent to the idea that IL-15 may become dysregulated in tissues, resulting in the direct activation of immune responses leading to tissue destruction. Our data suggests that IL-15 not only functions to enhance effector cell function for tumor control, but also enables tissue-resident innate lymphocytes to sense stressed, transformed tissues.

In RCC, clear cell and chromophobe are quite distinct in terms of their genetic and molecular characteristics, as well as their cell of origin, two factors that may regulate level of IL-15 expression in cancer cells. While the majority of both ccRCC and chRCC tumors are characterized by mutations in tumor suppressor genes, *VHL* in ccRCC and *FLCN* and *PTEN* in chRCC, chRCC tumors also have very high incidence of loss of

heterozygosity at multiple chromosomal locations [87]. This suggests that chRCC tumors are more genetically unstable, potentially resulting in more highly dysregulated cancer cells. This increase level in stress or cellular damage likely disrupts cellular homeostasis, a response of which may induce expression of IL-15 or other danger signals. The reaction to IL-15 expressed on distressed cells by local, tissue-resident cells is possibly an evolved host defense mechanism to detect aberrations to host cells.

Our studies suggest that $CD49a^{+}CD103^{+}$ innate lymphocytes are poised within tissues to combat local challenges. In human RCC patient samples, we observed a low percentage of $CD56^{bright}$ $CD49a^{+}CD103^{+}$ innate lymphocytes already present in adjacent normal kidney tissue. However, whether the accumulation of $CD56^{bright}$ $CD49a^{+}CD103^{+}$ innate lymphocytes in RCC tumors is the result of local expansion or recruitment into the tissue is unclear. In contrast to the $CD56^{bright}$ innate lymphocytes, $CD56^{dim}$ innate lymphocytes expressed a circulatory profile as exemplified by expression of *S1PR5, KLF2* and *CX3CR1*. These distinct localizations have implications for immunosurveillance. Circulating cells, like NK cells found in the blood, are poised to encounter systemic challenges that circulate throughout the body's blood stream and lymphatic system, in particular viral infections or hematological cancers. Similar to circulating $CD8^{+}$ T cells, who are primed by DCs in secondary lymphoid organs (SLO), circulating NK cells are likely to receive help in the form of cytokine production by APCs in SLO. Indeed, we report as others have that NK cells in the spleen require IL-15 expressed by myeloid cells for their survival and maturation.

It has been proposed and largely accepted that the two subsets of NK cells we observed in RCC patient tissues are linearly related [142]. $CD56^{bright}CD16^{+/-}$ ($CD56^{bright}$)

cells are found at very low frequency in the circulation but dominantly in tissues, while $CD56^{dim}CD16^{+}$ ($CD56^{dim}$) cells are found predominantly in the circulation. Canonically, $CD56^{bright}$ NK cells are thought to be the immediate precursor to $CD56^{dim}$ NK cells. With the recent advancement of ILC lineage elucidated in mice, whether these two populations indeed represent linear steps along a differentiation pathway or in fact are derived from distinct progenitors is not yet fully elucidated. Evidence exists for an NK-committed precursor found in the fetal liver, fetal bone marrow, adult bone marrow and tonsils that had no helper-ILC potential [143]. On the other hand, a recent study discovered a circulating ILC progenitor (ILCp) that could give rise to ILC1, ILC2 and ILC3, as well as a $CD56^{+}$ population that could seed the tissue [144]. Further description of the $CD56^{+}$ population in terms of level of expression and concurrent CD16 expression was not done. It therefore remains to be seen if $CD56^{bright}$, $CD56^{dim}$ or both can be derived from a circulating ILCp. While $CD56^{dim}$ NK cells have been observed in sites such as the lung and small intestine, whether or not $CD56^{dim}$ NK cells either from blood or tissue can convert to $CD49a^{+}CD103^{+}$ $CD56^{bright}$ cells in tissues remains unknown [145].

In our studies, loss of hematopoietic sources of IL-15 resulted in a reduction of circulating NK cells but had no effect on tissue-resident innate lymphocytes. Instead, local IL-15 signaling within the tissue was required to sustain the abundance and effector function of $CD3^{-}NK1.1^{+}$ $CD49a^{+}CD103^{+}$ innate lymphocytes. In addition to arguing against the conversion of circulating NK cells to tissue-resident cells, these data suggest that the distinct niche in which these cells reside provide the signals necessary for activation and/or homeostasis. Does that imply circulating and tissue-resident innate lymphocytes should be classified as discrete classes or subsets? Their fates may be

imprinted upon them during development or differentiation based on signals they receive, similar to how the recently described subsets of memory $CD8^+$ T cells differentiate from effector $CD8^+$ T cells with differing expression of CX3CR1 [146]. As the lineage and origin of discrete lymphocyte subsets continue to be elucidated, distinct differentiation states and localization of innate should be taken into consideration for effective, targeted cancer immunotherapy.

The work described in this dissertation adds knowledge to the classes of anti-tumor immune responses induced in human and murine tumors. We have shown that subtypes of cancer can have vastly different cytotoxic immune responses, which are regulated by cues received from the tumor microenvironment. Importantly, we demonstrated that IL-15 is a master regulator of phenotype and function of tissue-resident cytotoxic innate lymphocytes in both human and mouse tumors, and that subsets of innate lymphocytes have distinct requirements for cell-contact dependent IL-15 signaling depending on their localization. Significantly, we have shown that IL-15 expressed specifically by cancer cells is sensed by cytotoxic innate lymphocytes that accumulate in transformed tissue, likely representing an evolved mechanism of detection of cellular stress by tissue-resident innate lymphocytes serving as sentinels of tissue homeostasis.

REFERENCES

1. Chowdhury, D. and J. Lieberman, *Death by a thousand cuts: granzyme pathways of programmed cell death.* Annu Rev Immunol, 2008. **26**: p. 389-420.
2. Wang, S. and W.S. El-Deiry, *TRAIL and apoptosis induction by TNF-family death receptors.* Oncogene, 2003. **22**(53): p. 8628-33.
3. Germain, R.N., *T-cell development and the CD4-CD8 lineage decision.* Nat Rev Immunol, 2002. **2**(5): p. 309-22.
4. Schenkel, J.M. and D. Masopust, *Tissue-resident memory T cells.* Immunity, 2014. **41**(6): p. 886-97.
5. Masopust, D. and A.G. Soerens, *Tissue-Resident T Cells and Other Resident Leukocytes.* Annu Rev Immunol, 2019. **37**: p. 521-546.
6. McLane, L.M., M.S. Abdel-Hakeem, and E.J. Wherry, *CD8 T Cell Exhaustion During Chronic Viral Infection and Cancer.* Annu Rev Immunol, 2019. **37**: p. 457-495.
7. Chen, D.S. and I. Mellman, *Elements of cancer immunity and the cancer-immune set point.* Nature, 2017. **541**(7637): p. 321-330.
8. Chiossone, L., et al., *Natural killer cells and other innate lymphoid cells in cancer.* Nat Rev Immunol, 2018. **18**(11): p. 671-688.
9. Yokoyama, W.M., *The search for the missing 'missing-self' receptor on natural killer cells.* Scand J Immunol, 2002. **55**(3): p. 233-7.
10. Ljunggren, H.G. and K. Karre, *In search of the 'missing self': MHC molecules and NK cell recognition.* Immunol Today, 1990. **11**(7): p. 237-44.

11. Raulet, D.H. and N. Guerra, *Oncogenic stress sensed by the immune system: role of natural killer cell receptors.* Nat Rev Immunol, 2009. **9**(8): p. 568-80.

12. Morvan, M.G. and L.L. Lanier, *NK cells and cancer: you can teach innate cells new tricks.* Nat Rev Cancer, 2016. **16**(1): p. 7-19.

13. Vivier, E., et al., *Innate Lymphoid Cells: 10 Years On.* Cell, 2018. **174**(5): p. 1054-1066.

14. Dadi, S., et al., *Cancer Immunosurveillance by Tissue-Resident Innate Lymphoid Cells and Innate-like T Cells.* Cell, 2016. **164**(3): p. 365-77.

15. Glasner, A., et al., *Recognition and prevention of tumor metastasis by the NK receptor NKp46/NCR1.* J Immunol, 2012. **188**(6): p. 2509-15.

16. Halfteck, G.G., et al., *Enhanced in vivo growth of lymphoma tumors in the absence of the NK-activating receptor NKp46/NCR1.* J Immunol, 2009. **182**(4): p. 2221-30.

17. Smyth, M.J., *NK cells and NKT cells collaborate in host protection from methylcholanthrene-induced fibrosarcoma.* Int Immunol, 2008. **20**(4): p. 631.

18. Bjorkstrom, N.K., H.G. Ljunggren, and J. Michaelsson, *Emerging insights into natural killer cells in human peripheral tissues.* Nat Rev Immunol, 2016. **16**(5): p. 310-20.

19. Cichocki, F., B. Grzywacz, and J.S. Miller, *Human NK Cell Development: One Road or Many?* Front Immunol, 2019. **10**: p. 2078.

20. Huntington, N.D., J. Cursons, and J. Rautela, *The cancer-natural killer cell immunity cycle.* Nat Rev Cancer, 2020. **20**(8): p. 437-454.

21. Burnet, M., *Cancer: a biological approach. III. Viruses associated with neoplastic conditions. IV. Practical applications.* Br Med J, 1957. **1**(5023): p. 841-7.

22. Schumacher, T.N. and R.D. Schreiber, *Neoantigens in cancer immunotherapy.* Science, 2015. **348**(6230): p. 69-74.

23. Sharma, P. and J.P. Allison, *Immune checkpoint targeting in cancer therapy: toward combination strategies with curative potential.* Cell, 2015. **161**(2): p. 205-14.

24. Motzer, R.J., M.B. McHenry, and A.C. Chen, *Immune Checkpoint Blockade in Advanced Renal-Cell Carcinoma.* N Engl J Med, 2018. **379**(1): p. 92-93.

25. Baumeister, S.H., et al., *Coinhibitory Pathways in Immunotherapy for Cancer.* Annu Rev Immunol, 2016. **34**: p. 539-73.

26. Savage, P.A., et al., *Recognition of a ubiquitous self antigen by prostate cancer-infiltrating CD8+ T lymphocytes.* Science, 2008. **319**(5860): p. 215-20.

27. Willimsky, G. and T. Blankenstein, *Sporadic immunogenic tumours avoid destruction by inducing T-cell tolerance.* Nature, 2005. **437**(7055): p. 141-6.

28. Dunn, G.P., et al., *Cancer immunoediting: from immunosurveillance to tumor escape.* Nat Immunol, 2002. **3**(11): p. 991-8.

29. Hegde, P.S. and D.S. Chen, *Top 10 Challenges in Cancer Immunotherapy.* Immunity, 2020. **52**(1): p. 17-35.

30. Pardoll, D., *Cancer and the Immune System: Basic Concepts and Targets for Intervention.* Semin Oncol, 2015. **42**(4): p. 523-38.

31. Long, E.O., et al., *Controlling natural killer cell responses: integration of signals for activation and inhibition.* Annu Rev Immunol, 2013. **31**: p. 227-58.

32. Parham, P. and A. Moffett, *Variable NK cell receptors and their MHC class I ligands in immunity, reproduction and human evolution.* Nat Rev Immunol, 2013. **13**(2): p. 133-44.

33. Rahim, M.M., et al., *Ly49 receptors: innate and adaptive immune paradigms.* Front Immunol, 2014. **5**: p. 145.

34. Karre, K., et al., *Selective rejection of H-2-deficient lymphoma variants suggests alternative immune defence strategy.* Nature, 1986. **319**(6055): p. 675-8.

35. Raulet, D.H., *Missing self recognition and self tolerance of natural killer (NK) cells.* Semin Immunol, 2006. **18**(3): p. 145-50.

36. Anfossi, N., et al., *Human NK cell education by inhibitory receptors for MHC class I.* Immunity, 2006. **25**(2): p. 331-42.

37. Kim, S., et al., *Licensing of natural killer cells by host major histocompatibility complex class I molecules.* Nature, 2005. **436**(7051): p. 709-13.

38. Shifrin, N., D.H. Raulet, and M. Ardolino, *NK cell self tolerance, responsiveness and missing self recognition.* Semin Immunol, 2014. **26**(2): p. 138-44.

39. Boudreau, J.E., et al., *Cell-Extrinsic MHC Class I Molecule Engagement Augments Human NK Cell Education Programmed by Cell-Intrinsic MHC Class I.* Immunity, 2016. **45**(2): p. 280-91.

40. Hanke, T., et al., *Direct assessment of MHC class I binding by seven Ly49 inhibitory NK cell receptors.* Immunity, 1999. **11**(1): p. 67-77.

41. Aldrich, C.J., et al., *Identification of a Tap-dependent leader peptide recognized by alloreactive T cells specific for a class Ib antigen.* Cell, 1994. **79**(4): p. 649-58.

42. DeCloux, A., et al., *Dominance of a single peptide bound to the class I(B) molecule, Qa-1b.* J Immunol, 1997. **158**(5): p. 2183-91.

43. Kurepa, Z., C.A. Hasemann, and J. Forman, *Qa-1b binds conserved class I leader peptides derived from several mammalian species.* J Exp Med, 1998. **188**(5): p. 973-8.

44. Braud, V.M., et al., *HLA-E binds to natural killer cell receptors CD94/NKG2A, B and C.* Nature, 1998. **391**(6669): p. 795-9.

45. Rodgers, J.R. and R.G. Cook, *MHC class Ib molecules bridge innate and acquired immunity.* Nat Rev Immunol, 2005. **5**(6): p. 459-71.

46. Vance, R.E., et al., *Mouse CD94/NKG2A is a natural killer cell receptor for the nonclassical major histocompatibility complex (MHC) class I molecule Qa-1(b).* J Exp Med, 1998. **188**(10): p. 1841-8.

47. Kaiser, B.K., et al., *Structural basis for NKG2A/CD94 recognition of HLA-E.* Proc Natl Acad Sci U S A, 2008. **105**(18): p. 6696-701.

48. Kambayashi, T., et al., *The nonclassical MHC class I molecule Qa-1 forms unstable peptide complexes.* J Immunol, 2004. **172**(3): p. 1661-9.

49. Petrie, E.J., et al., *CD94-NKG2A recognition of human leukocyte antigen (HLA)-E bound to an HLA class I leader sequence.* J Exp Med, 2008. **205**(3): p. 725-35.

50. Burshtyn, D.N., et al., *Recruitment of tyrosine phosphatase HCP by the killer cell inhibitor receptor.* Immunity, 1996. **4**(1): p. 77-85.

51. Stebbins, C.C., et al., *Vav1 dephosphorylation by the tyrosine phosphatase SHP-1 as a mechanism for inhibition of cellular cytotoxicity.* Mol Cell Biol, 2003. **23**(17): p. 6291-9.

52. Gleimer, M. and P. Parham, *Stress management: MHC class I and class I-like molecules as reporters of cellular stress.* Immunity, 2003. **19**(4): p. 469-77.

53. Bauer, S., et al., *Activation of NK cells and T cells by NKG2D, a receptor for stress-inducible MICA.* Science, 1999. **285**(5428): p. 727-9.

54. Lanier, L.L., *NKG2D Receptor and Its Ligands in Host Defense.* Cancer Immunol Res, 2015. **3**(6): p. 575-82.

55. Abel, A.M., et al., *Natural Killer Cells: Development, Maturation, and Clinical Utilization.* Front Immunol, 2018. **9**: p. 1869.

56. Kennedy, M.K., et al., *Reversible defects in natural killer and memory CD8 T cell lineages in interleukin 15-deficient mice.* J Exp Med, 2000. **191**(5): p. 771-80.

57. Lodolce, J.P., et al., *IL-15 receptor maintains lymphoid homeostasis by supporting lymphocyte homing and proliferation.* Immunity, 1998. **9**(5): p. 669-76.

58. Burkett, P.R., et al., *Coordinate expression and trans presentation of interleukin (IL)-15Ralpha and IL-15 supports natural killer cell and memory CD8+ T cell homeostasis.* J Exp Med, 2004. **200**(7): p. 825-34.

59. Dubois, S., et al., *IL-15Ralpha recycles and presents IL-15 In trans to neighboring cells.* Immunity, 2002. **17**(5): p. 537-47.

60. Lodolce, J.P., et al., *T cell-independent interleukin 15Ralpha signals are required for bystander proliferation.* J Exp Med, 2001. **194**(8): p. 1187-94.

61. Sandau, M.M., et al., *Cutting edge: transpresentation of IL-15 by bone marrow-derived cells necessitates expression of IL-15 and IL-15R alpha by the same cells.* J Immunol, 2004. **173**(11): p. 6537-41.

62. Mishra, A., L. Sullivan, and M.A. Caligiuri, *Molecular pathways: interleukin-15 signaling in health and in cancer.* Clin Cancer Res, 2014. **20**(8): p. 2044-50.

63. Castillo, E.F. and K.S. Schluns, *Regulating the immune system via IL-15 transpresentation.* Cytokine, 2012. **59**(3): p. 479-90.

64. Cui, G., et al., *Characterization of the IL-15 niche in primary and secondary lymphoid organs in vivo.* Proc Natl Acad Sci U S A, 2014. **111**(5): p. 1915-20.

65. Gil-Cruz, C., et al., *Fibroblastic reticular cells regulate intestinal inflammation via IL-15-mediated control of group 1 ILCs.* Nat Immunol, 2016. **17**(12): p. 1388-1396.

66. Waldmann, T.A. and Y. Tagaya, *The multifaceted regulation of interleukin-15 expression and the role of this cytokine in NK cell differentiation and host response to intracellular pathogens.* Annu Rev Immunol, 1999. **17**: p. 19-49.

67. Castillo, E.F., et al., *Dendritic cells support the in vivo development and maintenance of NK cells via IL-15 trans-presentation.* J Immunol, 2009. **183**(8): p. 4948-56.

68. Ferlazzo, G., et al., *Distinct roles of IL-12 and IL-15 in human natural killer cell activation by dendritic cells from secondary lymphoid organs.* Proc Natl Acad Sci U S A, 2004. **101**(47): p. 16606-11.

69. Mortier, E., et al., *Macrophage- and dendritic-cell-derived interleukin-15 receptor alpha supports homeostasis of distinct CD8+ T cell subsets.* Immunity, 2009. **31**(5): p. 811-22.

70. Sosinowski, T., et al., *CD8alpha+ dendritic cell trans presentation of IL-15 to naive CD8+ T cells produces antigen-inexperienced T cells in the periphery with memory phenotype and function.* J Immunol, 2013. **190**(5): p. 1936-47.

71. Colpitts, S.L., et al., *Cutting edge: the role of IFN-alpha receptor and MyD88 signaling in induction of IL-15 expression in vivo.* J Immunol, 2012. **188**(6): p. 2483-7.

72. Mattei, F., et al., *IL-15 is expressed by dendritic cells in response to type I IFN, double-stranded RNA, or lipopolysaccharide and promotes dendritic cell activation.* J Immunol, 2001. **167**(3): p. 1179-87.

73. Adachi, T., et al., *Hair follicle-derived IL-7 and IL-15 mediate skin-resident memory T cell homeostasis and lymphoma.* Nat Med, 2015. **21**(11): p. 1272-9.

74. Liou, Y.H., et al., *Adipocyte IL-15 regulates local and systemic NK cell development.* J Immunol, 2014. **193**(4): p. 1747-58.

75. Mackay, L.K., et al., *Hobit and Blimp1 instruct a universal transcriptional program of tissue residency in lymphocytes.* Science, 2016. **352**(6284): p. 459-63.

76. Le Floc'h, A., et al., *Minimal engagement of CD103 on cytotoxic T lymphocytes with an E-cadherin-Fc molecule triggers lytic granule polarization via a phospholipase Cgamma-dependent pathway.* Cancer Res, 2011. **71**(2): p. 328-38.

77. Bosmuller, H.C., et al., *Combined Immunoscore of CD103 and CD3 Identifies Long-Term Survivors in High-Grade Serous Ovarian Cancer.* Int J Gynecol Cancer, 2016. **26**(4): p. 671-9.

78. Djenidi, F., et al., *CD8+CD103+ tumor-infiltrating lymphocytes are tumor-specific tissue-resident memory T cells and a prognostic factor for survival in lung cancer patients.* J Immunol, 2015. **194**(7): p. 3475-86.

79. Webb, J.R., K. Milne, and B.H. Nelson, *PD-1 and CD103 Are Widely Coexpressed on Prognostically Favorable Intraepithelial CD8 T Cells in Human Ovarian Cancer.* Cancer Immunol Res, 2015. **3**(8): p. 926-35.

80. Workel, H.H., et al., *CD103 defines intraepithelial CD8+ PD1+ tumour-infiltrating lymphocytes of prognostic significance in endometrial adenocarcinoma.* Eur J Cancer, 2016. **60**: p. 1-11.

81. Santana Carrero, R.M., et al., *IL-15 is a component of the inflammatory milieu in the tumor microenvironment promoting antitumor responses.* Proc Natl Acad Sci U S A, 2019. **116**(2): p. 599-608.

82. Guy, C.T., R.D. Cardiff, and W.J. Muller, *Induction of mammary tumors by expression of polyomavirus middle T oncogene: a transgenic mouse model for metastatic disease.* Mol Cell Biol, 1992. **12**(3): p. 954-61.

83. Lin, E.Y., et al., *Progression to malignancy in the polyoma middle T oncoprotein mouse breast cancer model provides a reliable model for human diseases.* Am J Pathol, 2003. **163**(5): p. 2113-26.

84. Cairns, P., *Renal cell carcinoma.* Cancer Biomark, 2010. **9**(1-6): p. 461-73.

85. Ricketts, C.J., et al., *The Cancer Genome Atlas Comprehensive Molecular Characterization of Renal Cell Carcinoma.* Cell Rep, 2018. **23**(1): p. 313-326 e5.

86. George, D.J. and W.G. Kaelin, Jr., *The von Hippel-Lindau protein, vascular endothelial growth factor, and kidney cancer.* N Engl J Med, 2003. **349**(5): p. 419-21.

87. Davis, C.F., et al., *The somatic genomic landscape of chromophobe renal cell carcinoma.* Cancer Cell, 2014. **26**(3): p. 319-330.

88. Storkel, S., et al., *Classification of renal cell carcinoma: Workgroup No. 1. Union Internationale Contre le Cancer (UICC) and the American Joint Committee on Cancer (AJCC).* Cancer, 1997. **80**(5): p. 987-9.

89. Amin, M.B., et al., *Prognostic impact of histologic subtyping of adult renal epithelial neoplasms: an experience of 405 cases.* Am J Surg Pathol, 2002. **26**(3): p. 281-91.

90. Przybycin, C.G., et al., *Chromophobe renal cell carcinoma: a clinicopathologic study of 203 tumors in 200 patients with primary resection at a single institution.* Am J Surg Pathol, 2011. **35**(7): p. 962-70.

91. Nickerson, M.L., et al., *Mutations in a novel gene lead to kidney tumors, lung wall defects, and benign tumors of the hair follicle in patients with the Birt-Hogg-Dube syndrome.* Cancer Cell, 2002. **2**(2): p. 157-64.

92. Pavlovich, C.P., et al., *Renal tumors in the Birt-Hogg-Dube syndrome.* Am J Surg Pathol, 2002. **26**(12): p. 1542-52.

93. Schmidt, L.S., et al., *Birt-Hogg-Dube syndrome, a genodermatosis associated with spontaneous pneumothorax and kidney neoplasia, maps to chromosome 17p11.2.* Am J Hum Genet, 2001. **69**(4): p. 876-82.

94. Shuch, B., et al., *Germline PTEN mutation Cowden syndrome: an underappreciated form of hereditary kidney cancer.* J Urol, 2013. **190**(6): p. 1990-8.

95. McGregor, B.A., et al., *Results of a Multicenter Phase II Study of Atezolizumab and Bevacizumab for Patients With Metastatic Renal Cell Carcinoma With Variant Histology and/or Sarcomatoid Features.* J Clin Oncol, 2020. **38**(1): p. 63-70.

96. Motzer, R.J., et al., *Survival outcomes and independent response assessment with nivolumab plus ipilimumab versus sunitinib in patients with advanced renal cell carcinoma: 42-month follow-up of a randomized phase 3 clinical trial.* J Immunother Cancer, 2020. **8**(2).

97. Motzer, R.J., et al., *Nivolumab plus ipilimumab versus sunitinib in first-line treatment for advanced renal cell carcinoma: extended follow-up of efficacy and safety results from a randomised, controlled, phase 3 trial.* Lancet Oncol, 2019. **20**(10): p. 1370-1385.

98. Motzer, R.J., et al., *Nivolumab plus Ipilimumab versus Sunitinib in Advanced Renal-Cell Carcinoma.* N Engl J Med, 2018. **378**(14): p. 1277-1290.

99. McDermott, D.F., et al., *Open-Label, Single-Arm, Phase II Study of Pembrolizumab Monotherapy as First-Line Therapy in Patients With Advanced Non-Clear Cell Renal Cell Carcinoma.* J Clin Oncol, 2021. **39**(9): p. 1029-1039.

100. Zhang, N. and M.J. Bevan, *CD8(+) T cells: foot soldiers of the immune system.* Immunity, 2011. **35**(2): p. 161-8.

101. Imai, T., et al., *Identification and molecular characterization of fractalkine receptor CX3CR1, which mediates both leukocyte migration and adhesion.* Cell, 1997. **91**(4): p. 521-30.

102. Cheuk, S., et al., *CD49a Expression Defines Tissue-Resident CD8(+) T Cells Poised for Cytotoxic Function in Human Skin.* Immunity, 2017. **46**(2): p. 287-300.

103. Sun, H., et al., *Tissue-resident lymphocytes: from adaptive to innate immunity.* Cell Mol Immunol, 2019. **16**(3): p. 205-215.

104. Gunesch, J.T., et al., *CD56 regulates human NK cell cytotoxicity through Pyk2.* Elife, 2020. **9**.

105. Zhou, Z., et al., *Granzyme A from cytotoxic lymphocytes cleaves GSDMB to trigger pyroptosis in target cells.* Science, 2020. **368**(6494).

106. Lieberman, J., *Granzyme A activates another way to die.* Immunol Rev, 2010. **235**(1): p. 93-104.

107. Ranson, T., et al., *IL-15 is an essential mediator of peripheral NK-cell homeostasis.* Blood, 2003. **101**(12): p. 4887-93.

108. Wagner, J.A., et al., *CD56bright NK cells exhibit potent antitumor responses following IL-15 priming.* J Clin Invest, 2017. **127**(11): p. 4042-4058.

109. Eckl, J., et al., *Transcript signature predicts tissue NK cell content and defines renal cell carcinoma subgroups independent of TNM staging.* J Mol Med (Berl), 2012. **90**(1): p. 55-66.

110. Schleypen, J.S., et al., *Cytotoxic markers and frequency predict functional capacity of natural killer cells infiltrating renal cell carcinoma.* Clin Cancer Res, 2006. **12**(3 Pt 1): p. 718-25.

111. Schleypen, J.S., et al., *Renal cell carcinoma-infiltrating natural killer cells express differential repertoires of activating and inhibitory receptors and are inhibited by specific HLA class I allotypes.* Int J Cancer, 2003. **106**(6): p. 905-12.

112. Simoni, Y., et al., *Human Innate Lymphoid Cell Subsets Possess Tissue-Type Based Heterogeneity in Phenotype and Frequency.* Immunity, 2017. **46**(1): p. 148-161.

113. Gao, Y., et al., *Tumor immunoevasion by the conversion of effector NK cells into type 1 innate lymphoid cells.* Nat Immunol, 2017. **18**(9): p. 1004-1015.

114. Guan, Y., et al., *Renal cell tumors convert natural killer cells to a proangiogenic phenotype.* Oncotarget, 2020. **11**(26): p. 2571-2585.

115. Freytag, S., et al., *Comparison of clustering tools in R for medium-sized 10x Genomics single-cell RNA-sequencing data.* F1000Res, 2018. **7**: p. 1297.

116. Haghverdi, L., et al., *Batch effects in single-cell RNA-sequencing data are corrected by matching mutual nearest neighbors.* Nat Biotechnol, 2018. **36**(5): p. 421-427.

117. Lun, A.T., D.J. McCarthy, and J.C. Marioni, *A step-by-step workflow for low-level analysis of single-cell RNA-seq data with Bioconductor.* F1000Res, 2016. **5**: p. 2122.

118. Levine, J.H., et al., *Data-Driven Phenotypic Dissection of AML Reveals Progenitor-like Cells that Correlate with Prognosis.* Cell, 2015. **162**(1): p. 184-97.

119. Xu, C. and Z. Su, *Identification of cell types from single-cell transcriptomes using a novel clustering method.* Bioinformatics, 2015. **31**(12): p. 1974-80.

120. Lu, L., et al., *Regulation of activated CD4+ T cells by NK cells via the Qa-1-NKG2A inhibitory pathway.* Immunity, 2007. **26**(5): p. 593-604.

121. Rapaport, A.S., et al., *The Inhibitory Receptor NKG2A Sustains Virus-Specific CD8(+) T Cells in Response to a Lethal Poxvirus Infection.* Immunity, 2015. **43**(6): p. 1112-24.

122. Franklin, R.A., et al., *The cellular and molecular origin of tumor-associated macrophages.* Science, 2014. **344**(6186): p. 921-5.

123. Bhowmick, N.A., et al., *TGF-beta signaling in fibroblasts modulates the oncogenic potential of adjacent epithelia.* Science, 2004. **303**(5659): p. 848-51.

124. Swonger, J.M., et al., *Genetic tools for identifying and manipulating fibroblasts in the mouse.* Differentiation, 2016. **92**(3): p. 66-83.

125. Snippert, H.J., et al., *Intestinal crypt homeostasis results from neutral competition between symmetrically dividing Lgr5 stem cells.* Cell, 2010. **143**(1): p. 134-44.

126. Gee, J.M., et al., *Imaging activity in neurons and glia with a Polr2a-based and cre-dependent GCaMP5G-IRES-tdTomato reporter mouse.* Neuron, 2014. **83**(5): p. 1058-72.

127. Orr, M.T., et al., *Development and function of CD94-deficient natural killer cells.* PLoS One, 2010. **5**(12): p. e15184.

128. Zhang, X., et al., *Synergized regulation of NK cell education by NKG2A and specific Ly49 family members.* Nat Commun, 2019. **10**(1): p. 5010.

129. Brodin, P., K. Karre, and P. Hoglund, *NK cell education: not an on-off switch but a tunable rheostat.* Trends Immunol, 2009. **30**(4): p. 143-9.

130. Brodin, P., et al., *Skewing of the NK cell repertoire by MHC class I via quantitatively controlled enrichment and contraction of specific Ly49 subsets.* J Immunol, 2012. **188**(5): p. 2218-26.

131. Joncker, N.T., et al., *NK cell responsiveness is tuned commensurate with the number of inhibitory receptors for self-MHC class I: the rheostat model.* J Immunol, 2009. **182**(8): p. 4572-80.

132. Kadri, N., T.L. Thanh, and P. Hoglund, *Selection, tuning, and adaptation in mouse NK cell education.* Immunol Rev, 2015. **267**(1): p. 167-77.

133. Mlecnik, B., et al., *Functional network pipeline reveals genetic determinants associated with in situ lymphocyte proliferation and survival of cancer patients.* Sci Transl Med, 2014. **6**(228): p. 228ra37.

134. Angelova, M., et al., *Evolution of Metastases in Space and Time under Immune Selection.* Cell, 2018. **175**(3): p. 751-765 e16.

135. Ewald, A.J., Z. Werb, and M. Egeblad, *Preparation of mice for long-term intravital imaging of the mammary gland.* Cold Spring Harb Protoc, 2011. **2011**(2): p. pdb prot5562.

136. Shreeve, N., et al., *The CD94/NKG2A inhibitory receptor educates uterine NK cells to optimize pregnancy outcomes in humans and mice.* Immunity, 2021.

137. Hoglund, P. and P. Brodin, *Current perspectives of natural killer cell education by MHC class I molecules.* Nat Rev Immunol, 2010. **10**(10): p. 724-34.

138. Wu, J. and L.L. Lanier, *Natural killer cells and cancer.* Adv Cancer Res, 2003. **90**: p. 127-56.

139. Jabri, B. and V. Abadie, *IL-15 functions as a danger signal to regulate tissue-resident T cells and tissue destruction.* Nat Rev Immunol, 2015. **15**(12): p. 771-83.

140. Abadie, V., et al., *IL-15, gluten and HLA-DQ8 drive tissue destruction in coeliac disease.* Nature, 2020. **578**(7796): p. 600-604.

141. Liu, R.B., et al., *IL-15 in tumor microenvironment causes rejection of large established tumors by T cells in a noncognate T cell receptor-dependent manner.* Proc Natl Acad Sci U S A, 2013. **110**(20): p. 8158-63.

142. Freud, A.G. and M.A. Caligiuri, *Human natural killer cell development.* Immunol Rev, 2006. **214**: p. 56-72.

143. Renoux, V.M., et al., *Identification of a Human Natural Killer Cell Lineage-Restricted Progenitor in Fetal and Adult Tissues.* Immunity, 2015. **43**(2): p. 394-407.

144. Lim, A.I., et al., *Systemic Human ILC Precursors Provide a Substrate for Tissue ILC Differentiation.* Cell, 2017. **168**(6): p. 1086-1100 e10.

145. Dogra, P., et al., *Tissue Determinants of Human NK Cell Development, Function, and Residence.* Cell, 2020. **180**(4): p. 749-763 e13.

146. Gerlach, C., et al., *The Chemokine Receptor CX3CR1 Defines Three Antigen-Experienced CD8 T Cell Subsets with Distinct Roles in Immune Surveillance and Homeostasis.* Immunity, 2016. **45**(6): p. 1270-1284.